Candida albicans exhibits distinct cytoprotective responses to anti-fungal drugs that facilitate the evolution of drug resistance

Samira Massahi

A Thesis

in

The Department

of

Biology

Presented in Partial Fulfillment of the Requirements

for the Degree of Master of Science (Biology) at

Concordia University

Montreal, Quebec, Canada

May 2020

CONCORDIA UNIVERSITY

School of Graduate Studies

This is to certify that the thesis prepared

By: Samira Massahi

Entitled: Molecular portraits of heterogeneity in Candida albicans population after treatment with antifungal compounds

and submitted in partial fulfillment of the requirements for the degree of

Master of Science (Biology)

complies with the regulations of the University and meets the accepted standards with respect to originality and quality.

Signed by the final Examining Committee:

_____Chair

Professor Malcolm Whiteway

_____ Examiner

Professor Isabelle Benoit Gelber

_____ Examiner

Professor Aashiq Kachroo

_____ Supervisor

Professor Michael Hallett

Approved by _____

Professor Patrick Gulick

_____2020 _____

Professor Andre G. Roy

Abstract

Candida albicans exhibits distinct cytoprotective responses to anti-fungal drugs that facilitate the evolution of drug resistance

Samira Massahi

Candida albicans is both a human commensal and opportunistic pathogen. Nosocomial infections due to pathogenic *C. albicans* are the fourth largest in North America and carry significant socioeconomic burden. Systemic *Candida* infections of immune-compromised individuals are frequently lethal even when treated optimally. Drug resistance is sometimes due to the pre-existence of genetic polymorphisms that bypass the mode of action of the drug. In other cases, resistance is acquired via the evolution of genetic polymorphisms. There is evidence that *C. albicans* possesses a drug tolerance response which “buys time” for individuals to gain such beneficial mutations. Our goal is to characterize this poorly understood epigenetic cytoprotective program at the single cell molecular level.

Our hypothesis is that individuals will respond differently to drug exposure. Some will not mount a sufficient epigenetic response and die, while others will survive using different pathways. We modified a single cell platform for the fungal setting and used it to transcriptionally profile thousands of treated and untreated cells at early (tolerance) and late (resistance) timepoints. Untreated populations exhibit multivariate epigenetic responses with individuals partitioning into distinct subpopulations, each with a unique survival strategy involving efflux pumps, chaperones, transport mechanisms, and cell wall maintenance. Cell imaging will be used to validate these observations. Whole genome DNA-sequencing will be used to determine if there is increased instability during the tolerance phase. Targeting the tolerance response concomitantly with standard therapies could represent an efficient approach to ablating clinical persistence.

Acknowledgements

I wish to express my sincere gratitude to my supervisor, Professor Michael Hallett, for his support, patience, helpful comments and great advice which guided me through this project. Thanks to his immense knowledge, I have learned a lot about data analysis and bioinformatics. I truly believe without his help, support and guidance, I would not be able to finish my master project.

I would also like to express my very great appreciation to professor Malcolm Whiteway for his valuable advice and willingness to give his time for the progress of this project.

My sincere thanks also goes to Dr Vanessa Dumeaux for offering me her precious time, advice and help in the establishment of Drop-seq protocol for Candida albicans.

I wish to extend my special thanks to Van Bettauer for his effort, dedication and hard work. If it is not for his help, I would not be able to finish this thesis and project. I have been lucky to have him as a friend and colleague throughout my master project.

I feel so grateful to have Sanny Khurdia, Shawn Simpson, Mathiew Harb and Eftyhios Kirbizakis from Hallett's lab as colleagues and friends help me through all steps of my project. Their passionate participation in this project encourages me to not get tired of all the barriers and to overcome them. I am also grateful for the assistance given by Dr Anna Carolina Borges Pereira Da Costa and Raha Omran from Whiteway lab.

And last but not least, I want to express my profound gratitude to my family, my mother, father and sister for their invaluable support and encouragement in each and every step of my life. This accomplishment would not have been possible without them.

Contribution of Authors

Van Bettauer and I are shared first authors on a manuscript that arises from this work (bioRxiv 914549). We both made intellectual contributions to all aspects of this work including concept and hypothesis generation, experimental design and logistics, execution of experiments, data quality control, data science, analysis and manuscript preparation. However, according to our expertise and background, we each had specific components of the project that were primarily our responsibilities. For example, I directed many of the wet lab assays and experiments due to my previous experience with fungal biology and laboratory techniques. This included preparation of C. albicans cultures, CRISPR/Cas9 transformations, microscopy experiments, and sample preparation upstream of single cell transcriptomics and bulk DNA sequencing. Bettauer on the other hand took primary responsibility for the statistical design of these experiments, bioinformatics required to identify good biomarkers for the microscopy, and the design of CRISPR guide RNAs. Bettauer's experience with deep learning and computational biology synergized with my knowledge of fungal biology during the analysis phases of this project.

S Khurdia, M Harb and S Simpson (all MSc candidates in Dr Hallett's lab) assisted with logistics and execution of DROP-seq experiments, helped prepare samples for sequencing, contributed knowledge and assistance with the development of bioinformatic pipelines and provided critical evaluation of the work. N Khosravi, who completed the graduate diploma project in Genomics and Biotechnology in Dr Hallett's lab, assisted with sample preparation and the execution of experiments. ACBP Costa and RP Omran from Dr Whiteway's lab provided support for assays and experiments with *C. albicans*, and critically evaluated results.

V Dumeaux assisted and supervised the development of the DROP-seq device, the bioinformatics analysis and with critical evaluations of the findings. M Whiteway provided the laboratory space, cell cultures and some reagents used in this effort, provided intellectual guidance in the project and assisted in the preparation of the manuscript. M Hallett provided funding for the project, supervised this work, and assisted in the preparation of this manuscript.

Table of Contents

List of Figures

Introduction

Candida albicans is both a human commensal and opportunistic pathogen. Nosocomial infections due to pathogenic *C. albicans* are the fourth most important in North America and are associated with significant socioeconomic burden[1,2]. Systemic *Candida* infections of immune-compromised individuals are frequently lethal even when treated optimally[3].

There are at least five classes of anti-fungal drugs: the polyenes, the azoles, the allylamines, the echinocandins, and the nucleoside analog flucytosine[4]. The first four attack a component of the pathogenic fungi that is distinct from the human host: the polyenes cause membrane leakage through interaction with ergosterol whereas the azoles and allylamines block the synthesis of ergosterol at different steps and the echinocandins attack the biosynthesis of the fungal cell wall. Flucytosine is metabolized into compounds that interfere with fungal DNA replication and RNA production; it is typically used in combination with the polyene amphotericin B.

The interaction between *C. albicans* and antifungal drugs is complex and multiple factors determine how the pathogen will be cleared or persist in the host individual. Persistence may be due to defects in the immune system of the host[5,6] or due to pre-existing or acquired genetic mechanisms of resistance[7]. For example, flucytosine resistance can result from mutations in the cytosine permease leading to a block in drug uptake, or by mutations in cytosine deaminase or uracil phosphoribosyltransferase that prevent the compound from being turned into a toxic analog[8]. Resistance to azoles can result from increased drug efflux[9–11] or mutations in the drug target *ERG11*[12]. Similarly, terbinafine resistance can arise from mutations in the drug target squalene epoxidase[13], while echinocandin resistance occurs through mutations in its target, the 1-3 beta glucan synthase[14]. Mutations in other elements can influence resistance more indirectly. For example, mutations in alternative components of the ergosterol pathway can provide resistance to azoles by preventing the blocked step from generating the highly detrimental sterols the wild type cells produce when Erg11 function is compromised[15]. Stress response pathways, particularly involving Hsp90 circuitry, are also linked to resistance to antifungal compounds[16]. Importantly, recent unbiased genomic profiling of 43 clinical isolates identified loss of heterozygosity events and single nucleotide polymorphisms in over 240 genes involved in adherence, filamentation, virulence and other processes, suggesting that genetic acquired

resistance may be achieved in many ways including via genomic instability[17–19]. There is now a substantial literature suggesting that *C. albicans*, like *S. cerevisiae*, generate large scale genomic variation as a means of adaptation[20–25], and there is some evidence that this could be facilitated by the parasexuality of the fungus[20,22,26–29].

C. albicans is well adapted to its role as an opportunistic pathogen with several distinct cellular morphologies that predominate in different niches. Drug response, resistance and clinical persistence are interwoven with these *C. albicans* morphologies including the white yeast form (round smooth cells) implicated in bloodstream dissemination, the opaque yeast form (rectangular or rod-shaped cells with large vacuoles) found predominantly in skin infections[30], and the hyphal form (filamentous long multifurcating strands) associated with tissue invasion[31]. Each morphology has unique underlying metabolic and regulatory characteristics that play cytoprotective roles against anti-fungals[32]. Several previous efforts have performed bulk RNA-sequencing to compare white opaque and filamentous[33–38]. These comparisons produced lists of genes that were differentially expressed (at the population level) between each two morphologies under different growth and stress conditions. Such a list of genes is often termed a *long-term adaptive transcriptional signature*, or simply *signature*. The signatures for Candida morphologies were distinct: although sharing many genes, each signature also contains many unique genes and processes.

Together, these molecular and cellular processes constitute the drug tolerance response, a short time interval post-treatment that is inherently epigenetic in nature, involving “reversible” regulatory programs and an absence of fixed genetic mutations. That is, the source of the cells physiological ability to survive in the presence of the inhibitory compound is not due to stable genomic modifications, but rests upon post-transcriptional programs such as position in the cell cycle, expression of stress genes, or random fluctuation in key cellular defense genes. Even when grown under standard laboratory conditions, isogenetic (or near isogenic) *Candida* populations respond differentially to antifungal drugs, with some fraction of the population exhibiting drug tolerance, defined as the ability of individuals to survive and grow at drug concentrations above the minimal inhibitory concentration (MIC)[39,40]. In general, tolerance is not nearly as well understood as drug resistance[41,42]. Bet hedging, for example, in response to environmental stress, has been observed in *S. cerevisiae*[43,44]. Tolerance also appears to be connected with reduced drug accumulation, where tolerant cells appear physiologically more

capable of preventing drug uptake or better at drug export. Although time scales are almost certainly longer within *in vivo* contexts, the tolerance phase, defined as the "lag time" between drug introduction and true acquired resistance, is relatively short; in some cases only a 48hr window is sufficient time for the fixation of advantageous genetic lesions[20,22,39].

Taken together this previous work suggests that the *C. albicans* drug tolerance response "buys cells time" in order to facilitate the appearance of *de novo* genetic mutations, thus increasing the chance of long-term survival. However, we do not fully understand these epigenetic programs and how they vary between drugs and environmental conditions. Our effort here is structured around the proposition that survival of any individual *C. albicans* cell, which does not already harbour a latent advantageous genetic mutation conferring drug resistance, is able to survive because it achieves an advantageous epigenetic configuration at the time of the drug challenge. This epigenetic configure provides a window for the generation of somatic mutational events for long-term resistance (**Figure 1A**). Previous genomic efforts to understand tolerance relied on bulk RNA-profiling, however in this case the transcriptional profiles describe only the "average" expression levels for each gene across all members of the population. Therefore, they were not able to measure perhaps subtle molecular events unique to individuals or small subpopulations. With bulk profiling, the tolerance response would need to be near universal, common across almost all members of the colony. The work discussed in the previous paragraph suggests that the tolerance response is not the same across all survivors in a population.

Here we are the first to modify a single cell sequencing approach based on nano-litre droplet sequencing (DROP-seq) for the fungal setting. DROP-seq is able to isolate individual cells in oil droplets, lysis the cells, capture mRNAs and barcode the resultant cDNA for next generation sequencing. Using our assay, we identify sub communities that successfully tolerate different anti-fungal agents with distinct modes of actions. We also present the first steps towards future investigations of single cell drug response dynamics using live cell imaging. In particular, we show how we will validate the existence of our subpopulations using fluorescent tagged genes. We also describe our first steps towards understanding if and how our distinct subpopulations (defined at the transcriptome level) are characterized at the genetic DNA level. Specifically, here since an isogenic (or near isogenic) SC5314 strain was used in our study, we expect that long-term resistance will be acquired over the course of our time series. Although the mRNAs captured by DROP-seq provide some clues as to what the nature of these genetic modifications,

more thorough large-scale whole genome DNA sequencing would allow us to better identify these events, especially large chromosome amplifications and losses. We present the first steps towards investigating the same populations of drug-challenged *C. albicans* at the genomic DNA level. We argue that a comprehensive characterization of the cytoprotective molecular pathways and processes could lead to new therapeutic approaches that seek to ablate the tolerance phase, thereby minimizing the likelihood of acquiring long-term drug resistance.

Results

A droplet-based single cell sequencing approach for fungi (fungal DROP-seq)

The *C. albicans* setting required an optimized protocol for cell preparation with specific techniques to remove the cell wall and induce stable spheroplasts, to stabilize and protect cellular RNA in situ (via RNAlater, a non-toxic reagent that rapidly permeates tissues and cells in unfrozen samples), and filtering steps to separate very large cells with hyphae morphologies. SC5314, a well established (circa 1984) lab grown strain (Squibb Inc.), were grown in YPD media alone (untreated, UT) or in the presence of an antifungal for either 48 or 72 hrs (**Methods 2, 3**). We chose a concentration of 0.01 mg/ml for both fluconazole (FCZ) and nystatin (NYS), representing a moderate dosage relative to their MIC_{50}s[8,45–48]. For caspofungin (CSP), a compound that interrupts cell wall biosynthesis[49–51], a concentration of 1 nanogram/ml. This is well below its MIC_{50} levels and chosen in order to increase the number of survivors of this compound (**Methods 3**). All cultures at all time points yielded a sufficient population of survivors for downstream DROP-seq profiling, although 72 hr Caspofungin (CSP-72) was excluded from the present study for logistical difficulties. In particular, we were able to recover too few cells from the culture due to adherence between intact cell walls (the colony will be revisited when all samples are re-processed). The cells were processed with our fungal DROP-seq device, and the captured material sequenced with Illumina NEXT-seq following a standard protocol[52,53] with ~200M read/sample (**Methods 4-6**). The raw sequencing data was subjected to our bioinformatics pipeline for read processing, data normalization and imputation (**Methods 7**). **Figure 1B, C** and **Supplemental Figure 1** provide summaries of the observed data post-sequencing, and the effects of normalization and imputation respectively. Results are comparable to previous studies[52] corrected for the size of the Candida transcriptome.

Different anti-fungals exhibit distinct transcriptional responses

We asked whether *C. albicans* populations exhibit distinct responses to different anti-fungal drugs. **Figure 2** provides an unsupervised clustering of the single cell expression profiles (UMAP, **Methods 8**) labelled with population of origin (panel **A**) . UMAP is a type of clustering that maps the expression profiles of cells to a manifold, a multidimensional nonlinear surface. The idea is that cells with similar expression profiles will reside close to one another on this manifold than cells that are not similar will be more distant. Then UMAP projects this multidimensional nonlinear surface to two dimensions for visualization. As such, the x and y units are unitless and it is dangerous to place too much meaning in large versus small gaps between disconnected clusters. This is because we are transforming high dimensional data (the expression of thousands of genes over thousands of cells) onto two dimen,sions. Alternative dimensionality reduction techniques and visualizations[54,55] produced qualitatively similar cell clusters (data not shown). Then after the UMAP embedding in two dimensions is established, we use Louvain clustering in the VISION package (panel **B**) to fracture this space into disjoint gene expression patterns. Like most classic clustering techniques, the number of clusters is a controllable parameter.

Although UT cells are likely near isogenic, they exhibit considerable transcriptional variation, bridging from some late FCZ-72 survivors (cluster 14) to late NYS-72 survivors (cluster 1). FCZ-72 and NYS-72 survivors have distinct gene expression patterns, each separating into two non-overlapping clusters. One subpopulation of CSP-48 and a subpopulation FCZ-48 are highly intermixed in clusters 9, 16, 18 and 20 (panel **B**). Far from this location, a second pair of subpopulations of CSP-48 and FCZ-48 form cluster 6. In fact, cluster 6 contains cells from almost all drugs and timepoints.

We next investigated whether specific processes and pathways were differential between the subpopulations highlighted in panels **A** and **B**. Towards this end, we collected from the literature genes or transcriptional signatures for relevant biological processes (**Methods 9**), and summarized the joint expression pattern of this set of genes for each cell using VISION (**Methods 10**). Drug resistance genes including those coding for efflux pumps were generally expressed lowest in UT cells **(Figure 2C)** as perhaps expected. Moreover, UT cells had the

most evidence of expressing the white yeast morphology and the least evidence of hyphae transcriptional signatures, compared to drug treated populations (**Figure 2D**). Nevertheless, *C. albicans* cell microscopy did not show as many hyphae/pseudohyphae morphologies as our data suggested (**Supplemental Figures 3 and 4**).

Many of the genes differentially expressed between UT and all drug treated populations were related to cellular morphology including *PFY1* (1.5 logFC), *WH11* (1.77), *PST1* (2.0). Also supporting the quality of our data, we observed that the inducible Environmental Stress Response (iESR)[56,57], a signature that should be upregulated in stressed cells, varied significantly across our panel and was inversely correlated with the expression of ribosomal proteins, which tend to be expressed higher in stable healthy cells[56] (**Figure 2E, F**). This suggests that the single cell approach is able to detect differences that bulk profiling was unable to find. We were able to verify that the clusters from Panel **B** are not primarily driven by cell cycle state (**Supplemental Figure 1, Methods 9**). Overall, we observe a varied response for many additional processes (**Figure 2G**). Together this suggests that *C. albicans* mounts distinct molecular responses to different classes of anti-fungal drugs.

Untreated colonies exhibit significant heterogeneity

We also observed from **Figure 2** that there is significant transcriptional heterogeneity across UT cells involving at least seven VISION clusters (**Panel B**). Of particular note, mustard cluster 6 is diverse, containing UT cells and cells from all drug/time points. Dark blue cluster 1 is intermixed with late NYS-72 survivors. Some remaining UT cells border late FCZ-72 survivors.

In order to better characterize molecular differences here, we restricted attention to only UT cells, applied Louvain clustering and identified 15 distinct transcriptional regions (**Figure 3A**). Three regions (cluster 8 versus cluster 12 versus clusters 2, 4 and 10) express the iESR; this signature is broadly anti-correlated with the ribosomal protein (RP) signature, which is generally considered a signature of healthy cells (**Figure 3B**). Our goal was then to characterize these three regions across our panel of signatures (**Figure 3E**). Cluster 8 strongly expresses most signatures except ergosterol and cell maintenance, suggesting the cells are very active although grown in an untreated environment with sufficient media, which was unexpected considering

these cells were not challenged by stressful situations. Cluster 12 most strongly expressed the cell maintenance and efflux pump signatures, but with moderate fluctuation in the remaining pathways. The regions defined by clusters 2, 4 and 10 are largely characterized by an absence, or possibly repression, of expression across most molecular processes, suggesting these cells are healthy.

At the gene level, we observe expression of the endoplasmic reticulum chaperone HSP70 localized to cluster 8, the ABC transporter *PRN3* localized to cluster 12, and *TTR1*, a dithiol glutaredoxin, is most highly expressed in clusters 2, 4 and 10 (**Figure 3C**). We located these UT cells which express markers *HSP70*, *PRN3* or *TTR1* back in the UMAP embedding for all cell populations (**Figure 3D**). *HSP70* is most highly expressed in mustard cluster 6 of **Figure 2B**, a highly diverse clustering containing UT cells and cells from each drug exposure. We asked what genes were strongly differentially expressed between these clusters and remaining cells (**Supplemental Table 3)** and found that many have well established roles in different stress responses including *HSP21*, *HGT6* and *CAS5* in the core stress response, *GAC1, XYL2* and *ADH2* in acid stress, *SOD3, YCF1* and *OXR1* in oxidative stress, consistent with the high expression of the iESR signature in this cluster (**Figure 2E**). Other genes are known hyphae morphology related genes including *YHB1, UCF1, XYL2, FAB1* and *REG1*, or genes with established roles in virulence including *HSP21* and *YHB1*.

PRN3 is mostly highly expressed in dark blue cluster 1 of **Figure 2B**, a cluster enriched for late NYS-72 survivors. We asked what genes were strongly differentially expressed between these dark blue cluster 1 of **Figure 2B** and neighbouring UT cells of cluster 11, and identified several genes with established roles in drug resistance (eg *RPL24, FMP45, ERG25*), biofilm formation (eg *TY37*), and cell wall maintenance (eg *PGA31*) (**Supplemental Table 4**). High iESR expression was also detected in this cluster. *TTR1* is most highly expressed in the mustard cluster 6 (where *HSP70* is expressed) but also uniquely expressed in the clusters predominated by UT cells (2,4,5,11,14) of **Figure 2B**. There was in general little evidence of expression of the iESR in these clusters.

Together the data supports the existence of three distinct subpopulations of UT cells, and provides preliminary evidence that these subpopulations expressed different transcriptional programs. This includes, but is not limited to, variability in iESR expression levels. The fact that high iESR expressing UT cells co-cluster with late FCZ-72 and NYS-72 survivors is consistent with the concept that a cell which “bet hedges” is more likely to survive.

To confirm the presence of the different subpopulations of UT cells, we are building genetically modified *C. albicans* strains that harbour *GFP*- and *RFP*-tagged Hsp70 and Ttr1 proteins respectively (**Methods 11a-c, Supplemental Table 1**). The resultant transformed fluorescence proteins represent fusion proteins and not *C. albicans* gene replacement by the *GFP* or *RFP*. At present, we have successfully completed the single RFP-Ttr1 strain, which is now frozen down in response to COVID-19 (**Supplemental Figure 5**). When we are able, we will complete the construction of the double mutant with *GFP*-tagged Hsp70, and grow UT cells in the same manner as for single cell sequencing (**Methods 3**). The colonies will then be subjected to live cell fluorescent imaging (**Methods 11d**) to test for the presence of two distinct non-overlapping sub-populations of cells.

Two distinct subpopulations are observed during the tolerance phase after treatment with fluconazole

Figure 2A suggests that isogenic (or near isogenic) individuals respond differentially to the same challenge. In particular, there are two distinct subpopulations of FCZ-48 survivors: clusters 9, 16, 18, 20 versus the second subpopulation in mustard cluster 6 (**Figure 2B**). To better characterize the molecular differences between the two subpopulations, we restricted attention to only FCZ-48 cells and applied Louvain clustering (**Figure 4A)**. The FCZ-48 cells in the brown and pink clusters 6 and 7 map exclusively to the highly diverse mustard cluster 6 of **Figure 2B** discussed previously. We refer to these two clusters as Response A, and the remaining clusters as response B. Differences in iESR expression broadly characterize the two responses (**Figure 4B)**.

Response A shows higher expression for most pathways (**Figure 4E**) including mechanisms established in the literature[11,12,45,59] as important to fluconazole resistance including cell membrane, oxidative stress and ergosterol pathway members (**Figure 4C**).

We hypothesized that cells exhibiting response A are more likely to survive to 72 hours. To test this hypothesis, we selected markers *UCF1* and *CMD1* that are strongly differentially expressed between response A and B (**Figure 4D**). UCF1 (Up-regulated by CAMP in Filamentous growth 1) exhibits higher expression in Response A. Consistent with our hypothesis, down-regulation of *UCF1* is associated with resistance to FCZ. Ca2+ binding protein *CMD1* (Calmodulin) regulates many Ca2+ independent processes related to cellular morphology, growth and mitosis. It is not expressed in Response A and shows variable expression across Response B.

To confirm the presence of two different subpopulations in FCZ-48 populations, we are building genetically modified *C. albicans* strains that harbour *GFP*- and *RFP*-tagged for Ucf1 and for Cmd1 proteins respectively (**Methods 11a-c, Supplemental Table 1**). These two genes are each expressed in two different *C albicans* subpopulations 48hrs post FCZ treatment. There is no evidence of any FCZ-48 survivors that express both genes simultaneously. Therefore, we transform both genes with GFP and RFP to emit different fluorescent signals, we expect to see two visible non-overlapping subpopulations at 48 hours. Our hope is that expression at the transcriptional level will be well correlated with protein fluorescence. We can also follow our FP cells from drug treatment to 48hrs to 72 hrs and beyond. This will provide evidence of whether both subpopulations (one defined by the presence of Ucf1 and absence of Cmd1, one defined by the absence of Uc1 and the presence of Cmd1) contribute survivors to later time points. In summary, the single cell expression profiles identify novel subpopulations and the microscopy allows us to “link” these subpopulations over time along the path from tolerance to resistance.

At present, we have successfully completed the single *RFP* Cmd1 strain, which is now frozen down in response to COVID-19 (**Supplemental Figure 5**). When we are able, we will complete the construction of the double mutant with *GFP*-tagged Ucf1, and grow FCZ-48 cells in the same manner as for single cell sequencing (**Methods 3**). The colonies will then be subjected to live

cell fluorescent imaging (**Methods 11d**) to test for the presence of two distinct non-overlapping sub-populations of cells.

We note that CSP-48 survivors intermix with the FCZ-48 survivors in both response A and B, suggesting that although caspofungin and fluconazole are different classes of anti-fungals with distinct modes of action, patterns of heterogeneity are conserved. We will use the genetically modified *C. albicans* strains with *GFP*-tagged Ucf1 and *RFP*-tagged Cmd1, but this time exposed the population to CSP-48 at the same concentration levels as was used for single cell sequencing. This experiment, which was interrupted will resume when the COVID-19 lockdown ends.

There is little evidence of multiple subpopulations across NYS-48 survivors with the vast majority of cells restricted to response A. Since our cell membrane signature is much higher expressed in Response A compared to B, we conjecture that cells that lowly express this process are highly sensitive to nystatin treatment as it specifically disrupts membrane function.

Two distinct subpopulations are observed in late 72 hours survivors after treatment with fluconazole

Figure 2A suggests that late 72 hour survivors of fluconazole treatment partition into two distinct subpopulations. The first population resides at the convergence of clusters 3, 11 and 14, and overlap with outlier UT cells (**Figure 2B**). The second population is contained exclusively within cluster 7, and resides in close proximity to Response A observed at the 48 hour time point. UMAP-based visualizations of FCZ-72 identify two main subpopulations (clusters 2 and 7 versus the remaining eight clusters; **Figure 5A**). Cells from clusters 2 and 7 correspond exclusively to Response A and the remainder to Response B (**Figure 5C**). The pathways and processes differentially expressed between these two subpopulations share many similarities to the observations made in the context of 48 hour post-FCZ treatment (**Figure 5B**).

We observe however that the FCZ-72 population closest to Response B has shifted slightly towards the expression profiles of UT in comparison to the FCZ-48 Response B cells (**Figure**

2A). We searched our signatures for those whose expression at 72 hours more closely resembled UT cells, in comparison to early 48 hour treatment. Both the ergosterol and efflux pathways were more lowly expressed in both FCZ-72 and UT cells than in FCZ-48. Conversely, stress pathways including oxidative stress, heat shock and the iESR are more highly expressed in the FCZ-72 and UT cells than in FCZ-48 (**Figure 5D**). In general, the expression changes associated with Response B are difficult to interpret; however they do suggest the tolerance phase at 48 hours may be stochastically probing different combinations of responses to survive, and survival of these cells, even if it is less likely than Response A, may involve the ablation of unnecessary cytoprotective pathways.

To examine the dynamics of these subpopulations from untreated, through the tolerance phase to late survivors at 72 hours, we selected two markers *WH11* and *YHB1* that showed differential expression between the two responses and variability across the time points (**Figure 6A,B**). *WH11* is expressed specifically in white-phase yeast-form cells and is similar in structure to *S. cerevisiae GLP1*, a gene coding for a plasma membrane protein involved in membrane organization and involved in maintaining organization during stress conditions. *WH11* is strongly expressed in almost all UT cells (both in Response A and B), loses expression in FCZ-48 but regains expression in FCZ-72 in Response B. The nitric oxide dioxygenase *YHB1* is only expressed in cells occurring in Response A at all time points UT, FCZ-48 and FCZ-72.

To confirm the presence of two different subpopulations in FCZ-72 populations, we again are creating double genetic mutant strains contain fluorescent markers for both Wh11 (RFP) and Yhb1 (*GFP*) (**Methods 11a-c, Supplemental Table 1, Supplemental Figure 5**). At present, we have successfully completed the single *RFP* Wh11 strain, which is now frozen down in response to covid-19 (**Supplemental Figure 5**). When we are able, we will complete the construction of the double mutant with *GFP*-tagged Yhb1, and grow FCZ-72 cells in the same manner as for single cell sequencing (**Methods 3**). The colonies will then be subjected to live cell fluorescent imaging (**Methods 11d**) to test for the presence of two distinct non-overlapping sub-populations of cells. We will also examine the FCZ-48 markers Ucf1 and Cmd1 at 72 hours.

Two distinct subpopulations are observed in late 72 hours survivors after treatment with nystatin

Late surviving NYS-72 cells exhibited evidence of transcriptional heterogeneity with two subpopulations consisting of cluster 6 or clusters 1, 17, and 19 in **Figure 2B**. Both subpopulations are contained in our so-called Response A. Due to technical reasons the NYS-48 profiles produced fewer than expected cells, although these same two Response A subpopulations are also observed during the tolerance phase.

Figure 7A depicts the relationships between just NYS-72 cells. Here, green toned clusters 8 and 9 correspond to the cluster 6 in **Figure 2B**, a highly diverse cluster that contains cells from all populations. Although there is no difference in expression of the iESR or ribosomal protein (RP) signatures, expression of the white, heat shock proteins (HSP), oxidative, iron stress and membrane signatures are all localized to cluster 6 (**Figure 7B-E**).

Since *UCF1* is expressed exclusively in cluster 6, we will also use our *GFP*-tagged *C. albicans* to observe cell growth in the presence of NYS.

DNA level investigations of drug tolerance and resistance

We sought to further investigate the findings obtained from single cell transcriptomic and phenotypic data at the DNA level. In particular, we are interested in understanding if and how an isogenic (or near isogenic) founder population can generate genetic polymorphisms that incur long time "true" genetic drug resistance. As reviewed above, there is evidence for such dynamic processes during the tolerance phase including the whole genome DNA profiling of Ford et al. with clinical isolates of *C. albicans*[60]. Importantly, Ford et al. are able to argue that specific chromosomal amplifications, polymorphisms and loss of heterozygosity (LOH) events are persistent, statistically over-represented and recurring. Rosenberg et al.[42] also showed that *de novo* genomic modifications occurred after challenging *C. albicans* with drugs after just 48 hours.

We grew C. albicans colonies in an identical manner as for the single cell transcriptomics except we included two additional later time points at 6 and 12 days (**Methods 2, 3 and 12a**). As it remains too costly to sequence full genomes at the single cell level, we extracted genomic DNA

(gDNA) of each colony in bulk and prepared it for Illumina-based next generation sequencing (**Methods 12b**). Careful analysis and previous efforts[17,18] converged on a recommended depth of 100 fold DNA coverage. The gDNA samples passed quality control criteria (**Supplemental Figures 6-9**) and were sent for sequencing, but were halted due to the COVID-19 lockdown. The computational pipeline is in place (**Methods 12c**). As these DNA profiles are bulk and not single cell, the computational challenge will be to "align" as best possible the observed frequencies of events with the relative size of subpopulations as observed by single cell transcriptomics and microscopy, and to identify driver genes within regions of chromosomal aberrations. We anticipate that we will be able to identify candidate genomic loci that are markers of each subpopulation across the time points and drug conditions; these markers can then be evaluated by alternative methods such as fluorescence in situ hybridization (FISH). This method would allow us to identify these genetic events in the context of our single cell mRNA-defined subpopulations.

Discussion

C. albicans SC5314 populations, either untreated or grown in the presence of one of three anti-fungals, were transcriptionally profiled using a nano-litre droplet-based single cell sequencing approach optimized for the fungal setting. The untreated population is likely isogenic or near isogenic, thereby minimizing the chance for preexisting genetic polymorphisms that confers resistance. In terms of **Figure 1A**, the untreated population before t_0 is green only. In support of this, we observe heterogeneity in gene expression across the untreated population but do not observe distinct subpopulations with clear boundaries (**Figure 2A**), with perhaps the exception of a few cells that belong to the mustard colored cluster 6 of **Figure 2B**. Some but not all of this variability is explained by variation in cell cycle. In fact, over the 15 clusters found computationally across this population, many different processes show differential expression including the induced environmental stress response (iESR), ribosomal proteins (RP) and other processes linked to drug response/stress including efflux pumps. In general, untreated cells expressing the iESR fall at the edges of the untreated cloud and inter-mix with late survivors challenged by anti-fungals. Our DNA sequencing effort, when it resumes post-lockdown, will allow us to better estimate how truly isogenic the founder population is in our experiments.

Microscopy confirms that the vast majority (>99%) of the cells in the untreated populations are of the white yeast morphology, however gene expression signatures for early germ bud and late hyphae stages do show variability. We conjecture that is at least in part due to limitations in the way that these signatures from the literature were formed. That is, methodology from previous studies used supervised analysis of gene expression profiles between white yeast and other morphologies in bulk populations. Such bulk-derived lists of genes may not be sufficiently robust to capture a presumably multi-step trajectory between the target morphologies. This is an example of Simpson's paradox[61]. We conjecture that even healthy cells cycle through regulatory programs that represent proto-opaque, budding or filamentous morphologies. In other words, healthy cells "bet hedge" with various stress responses including an inclination towards a change in morphology. The most extreme example of this are those untreated cells that fall within mustard cluster 6 of **Figure 2B**. These are very active cells expressing many pathways

simultaneously. We conjecture that untreated cells in the core or upper region of **Figure 2A** do not successfully transition to the tolerance phase (**Figure 1A**, green region B).

Each drug challenged population was profiled after 48 hours, a latency chosen to provide sufficient time for the drug to influence the colony but too short to allow genetic adaptation and resistance. Survivors profiled at 48hrs under both fluconazole and caspofungin largely partition into two subpopulations, which we have termed response A and B throughout this manuscript. In broad terms, cells exhibiting response A appear transcriptionally active, expressing many stress and maintenance pathways including the proto-filamentous signatures described above. This latter statement is supported by microscopy of the populations that establish a higher fraction of filamentous cells in response A compared to response B. When we resume post-covid-19 lockdown, our genetically modified *C. albicans* strains expressing fluorescent reporters will allow us to determine whether or not both response A and B at 48 hours contribute cells that survive to 72 hours. If so, this would suggest that cells have distinct survival paths. Perhaps response A represents an aggressive *tour de force* while response B represents a more passive cell arrest strategy.

In fact, the fluconazole and caspofungin populations intermix in both response A and B, even though they represent two distinct classes of antifungals with different modes of action (disrupting ergosterol versus cell wall biosynthesis), suggesting that cells choose a survival path that is in some cases independent of the specific drug. We are currently investigating whether this bimodal response is maintained for other -azoles and other -fungins including additional drugs representative of all five classes of anti-fungals.

Our data suggests that 72 hour survivors, which have presumably had sufficient time to develop genetic resistance, originate from both A and B responses at 48 hours. This is apparent from the single cell transcriptomics-based clustering. Our double genetic mutants with live cell imaging experiments post-lockdown will provide more insight into this phenomena. Given that response A individuals are more active transcriptionally, we would conjecture that this response is enriched for individuals with acquired genetic resistance (yellow type of **Figure 1A**) with

response B relatively enriched perhaps for individuals who solely exploited epigenetic regulatory programs to survive the chemical insult (orange type of **Figure 1A**). We are also currently conducting experiments with pulse drug delivery to better ablate cell escape simply due to better guarantee the population is continually challenged to evolve resistance following Cowen and colleagues[62]. We are also exploring a greater range of concentrations including the $MIC_{25,}$ and MPC (Mutant Prevention Concentration)[63] following EUCAST guidelines (www.eucast.org). In particular, we are extending our time series with DROP-seq to 6 and 12 days with a re-pulse of drug and fresh media at 3 and 9 days.

We are currently revisiting the concentrations of lysis buffer and zymolyase in the protocol in order to increase mRNA yield during the DROP-seq step **(Methods 4 and 5).** We are in the process of re-running all drugs and timepoints in order to address issues of reproducibility, batch effect, statistical power[64] and correct technical problems related to nystatin and caspofungin in the first round of profiles. This new set of experiments will also extend our repertoire of drugs to amphotericin B, flucytosine and rapamycin, and to a new media sorbose, which was previously confirmed to have a role in causing genome instability in *C.albicans*[19].

Our focus now has strongly shifted towards combining the transcriptomic data with whole genome DNA sequencing to identify plausible molecular mechanisms for rapid evolution perhaps based on genomic neoplasticity and instability[20–24,26,27]. The ability to identify genetic polymorphisms including large-scale chromosomal aberrations that are specific to subpopulations may provide insight into general mechanisms exploited by *C. albicans* during the tolerance phase in order to “try out” many combinations of responses perhaps not unlike how genomic instability and neoplasticity drive innovation in tumors.

This additional data at both the DNA and mRNA levels will allow us to move towards fuller pseudotime trajectories[65–72], a common powerful approach in single cell studies, that frame-by-frame track changes from untreated through tolerant to resistant cells. The number of cells per sample and the number of distinct transcripts harvested per cell are two factors that have been challenged for pseudotime reconstructions. However, conceptually a more difficult

challenge lies in the fact that expression profiles of 72 hour survivors (perhaps not surprisingly) map closer to untreated cells than 48 hour tolerance cells. This is in part, but not exclusively, due to the fact that the induced environmental stress response involves several hundred genes, and it is most strongly expressed in early stages.

Combination therapies use more than one drug simultaneously to reduce the probability of acquiring resistance, permit the use of lower levels of each individual drug, and improve treatment specificity[73–75]. They are now used in many contexts, however, identifying synergizing compounds is challenging, and mechanistic explanations are difficult to establish[76]. A molecular level understanding of drug tolerance in *C. albicans* will open a door to a long corridor that ends in a new type of therapeutic that targets the tolerance phase. By careful examination of the trajectories across different conditions, drugs and concentrations, we can identify the most likely “cut-points" along these paths, that when targeted, would eliminate the grace period for an individual to acquire resistance.

Materials and Methods

1. Nanolitre droplet-based single cell RNA-sequencing (DROP-seq) for Fungi

Yeast (*S. cerevisiae*) has previously been examined by single cell sequencing using the Fluidigm C1 system but this handles less than 100 cells[57]. Jackson et al[77] sequenced ~40K *S. cerevisiae* cells with the commercial Chromium (10X Inc.) system. We opted to build a fungal DROP-seq modified from the original approach presented in Macosko et al[52,53], to address issues of cost and flexibility in comparison with commercial alternatives. In general, DROP-seq devices have been shown to be near equivalent to commercial systems[78]. In particular, here we built a printed circuit board to control microfluidic flow inspired by Stephenson et al[79], and 3D printed plastic syringe pumps and cheap cameras inspired by Booeshaghi et al[80] . The cost per device is well below $1K CDN.

2. Strains and media

C. albicans SC5314, cells were grown in YPD liquid media (2% D-glucose, 2% peptone, 1% yeast extract, 0.01% uridine) and incubated at 30°C for 12-16 hours. Afterwards an aliquot of 10^8 cells (representing 10ml of culture with OD 1 in 600nm) was taken and used as the untreated sample. We then pelleted the cells with centrifugation, discarded the supernatant and introduced 1ml RNAlater (Sigma # R0901) and froze the resultant colony at -20°C for later use in the DROP-seq. Other aliquots were used for drugs treatment experiments. In order to have enough log-phase cells for our multiple drugs in different timepoints, we used the following protocol. Cells were pelleted and resuspended in 1ml of YPD. Then, 250µl of this suspension was combined with 15ml of fresh YPD and placed in a shaker incubator at 30 °C for 4-5 hours. Finally, on the order of 10^8 of these cells were placed in 10ml of YPD. Each suspension was then subjected to drug treatment.

3. Anti-fungal drug treatment

A concentration of 0.01 mg/ml was chosen for both fluconazole (Sigma #F8929) and nystatin (Sigma #N6261), representing a moderate dosage relative to their reported MIC50 levels[10,46–48,81]. A concentration of 1ng/ml was used for caspofungin (Sigma #SML0425), a compound that interrupts cell way biosynthesis[50,51,82]; this is well below its reported MIC50 levels and chosen in order to ensure a sufficient number of survivors to generate single cell profiles.

The target drug was delivered to the individual colonies from step 2 and incubated at 30 °C for 48 or 72 hours. Cells at these time points were strained (pluriStrainer® 20 µm) and collected in fresh tubes. This was done in order to minimize the likelihood that the microfluidic chip would block due to large hyphae and pseudohyphae morphologies. We observed that germ tubes up to four times the length of the mother cell can still be processed for drop-seq analysis (**Supplemental Figures 3, 4** and additional quantitative analysis in progress). Such cells are well within the hyphal transcriptional profile. This suggests that our profiles do contain hyphae and pseudohyphae cells.

4. <u>Spheroplasts</u>

The *C. albicans* setting required an optimized protocol for cell preparation with specific techniques to remove the cell wall and induce stable spheroplasts. Towards this end, we experimented with different concentrations of zymolyase (0.1, 0.2 and 0.4U zymolyase (BioShop # ZYM002) with 10^7 cells in 100 ul of sorbitol 1M at different time points (stored at 37 °C for 10, 20, 30 mins) before processing with the DROP-seq. To compare against untreated populations cells were stained with calcofluor white and imaged with microscopy (Leica DM6000). We concluded that concentrations in the range 0.1-0.2U after 20 minutes are able to induce spheroplasts that remain sufficiently stable for processing with our DROP-seq . These represent concentrations similar to the protocol for 10x from Jackson et al.

5. <u>Cell preparation</u>

Drug treated colonies at either the 48 or 72 hours were pelleted by brief centrifugation and washed two times with 1ml RNAlater. Cells were then resuspended in 0.5ml of RNAlater and stored at room temperature for one hour, following the company's protocol. Afterwards, they were put in -20 °C for at least 24 hours before passing through the DROP-seq. At the time of cell preparation for the DROP-seq protocol, an aliquot of 10^7 (OD=0.68 in 660 nm) cells from each colony was taken, and each colony was washed three times with sorbitol 1M. The cells were then resuspended in 100µl sorbitol 1M + 0.2 U Zymolyase and incubated at 37 °C for 20 minutes (as per our findings in **Methods 3**). The use of RNAlater before this step minimizes the chance of any transcripts changes during Zymolyase treatment. Next, the cells were pelleted and resuspended again in 0.5ml of cold and fresh RNAlater for five minutes. The cells were then washed (centrifuged and pelleted) with 1ml of washing buffer (1M sorbitol, 10mM TRIS pH 8,

100ug/ml BSA) three times. Finally, 10^6 cells (OD=0.08 in 660nm) were resuspended in 1.2 ml of the washing buffer. This cell suspension was then used as input to the DROP-seq device.

6. Fungal DROP-seq protocol

Cell preparation generally follows the protocol given by Macosko et al[52,53] with some exceptions. Whereas Macosko et al recommends a ratio of 100K cells to 120K beads for DROP-seq, we found that a ratio of 1M cells, for 120K beads generated a sufficient yield of cDNA as per the Agilent Tapestation. We hypothesise this is perhaps due to the fact that Candida cells are much smaller than mammalian cells, and therefore more cells tend to not be captured in droplets. Jackson et al[77] used 5M cells as input to the Chromium (10X Inc.) system. Furthermore, whereas Macosko et al. use 1ml of lysis buffer, we used 1.2 ml, and instead of 13 PCR cycles, we used 17 (Jackson et al. used 10 cycles). Samples were sequenced using the Illumina NextSeq500 following a standard protocol[52] (200M reads/sample).

7. Bioinformatics and statistics for the single cell profiles

In general, all computations were performed using Python version 3.67 or R version 3.6.1. Gene abundances were estimated from raw sequencing data using the end-to-end pipeline Alevin[83] which optimizes UMI deduplication and reduces the number of discarded (multi-mapped) reads. SCANPY[84], a python-based toolkit for analyzing single-cell gene expression data was used for data quality control and preprocessing. We selected cells with at least 30 genes and 50 read counts under the condition that less than half were found in ribosomal genes (RDN). We removed genes that were observed to be expressed in less than 20 cells. Normalization, imputation and batch correction were performed by scVI[85,86], a tool which implements a probabilistic model of mRNA capture and uses a variational autoencoder to estimate priors across batches and conditions (**Supplemental Figure 1**).

8. Approaches for identifying subpopulations with distinct states and expression patterns

To identify subpopulations of cells with similar gene expression patterns in an unsupervised manner, dimensionality reduction and visualization was based on UMAP[87] with Louvain[88] clustering.

UMAP. Traditional gene clustering used Pearson correlation distance (or a similar metric such as Euclidean distance) to identify and group genes or samples that had similar behavior. Single cell

analysis does not do well with such traditional approaches for a number of reasons. Perhaps the main limitation is that many genes have “zero counts” in many cells. Zero counts can occur because the transcript is truly not in the cell (we term this a biological zero) or because the technology misses it (a technical false negative). The single cell community turned to more complicated non-linear manifold embeddings and sophisticated machine learning techniques to help with this problem. You can think of a manifold as a sort of continuous cloud in three dimensions (although the data is much higher dimensional). The cells are mapped to this non-linear surface. The fact that it is non-linear (as compared to linear embeddings typical of classic clustering) gives many more degrees of freedom to retain “neighbourhood properties”. That is, we can map our cells onto the surface of this curvy shape in high dimensional space so that two cells that have similar transcriptional profiles are almost always close to each other, across our panels with 1000s of cells. Then UMAP takes the shape of a high-dimensional surface and projects the cells and their expression profile onto a two-dimensional plane (what you see in Figures 2-6). Again the algorithm tries to conserve nearest neighbor relationships: points near each other on the multidimensional manifold are also close to each other on the two-dimensional plane. That is, similar cells co-cluster.

Louvain is a so-called *community detection* algorithm. The principle is that it builds a graph where nodes are cells and two cells are connected if they have similar transcriptional profiles. Conceptually each cell builds a community consisting of its k nearest neighbors graph as defined by their similarity in gene expression profiles. Finally, the algorithm considers what every cell believes is its neighbourhood and forms a consensus of clusters across the data.

9. Gene signatures

Supplemental Table 2 lists all of the gene signatures used throughout the analysis. In some cases, gene signatures from the literature arise from studies in other organisms and therefore required orthology mappings to *C. albicans*. For example, the *S. cerevisiae* derived Environmental Stress Response (ESR)[56] contains 859 genes and is divided into three broad categories called the induced ESR (iESR; genes that are differentially regulated in response to environmental xenobiotics, conditions or other challenges), the ribosomal proteins (RP) and the

ribosomal biogenesis genes (RiBi; involved in rRNA production, growth and cell division). To generate a *C. albicans* version of the ESR, we downloaded *C. albicans* (strain SC5314) assembly 21 and Sc (S288C) orthology maps from the Candida Genome Database (http://www.candidagenome.org/), and synteny maps from the Candida Gene Order Browser[89] at this website. For each *S. cerevisiae* gene we almost always used synteny as the primary attribute determining the correct *C. albicans* orthologue. When these databases failed to identify a *C. albicans* gene, we manually evaluated the quality of the reciprocal best BLAST-protein alignment between *S. cerevisiae* and *C. albicans*. In total, orthologs for 642 of the 859 *S. cerevisiae* ESR genes were identified (**Supplemental Table 5**).

The list of gene signatures consists of the following: ras pathway[36] , ergosterol biosynthesis[12,90] ,hyphae morphology[91] , calcineurin pathway[92,93] , oxidative stress[94], cell wall biosynthesis[49,95] , efflux pumps[10,11], pseudohyphal morphology[96] , heat shock[97] , biofilm[38] , opaque morphology[98] , iron starvation[56,82] , parasexual and meiosis[28,99] , germ tubes[98] , white morphology and early filamentous morphology[100] . The genes for each signature are listed in **Supplemental Table 2** and **5**.

10. Approaches for exploring the molecular components of subpopulations

Our univariate analyses started with a simple Welch *t*-test to identify genes that are strongly differentially expressed between two given target populations. Five of 6 markers were significant at a pvalue of 0.01, however we did not make adjustments for multiple testing nor false discovery. Rather we focused on a choice of genes that had the most evidence of differential expression between the subpopulations to serve as good biomarkers in the downstream microscopy validation studies. When selecting for marker genes, we narrowed our focus towards genes that were strongly up-regulated in one cluster. Our multivariate analyses started with the VISION tool[101] to identify sets of genes that are strongly differential between two given target populations. Given a gene signature (**Methods 9**), VISION computes a signature score based on a combination of gene expression and a precomputed cell-cell similarity map. A representative score for each signature is computed for every cell, which is calculated as the sum of expression values of positive genes minus the sum of expression of negative genes. The sign of a gene is determined as follows: genes which are known to be up-regulated in a biological process are given a positive sign, while genes that are known to be down-regulated in

a biological process are given a negative sign. In cases where sign information is not known, every gene is given a positive value. Each signature score is divided by the total number of genes in the signature. Additionally, each signature is z-normalized using the expected mean and variance of a random signature with the same number of positive/negative genes.

11. Live cell imaging

Our goal is to use live cell imaging to validate subpopulations identified with the single cell transcriptional profiles. We proceeded as follows.

11a. Genes were selected whose expression profiles were differential expressed between subpopulations at each time point as described in **Methods 5**. This list of genes was winnowed down to one gene in each subpopulation with high expression levels. We limited validation studies to the two most distinct subpopulations at each time point (UT, FCZ 48h, FCZ 72h). In this manner, we required three pairs of marker genes, one tagged with GFP and one with RFP.

11b. Primers were designed for these six target genes (**Supplemental Table 1**). Strain SN76(*his1Δ/his1Δ, arg4Δ/arg4Δ, ura3Δ/ura3Δ*) was chosen for gene tagging, since it is a derivative strain of SC5314 but with multiple auxotrophic markers. These markers allow for convenient selection of cells which have successfully integrated the fluorescent protein in addition to the auxotroph marker (eg *HIS1*) via homologous recombination at the 3' position of the target genes (**Supplemental Figure 5B**).

11c. Benchling (https://benchling.com) was used to design the sgRNAs and we followed the CRISPR/Cas9 protocol with the plasmid pV1093 from Min et al[102]. This includes two PCR reactions to fuse the SNR52 promoter to the sgRNA scaffold and terminator. The third PCR reaction amplifies the final sgRNA cassettes. Two different plasmids pENO1-iRFP-NATr (Addgene Inc) and pFA-GFP-HIS1 were used to design the repair segment. The construction of the Cas9 cassette proceeded as per Min et al. Amplification of the Cas9 cassette with PCR used the following schedule: 98°C for 3 minutes, 98°C for 30 seconds, 63°C for 30 seconds, 72°C for

5 minutes and 30 seconds. Steps 2 to 4 have been repeated for 34 rounds followed by 72°C for 10 minutes and finally the reaction finished in 4°C. The repair DNA must be amplified with the designed primers described in **Supplemental Table 1** in 8-12 PCR tubes with 0.1µl plasmid (500ng/ml), 2.5µl forward primer, 2.5µl reverse primer, 1µl 10mM dNTP, 33.65µl nuclease free water, 10µl 5X HF PCR buffer and 0.25µl phusion polymerase in each tube.

11d. Preparation of cell colonies for microscopy. Cells that were successfully transformed were grown and harvested for each drug at each timepoint in a manner identical to that used for the single cell experiments (**Methods 4**). At time of microscopy, 10^6 cells were collected, washed with H2O and transferred to minimum media to minimize the background noise from normal YPD media. After, cells were mounted onto the uSlide and imaged with Nikon Ti microscope and Photometric camera each five minutes for three hours.

12. <u>Bulk DNA-sequencing</u>

12a. DNA was extracted from UT and drug treated cells after 48hrs, 72hrs, 6 days and 12 days (**Methods 3**). Since the media was saturated with cells at 72 hours, we sampled 10^8 cells from the population and added 10ml of new media with a second pulse of the drug to the culture. Cells were harvested for sequencing at 6 days. This procedure was repeated at the 9 day time point for cells to be harvested at day 12. Before harvesting, cells were maintained at 30°C in an incubator with rotation.

12b. When isolating genomic DNA (gDNA), 1.5ml of saturated media (approximately 8-10 A600 units for each ml) were pelleted as specified by the MasterPure Yeast DNA Purification Kit Protocol (Epicentre #MPY80200). Concentration and fragment length of the gDNA was measured using a 4150 Tapestation (Agilent) on a Genomic DNA ScreenTape (Agilent #5067-5365) (**Supplemental Figures 6-9**). The Nextera XT (Illumina #FC-131-1024) kit was used for tagmentation following the protocol from the manufacturer. All 13 samples were then multiplexed using the Nextera XT Indexing Primers and sent for sequencing utilizing the

NextSeq 500 platform. A mid-throughput chip with 2 x 80bp paired-end reads (Ilumina #20024904) is expected to generate a total of 20.8 billion nucleotides.

We rationalized that a average sequencing depth of 100x would provide sufficient power to detect (1) SNPs, (2) ploidy (haploid versus diploid versus tetraploid), (3) gains (from aneuploidy) and (4) losses (from aneuploidy), under several assumptions including that Response A has a set of defining genomic events that are common to almost all Response A cells and similarly Response B has a set of defining genomic events that almost all Response B cells have. Our depth of 100x is sufficient to identify events with a p-value < 0.05 under a broad range of different scenarios (eg a defining SNP of Response A occurs in a tetraploid genome, a loss of heterozygosity event occurs in a haploid genome). We stress that our independent power analysis (not shown) arrived at the same sequencing depth requirement as others in this domain[17,18].

The SC5314 genome is approximately 14.28 Mbp and therefore requires 1.428 billion base pairs for each sequencing run per sample to generate an expected 100x coverage. As we have 13 multiplexed samples in total, this requires 13 * 1.428 = 18.546 billion nucleotides, a number less than the expected 20.8 billion nucleotides generated by a full run of the NextSeq 500.

12.c Bioinformatics analysis will follow Ford et al.[17], a previous effort from the Broad Institute that sequenced whole genome DNA of clinical *C. albicans* samples. All reads will be mapped to the SC5314 reference genome (**Methods 9**) using the BWA alignment tool (version 0.7.1.7). Single nucleotide polymorphisms (SNPs will be identified using HaplotypeCaller (GATK version 4.1.4.1) and unreliable SNPs will be identified using the GATK Variant Filtration module, with the version 4 best practices annotation filters (QD < 2.0), MQ < 40.0, FS > 60.0, HaplotypeScore > 13.0, MQRankSum < -12.5, ReadPosRankSum < -8.0). A SNP matrix of all samples by position will be computed where an entry is 1 if a sample has a SNP at that position and 0 otherwise. We will also exploit the approaches in Ford et al. for determining copy number variation and loss of heterozygosity (LOH).

References

1. Zaoutis TE, Argon J, Chu J, Berlin JA, Walsh TJ, Feudtner C. The epidemiology and attributable outcomes of candidemia in adults and children hospitalized in the United States: a propensity analysis. *Clin Infect Dis Off Publ Infect Dis Soc Am*. 2005;41(9):1232-1239. doi:10.1086/496922
2. Benedict K, Jackson BR, Chiller T, Beer KD. Estimation of Direct Healthcare Costs of Fungal Diseases in the United States. *Clin Infect Dis Off Publ Infect Dis Soc Am*. 2019;68(11):1791-1797. doi:10.1093/cid/ciy776
3. Kullberg BJ, Arendrup MC. Invasive Candidiasis. *N Engl J Med*. 2015;373(15):1445-1456. doi:10.1056/NEJMra1315399
4. Roemer T, Krysan DJ. Antifungal drug development: challenges, unmet clinical needs, and new approaches. *Cold Spring Harb Perspect Med*. 2014;4(5). doi:10.1101/cshperspect.a019703
5. Siikala E, Rautemaa R, Richardson M, Saxen H, Bowyer P, Sanglard D. Persistent Candida albicans colonization and molecular mechanisms of azole resistance in autoimmune polyendocrinopathy-candidiasis-ectodermal dystrophy (APECED) patients. *J Antimicrob Chemother*. 2010;65(12):2505-2513. doi:10.1093/jac/dkq354
6. Kirchner FR, Littringer K, Altmeier S, et al. Persistence of Candida albicans in the Oral Mucosa Induces a Curbed Inflammatory Host Response That Is Independent of Immunosuppression. *Front Immunol*. 2019;10:330. doi:10.3389/fimmu.2019.00330
7. Hokken MWJ, Zwaan BJ, Melchers WJG, Verweij PE. Facilitators of adaptation and antifungal resistance mechanisms in clinically relevant fungi. *Fungal Genet Biol FG B*. 2019;132:103254. doi:10.1016/j.fgb.2019.103254
8. Shokohi T, Badali H, Amirrajab N, Ataollahi MR, Kouhpayeh SA, Afsarian MH. In vitro activity of five antifungal agents against Candida albicans isolates, Sari, Iran. *Curr Med Mycol*. 2016;2(2):34-39. doi:10.18869/acadpub.cmm.2.2.8
9. Sanglard D, Odds FC. Resistance of Candida species to antifungal agents: molecular mechanisms and clinical consequences. *Lancet Infect Dis*. 2002;2(2):73-85.
10. Sanglard D, Ischer F, Calabrese D, Micheli M, Bille J. Multiple resistance mechanisms to azole antifungals in yeast clinical isolates. *Drug Resist Updat Rev Comment Antimicrob Anticancer Chemother*. 1998;1(4):255-265.
11. Sanglard D. Emerging Threats in Antifungal-Resistant Fungal Pathogens. *Front Med*. 2016;3:11. doi:10.3389/fmed.2016.00011
12. Sanglard D, Ischer F, Parkinson T, Falconer D, Bille J. Candida albicans mutations in the ergosterol biosynthetic pathway and resistance to several antifungal agents. *Antimicrob Agents Chemother*. 2003;47(8):2404-2412. doi:10.1128/aac.47.8.2404-2412.2003
13. Osborne CS, Leitner I, Favre B, Ryder NS. Amino acid substitution in Trichophyton rubrum squalene epoxidase associated with resistance to terbinafine. *Antimicrob Agents Chemother*. 2005;49(7):2840-2844. doi:10.1128/AAC.49.7.2840-2844.2005
14. Balashov SV, Park S, Perlin DS. Assessing resistance to the echinocandin antifungal drug caspofungin in Candida albicans by profiling mutations in FKS1. *Antimicrob Agents Chemother*. 2006;50(6):2058-2063. doi:10.1128/AAC.01653-05
15. Kelly SL, Lamb DC, Corran AJ, Baldwin BC, Kelly DE. Mode of action and resistance to azole antifungals associated with the formation of 14 alpha-methylergosta-8,24(28)-dien-3 beta,6 alpha-diol. *Biochem Biophys Res Commun*. 1995;207(3):910-915. doi:10.1006/bbrc.1995.1272
16. Robbins N, Uppuluri P, Nett J, et al. Hsp90 governs dispersion and drug resistance of fungal biofilms. *PLoS Pathog*. 2011;7(9):e1002257-e1002257. doi:10.1371/journal.ppat.1002257
17. Ford CB, Funt JM, Abbey D, et al. The evolution of drug resistance in clinical isolates of Candida

albicans. *eLife*. 2015;4:e00662. doi:10.7554/eLife.00662
18. Mixão V, Hansen AP, Saus E, Boekhout T, Lass-Florl C, Gabaldón T. Whole-Genome Sequencing of the Opportunistic Yeast Pathogen Candida inconspicua Uncovers Its Hybrid Origin. *Front Genet*. 2019;10:383. doi:10.3389/fgene.2019.00383
19. Tucker C, Bhattacharya S, Wakabayashi H, et al. Transcriptional Regulation on Aneuploid Chromosomes in Diverse Candida albicans Mutants. *Sci Rep*. 2018;8. doi:10.1038/s41598-018-20106-9
20. Forche A, Abbey D, Pisithkul T, et al. Stress Alters Rates and Types of Loss of Heterozygosity in Candida albicans. Boothroyd JC, ed. *mBio*. 2011;2(4):e00129-11. doi:10.1128/mBio.00129-11
21. Rosenberg SM. Stress-Induced Loss of Heterozygosity in Candida: a Possible Missing Link in the Ability to Evolve. *mBio*. 2011;2(5):e00200-11. doi:10.1128/mBio.00200-11
22. Selmecki A, Forche A, Berman J. Genomic plasticity of the human fungal pathogen Candida albicans. *Eukaryot Cell*. 2010;9(7):991-1008. doi:10.1128/EC.00060-10
23. Selmecki A. Aneuploidy and Isochromosome Formation in Drug-Resistant Candida albicans. *Science*. 2006;313(5785):367-370. doi:10.1126/science.1128242
24. Selmecki AM, Dulmage K, Cowen LE, Anderson JB, Berman J. Acquisition of aneuploidy provides increased fitness during the evolution of antifungal drug resistance. *PLoS Genet*. 2009;5(10):e1000705. doi:10.1371/journal.pgen.1000705
25. Avramovska O, Hickman MA. *Ploidy Determines the Consequences of Antifungal-Induced Mutagenesis in Candida Albicans, a Human Fungal Pathogen*. Genetics; 2019. doi:10.1101/686881
26. Hickman MA, Paulson C, Dudley A, Berman J. Parasexual Ploidy Reduction Drives Population Heterogeneity Through Random and Transient Aneuploidy in *Candida albicans*. *Genetics*. 2015;200(3):781-794. doi:10.1534/genetics.115.178020
27. Popp C, Ramírez-Zavala B, Schwanfelder S, Krüger I, Morschhäuser J. Evolution of Fluconazole-Resistant Candida albicans Strains by Drug-Induced Mating Competence and Parasexual Recombination. *mBio*. 2019;10(1). doi:10.1128/mBio.02740-18
28. Hirakawa MP, Chyou DE, Huang D, Slan AR, Bennett RJ. Parasex Generates Phenotypic Diversity *de Novo* and Impacts Drug Resistance and Virulence in *Candida albicans*. *Genetics*. 2017;207(3):1195-1211. doi:10.1534/genetics.117.300295
29. Forche A, Alby K, Schaefer D, Johnson AD, Berman J, Bennett RJ. The Parasexual Cycle in Candida albicans Provides an Alternative Pathway to Meiosis for the Formation of Recombinant Strains. Heitman J, ed. *PLoS Biol*. 2008;6(5):e110. doi:10.1371/journal.pbio.0060110
30. Xie JL, Polvi EJ, Shekhar-Guturja T, Cowen LE. Elucidating drug resistance in human fungal pathogens. *Future Microbiol*. 2014;9(4):523-542. doi:10.2217/fmb.14.18
31. Desai JV. Candida albicans Hyphae: From Growth Initiation to Invasion. *J Fungi Basel Switz*. 2018;4(1). doi:10.3390/jof4010010
32. Loo AS, Muhsin SA, Walsh TJ. Toxicokinetic and mechanistic basis for the safety and tolerability of liposomal amphotericin B. *Expert Opin Drug Saf*. 2013;12(6):881-895. doi:10.1517/14740338.2013.827168
33. Martin R, Albrecht-Eckardt D, Brunke S, Hube B, Hünniger K, Kurzai O. A core filamentation response network in Candida albicans is restricted to eight genes. *PloS One*. 2013;8(3):e58613. doi:10.1371/journal.pone.0058613
34. Noble SM, Gianetti BA, Witchley JN. Candida albicans cell-type switching and functional plasticity in the mammalian host. *Nat Rev Microbiol*. 2017;15(2):96-108. doi:10.1038/nrmicro.2016.157
35. Kim J, Lee J-E, Lee J-S. Histone deacetylase-mediated morphological transition in Candida albicans. *J Microbiol*. 2015;53(12):805-811. doi:10.1007/s12275-015-5488-3
36. Inglis DO, Sherlock G. Ras signaling gets fine-tuned: regulation of multiple pathogenic traits of Candida albicans. *Eukaryot Cell*. 2013;12(10):1316-1325. doi:10.1128/EC.00094-13

37. Huang G. Regulation of phenotypic transitions in the fungal pathogen *Candida albicans*. *Virulence*. 2012;3(3):251-261. doi:10.4161/viru.20010
38. Huang MY, Woolford CA, May G, McManus CJ, Mitchell AP. Circuit diversification in a biofilm regulatory network. *PLoS Pathog*. 2019;15(5):e1007787. doi:10.1371/journal.ppat.1007787
39. Delarze E, Sanglard D. Defining the frontiers between antifungal resistance, tolerance and the concept of persistence. *Drug Resist Updat Rev Comment Antimicrob Anticancer Chemother*. 2015;23:12-19. doi:10.1016/j.drup.2015.10.001
40. Fridman O, Goldberg A, Ronin I, Shoresh N, Balaban NQ. Optimization of lag time underlies antibiotic tolerance in evolved bacterial populations. *Nature*. 2014;513(7518):418-421. doi:10.1038/nature13469
41. Delarze E, Sanglard D. Defining the frontiers between antifungal resistance, tolerance and the concept of persistence. *Drug Resist Updat Rev Comment Antimicrob Anticancer Chemother*. 2015;23:12-19. doi:10.1016/j.drup.2015.10.001
42. Rosenberg A, Ene IV, Bibi M, et al. Antifungal tolerance is a subpopulation effect distinct from resistance and is associated with persistent candidemia. *Nat Commun*. 2018;9(1):2470. doi:10.1038/s41467-018-04926-x
43. Gasch AP. Comparative genomics of the environmental stress response in ascomycete fungi. *Yeast Chichester Engl*. 2007;24(11):961-976. doi:10.1002/yea.1512
44. Gasch AP, Yu FB, Hose J, et al. Single-cell RNA sequencing reveals intrinsic and extrinsic regulatory heterogeneity in yeast responding to stress. Balaban N, ed. *PLOS Biol*. 2017;15(12):e2004050. doi:10.1371/journal.pbio.2004050
45. Sanglard D, Ischer F, Calabrese D, Micheli M, Bille J. Multiple resistance mechanisms to azole antifungals in yeast clinical isolates. *Drug Resist Updat Rev Comment Antimicrob Anticancer Chemother*. 1998;1(4):255-265.
46. Diaz MC, Camponovo R, Araya I, Cerda A, Santander MP, Carrillo-Munoz AJ. [Identification and in vitro antifungal susceptibility of vaginal Candida spp. isolates to fluconazole, clotrimazole and nystatin]. *Rev Espanola Quimioter Publicacion Of Soc Espanola Quimioter*. 2016;29(3):151-154.
47. Girmenia C, Tuccinardi C, Santilli S, et al. In vitro activity of fluconazole and voriconazole against isolates of Candida albicans from patients with haematological malignancies. *J Antimicrob Chemother*. 2000;46(3):479-483. doi:10.1093/jac/46.3.479
48. Yuksekkaya S, Findik D, Arslan U. [Molecular epidemiology and antifungal susceptibility of Candida species isolated from urine samples of patients in intensive care unit]. *Mikrobiyol Bul*. 2011;45(1):137-149.
49. Yang F, Zhang L, Wakabayashi H, et al. Tolerance to Caspofungin in Candida albicans Is Associated with at Least Three Distinctive Mechanisms That Govern Expression of FKS Genes and Cell Wall Remodeling. *Antimicrob Agents Chemother*. 2017;61(5). doi:10.1128/AAC.00071-17
50. Stevens DA, Espiritu M, Parmar R. Paradoxical effect of caspofungin: reduced activity against Candida albicans at high drug concentrations. *Antimicrob Agents Chemother*. 2004;48(9):3407-3411. doi:10.1128/AAC.48.9.3407-3411.2004
51. Cappelletty D, Eiselstein-McKitrick K. The echinocandins. *Pharmacotherapy*. 2007;27(3):369-388. doi:10.1592/phco.27.3.369
52. Macosko EZ, Basu A, Satija R, et al. Highly Parallel Genome-wide Expression Profiling of Individual Cells Using Nanoliter Droplets. *Cell*. 2015;161(5):1202-1214. doi:10.1016/j.cell.2015.05.002
53. Macosko E, Goldman M, Lab M, Mccarroll S. Drop-Seq Laboratory Protocol. Published online 2015. http://mccarrolllab.com/wp-content/uploads/2015/05/Online-Dropseq-Protocol-v.-3.1-Dec-2015.pdf
54. van der Maaten L, Hinton G. Visualizing data using t-SNE. *J Machine Learning Research*. 2008;9:2579-2605.

55. Moon KR, van Dijk D, Wang Z, et al. PHATE: A Dimensionality Reduction Method for Visualizing Trajectory Structures in High-Dimensional Biological Data. *bioRxiv*. Published online January 1, 2017:120378. doi:10.1101/120378
56. Gasch AP. Comparative genomics of the environmental stress response in ascomycete fungi. *Yeast Chichester Engl*. 2007;24(11):961-976. doi:10.1002/yea.1512
57. Gasch AP, Yu FB, Hose J, et al. Single-cell RNA sequencing reveals intrinsic and extrinsic regulatory heterogeneity in yeast responding to stress. Balaban N, ed. *PLOS Biol*. 2017;15(12):e2004050. doi:10.1371/journal.pbio.2004050
58. Enjalbert B, Nantel A, Whiteway M. Stress-induced gene expression in Candida albicans: absence of a general stress response. *Mol Biol Cell*. 2003;14(4):1460-1467. doi:10.1091/mbc.e02-08-0546
59. Sanglard D, Odds FC. Resistance of Candida species to antifungal agents: molecular mechanisms and clinical consequences. *Lancet Infect Dis*. 2002;2(2):73-85.
60. Ford CB, Funt JM, Abbey D, et al. The evolution of drug resistance in clinical isolates of Candida albicans. *eLife*. 2015;4:e00662. doi:10.7554/eLife.00662
61. Wagner CH. Simpson's Paradox in Real Life. *Am Stat*. 1982;36(1):46. doi:10.2307/2684093
62. Polvi EJ, Li X, O'Meara TR, Leach MD, Cowen LE. Opportunistic yeast pathogens: reservoirs, virulence mechanisms, and therapeutic strategies. *Cell Mol Life Sci CMLS*. 2015;72(12):2261-2287. doi:10.1007/s00018-015-1860-z
63. Hansen GT, Blondeau JM. Mutant prevention concentration as a strategy to minimize antimicrobial resistance: a timely concept but will its acceptance be too late? *Therapy*. 2005;2(1):61-66. doi:10.2217/14750708.2.1.61
64. Svensson V, Natarajan KN, Ly L-H, et al. Power analysis of single-cell RNA-sequencing experiments. *Nat Methods*. 2017;14:381.
65. Moon KR, van Dijk D, Wang Z, et al. PHATE: A Dimensionality Reduction Method for Visualizing Trajectory Structures in High-Dimensional Biological Data. *bioRxiv*. Published online January 1, 2017:120378. doi:10.1101/120378
66. Welch JD, Kozareva V, Ferreira A, Vanderburg C, Martin C, Macosko EZ. Single-Cell Multi-omic Integration Compares and Contrasts Features of Brain Cell Identity. *Cell*. 2019;177(7):1873-1887.e17. doi:10.1016/j.cell.2019.05.006
67. Setty M, Tadmor MD, Reich-Zeliger S, et al. Wishbone identifies bifurcating developmental trajectories from single-cell data. *Nat Biotechnol*. 2016;34(6):637-645. doi:10.1038/nbt.3569
68. Qiu X, Mao Q, Tang Y, et al. Reversed graph embedding resolves complex single-cell developmental trajectories. *bioRxiv*. Published online January 1, 2017:110668. doi:10.1101/110668
69. Rizvi AH, Camara PG, Kandror EK, et al. Single-cell topological RNA-seq analysis reveals insights into cellular differentiation and development. *Nat Biotechnol*. 2017;35(6):551-560. doi:10.1038/nbt.3854
70. Trapnell C, Cacchiarelli D, Grimsby J, et al. The dynamics and regulators of cell fate decisions are revealed by pseudotemporal ordering of single cells. *Nat Biotechnol*. 2014;32:381.
71. Papalexi E, Satija R. Single-cell RNA sequencing to explore immune cell heterogeneity. *Nat Rev Immunol*. 2017;18:35.
72. Rosenberg AB, Roco CM, Muscat RA, et al. Single-cell profiling of the developing mouse brain and spinal cord with split-pool barcoding. *Science*. 2018;360(6385):176. doi:10.1126/science.aam8999
73. Cihlar T, Fordyce M. Current status and prospects of HIV treatment. *Curr Opin Virol*. 2016;18:50-56. doi:10.1016/j.coviro.2016.03.004
74. Nabholtz J-MA, Reese DM, Lindsay M-A, Riva A. Combination chemotherapy for metastatic breast cancer. *Expert Rev Anticancer Ther*. 2002;2(2):169-180. doi:10.1586/14737140.2.2.169
75. Rao GG, Li J, Garonzik SM, Nation RL, Forrest A. Assessment and modelling of antibacterial combination regimens. *Clin Microbiol Infect Off Publ Eur Soc Clin Microbiol Infect Dis*.

2018;24(7):689-696. doi:10.1016/j.cmi.2017.12.004
76. Cui J, Ren B, Tong Y, Dai H, Zhang L. Synergistic combinations of antifungals and anti-virulence agents to fight against Candida albicans. *Virulence*. 2015;6(4):362-371. doi:10.1080/21505594.2015.1039885
77. Jackson CA, Castro DM, Saldi G-A, Bonneau R, Gresham D. Gene regulatory network reconstruction using single-cell RNA sequencing of barcoded genotypes in diverse environments. *bioRxiv*. Published online 2019:581678. doi:10.1101/581678
78. Zhang X, Li T, Liu F, et al. *Comparative Analysis of Droplet-Based Ultra-High-Throughput Single-Cell RNA-Seq Systems*. Genomics; 2018. doi:10.1101/313130
79. Stephenson W, Donlin LT, Butler A, et al. Single-cell RNA-seq of rheumatoid arthritis synovial tissue using low-cost microfluidic instrumentation. *Nat Commun*. 2018;9(1):791. doi:10.1038/s41467-017-02659-x
80. Booeshaghi AS, Beltrame E da V, Bannon D, Gehring J, Pachter L. Design principles for open source bioinstrumentation: the poseidon syringe pump system as an example. *bioRxiv*. Published online January 17, 2019:521096. doi:10.1101/521096
81. Shokohi T, Badali H, Amirrajab N, Ataollahi MR, Kouhpayeh SA, Afsarian MH. In vitro activity of five antifungal agents against Candida albicans isolates, Sari, Iran. *Curr Med Mycol*. 2016;2(2):34-39. doi:10.18869/acadpub.cmm.2.2.8
82. Yang F, Zhang L, Wakabayashi H, et al. Tolerance to Caspofungin in Candida albicans Is Associated with at Least Three Distinctive Mechanisms That Govern Expression of FKS Genes and Cell Wall Remodeling. *Antimicrob Agents Chemother*. 2017;61(5). doi:10.1128/AAC.00071-17
83. Srivastava A, Malik L, Smith T, Sudbery I, Patro R. Alevin efficiently estimates accurate gene abundances from dscRNA-seq data. *Genome Biol*. 2019;20(1):65. doi:10.1186/s13059-019-1670-y
84. Wolf FA, Angerer P, Theis FJ. SCANPY: large-scale single-cell gene expression data analysis. *Genome Biol*. 2018;19(1):15. doi:10.1186/s13059-017-1382-0
85. Lopez R, Regier J, Cole MB, Jordan MI, Yosef N. Deep generative modeling for single-cell transcriptomics. *Nat Methods*. 2018;15(12):1053-1058. doi:10.1038/s41592-018-0229-2
86. Xu C, Lopez R, Mehlman E, Regier J, Jordan MI, Yosef N. Harmonization and Annotation of Single-cell Transcriptomics data with Deep Generative Models. *bioRxiv*. Published online January 1, 2019:532895. doi:10.1101/532895
87. Becht E, McInnes L, Healy J, et al. Dimensionality reduction for visualizing single-cell data using UMAP. *Nat Biotechnol*. 2019;37(1):38-44. doi:10.1038/nbt.4314
88. Blondel VD, Guillaume J-L, Lambiotte R, Lefebvre E. Fast unfolding of communities in large networks. *J Stat Mech Theory Exp*. 2008;2008(10):P10008. doi:10.1088/1742-5468/2008/10/p10008
89. Fitzpatrick DA, O'Gaora P, Byrne KP, Butler G. Analysis of gene evolution and metabolic pathways using the Candida Gene Order Browser. *BMC Genomics*. 2010;11:290. doi:10.1186/1471-2164-11-290
90. Lv Q-Z, Yan L, Jiang Y-Y. The synthesis, regulation, and functions of sterols in Candida albicans: Well-known but still lots to learn. *Virulence*. 2016;7(6):649-659. doi:10.1080/21505594.2016.1188236
91. Desai JV. Candida albicans Hyphae: From Growth Initiation to Invasion. *J Fungi*. 2018;4(1). doi:10.3390/jof4010010
92. Yu S-J, Chang Y-L, Chen Y-L. Calcineurin signaling: lessons from Candida species. *FEMS Yeast Res*. 2015;15(4). doi:10.1093/femsyr/fov016
93. Gong Y, Li T, Yu C, Sun S. Candida albicans Heat Shock Proteins and Hsps-Associated Signaling Pathways as Potential Antifungal Targets. *Front Cell Infect Microbiol*. 2017;7. doi:10.3389/fcimb.2017.00520
94. Pais P, Galocha M, Teixeira MC. Genome-Wide Response to Drugs and Stress in the Pathogenic

Yeast Candida glabrata. *Prog Mol Subcell Biol*. 2019;58:155-193. doi:10.1007/978-3-030-13035-0_7
95. Gow NAR, Latge J-P, Munro CA. The Fungal Cell Wall: Structure, Biosynthesis, and Function. *Microbiol Spectr*. 2017;5(3). doi:10.1128/microbiolspec.FUNK-0035-2016
96. Merson-Davies LA, Odds FC. A morphology index for characterization of cell shape in Candida albicans. *J Gen Microbiol*. 1989;135(11):3143-3152. doi:10.1099/00221287-135-11-3143
97. Robbins N, Uppuluri P, Nett J, et al. Hsp90 Governs Dispersion and Drug Resistance of Fungal Biofilms. *PLoS Pathog*. 2011;7(9). doi:10.1371/journal.ppat.1002257
98. Si H, Hernday AD, Hirakawa MP, Johnson AD, Bennett RJ. Candida albicans White and Opaque Cells Undergo Distinct Programs of Filamentous Growth. Mitchell AP, ed. *PLoS Pathog*. 2013;9(3):e1003210. doi:10.1371/journal.ppat.1003210
99. Forche A, Alby K, Schaefer D, Johnson AD, Berman J, Bennett RJ. The Parasexual Cycle in Candida albicans Provides an Alternative Pathway to Meiosis for the Formation of Recombinant Strains. *PLOS Biol*. 2008;6(5):e110. doi:10.1371/journal.pbio.0060110
100. Martin R, Albrecht-Eckardt D, Brunke S, Hube B, Hünniger K, Kurzai O. A Core Filamentation Response Network in Candida albicans Is Restricted to Eight Genes. *PLoS ONE*. 2013;8(3). doi:10.1371/journal.pone.0058613
101. DeTomaso D, Jones MG, Subramaniam M, Ashuach T, Ye CJ, Yosef N. Functional interpretation of single cell similarity maps. *Nat Commun*. 2019;10(1):4376. doi:10.1038/s41467-019-12235-0
102. Min K, Ichikawa Y, Woolford CA, Mitchell AP. *Candida albicans* Gene Deletion with a Transient CRISPR-Cas9 System. Imperiale MJ, ed. *mSphere*. 2016;1(3). doi:10.1128/mSphere.00130-16

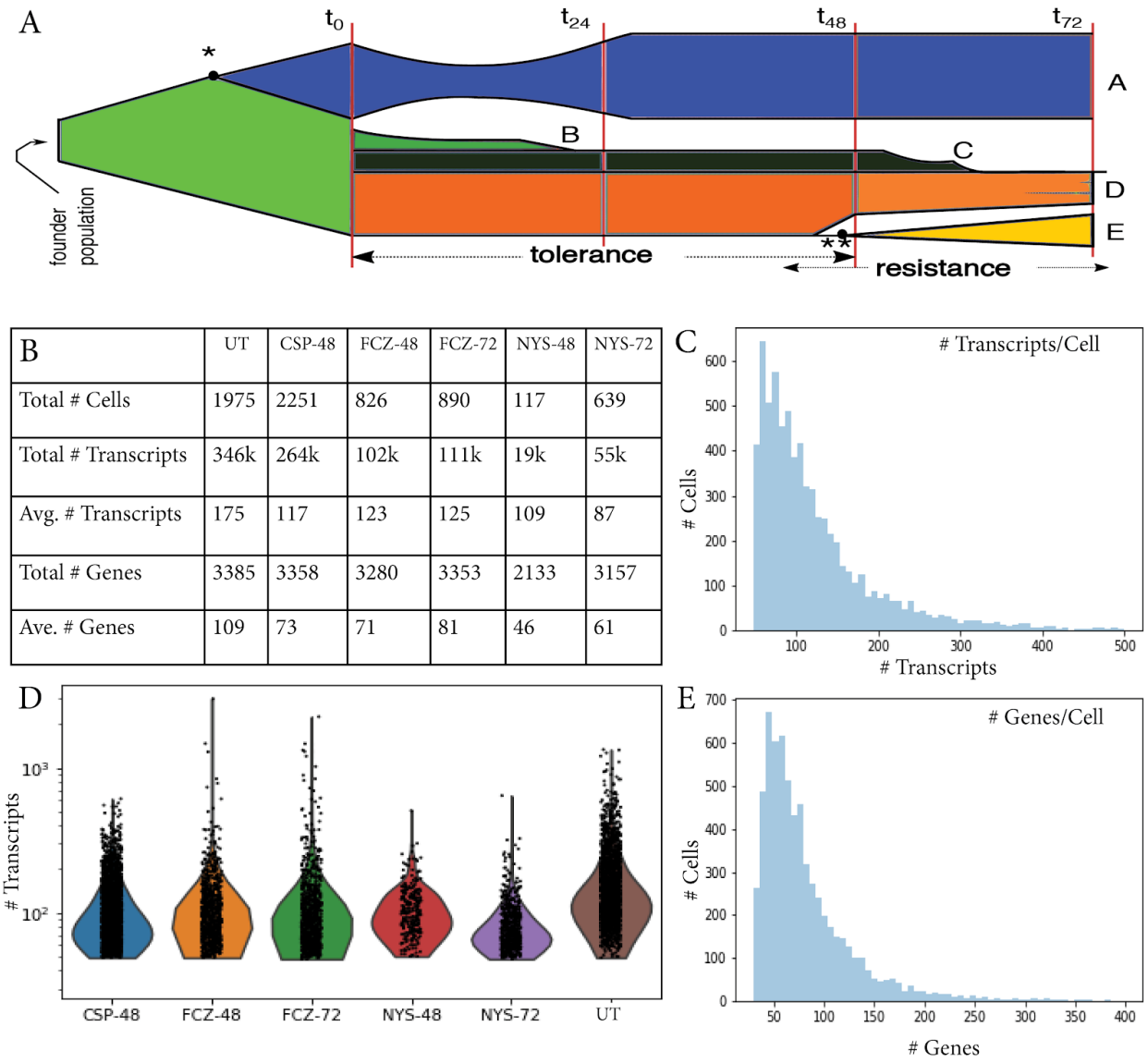

B	UT	CSP-48	FCZ-48	FCZ-72	NYS-48	NYS-72
Total # Cells	1975	2251	826	890	117	639
Total # Transcripts	346k	264k	102k	111k	19k	55k
Avg. # Transcripts	175	117	123	125	109	87
Total # Genes	3385	3358	3280	3353	2133	3157
Ave. # Genes	109	73	71	81	46	61

Figure 1 A. The potential trajectories of a fungal population challenged with an antifungal agent at time t_0.The pre-existence or the quick evolution in the founder population of a latent advantageous mutation (* and subsequent blue fraction) before drug exposure confers survival (population A). The remaining populations B-E lack such a preexisting mutation. Cells that do not mount a sufficient epigenetic tolerance defense die off (B). This proposal is focused on populations C,D,E that are each able to enlist an appropriate tolerance response. In some subpopulations (E), genetic events ultimately occur that confer long-term resistance (**, **yellow**),

whereas other subpopulations (C) may die off. Some subpopulations (D) may survive the drug through epigenetic modulation alone. **B.** Survey of results from fungal DROP-seq across different populations. **C.** Histogram describing the number of cells with observed levels of transcripts. **D.** Violin plots describing the distribution of transcript numbers. **E.** Histogram describing the number of cells with observed levels of genes.

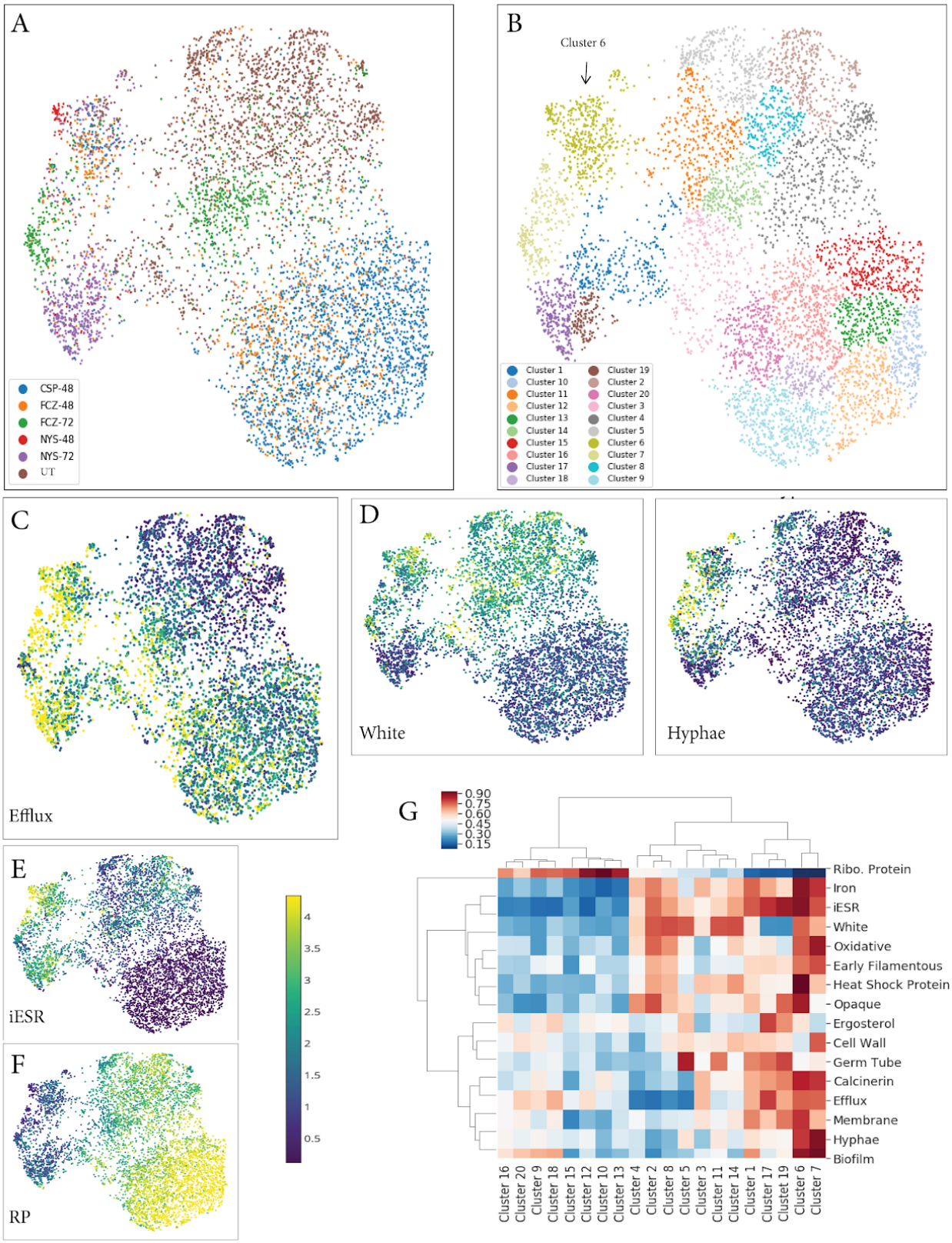
A
CSP-48
FCZ-48
FCZ-72
NYS-48
NYS-72
UT
B
Cluster 6
Cluster 1
Cluster 10
Cluster 11
Cluster 12
Cluster 13
Cluster 14
Cluster 15
Cluster 16
Cluster 17
Cluster 18
Cluster 19
Cluster 2
Cluster 20
Cluster 3
Cluster 4
Cluster 5
Cluster 6
Cluster 7
Cluster 8
Cluster 9
C
Efflux
D
White
Hyphae
E
iESR
F
RP
4
3.5
3
2.5
2
1.5
1
0.5
G
0.90
0.75
0.60
0.45
0.30
0.15
Ribo. Protein
Iron
iESR
White
Oxidative
Early Filamentous
Heat Shock Protein
Opaque
Ergosterol
Cell Wall
Germ Tube
Calcinerin
Efflux
Membrane
Hyphae
Biofilm
Cluster 16
Cluster 20
Cluster 9
Cluster 18
Cluster 15
Cluster 12
Cluster 10
Cluster 13
Cluster 4
Cluster 2
Cluster 8
Cluster 5
Cluster 3
Cluster 11
Cluster 14
Cluster 1
Cluster 17
Clustet 19
Cluster 6
Cluster 7

Figure 2 A. UMAP based visualization of the relationship between all *C. albicans* populations labelled by population of origin. Color codes for the cells are shown in the bottom left of the UMAP. For example, brown dots/cells are untreated (UT). **B.** UMAP embedding from A but here color reflects unsupervised Louvain found that many have well established roles in different stress responses including *HSP21, HGT6* and *CAS5* (core stress response), *GAC1, XYL2* and *ADH2* in acid stress, *SOD3, YCF1* and *OXR1* in clustering using VISION. **C.** Pattern of expression of the efflux pump gene signature mapped onto the UMAP embedding of A. **D.** Pattern of expression of white and hyphae gene signatures. **E, F.** Pattern of expression for the iESR and Ribosomal Protein (RP) signatures. **G.** Summary of expression of our collection of all signatures across the (unsupervised) Louvain clusters across all cell populations.

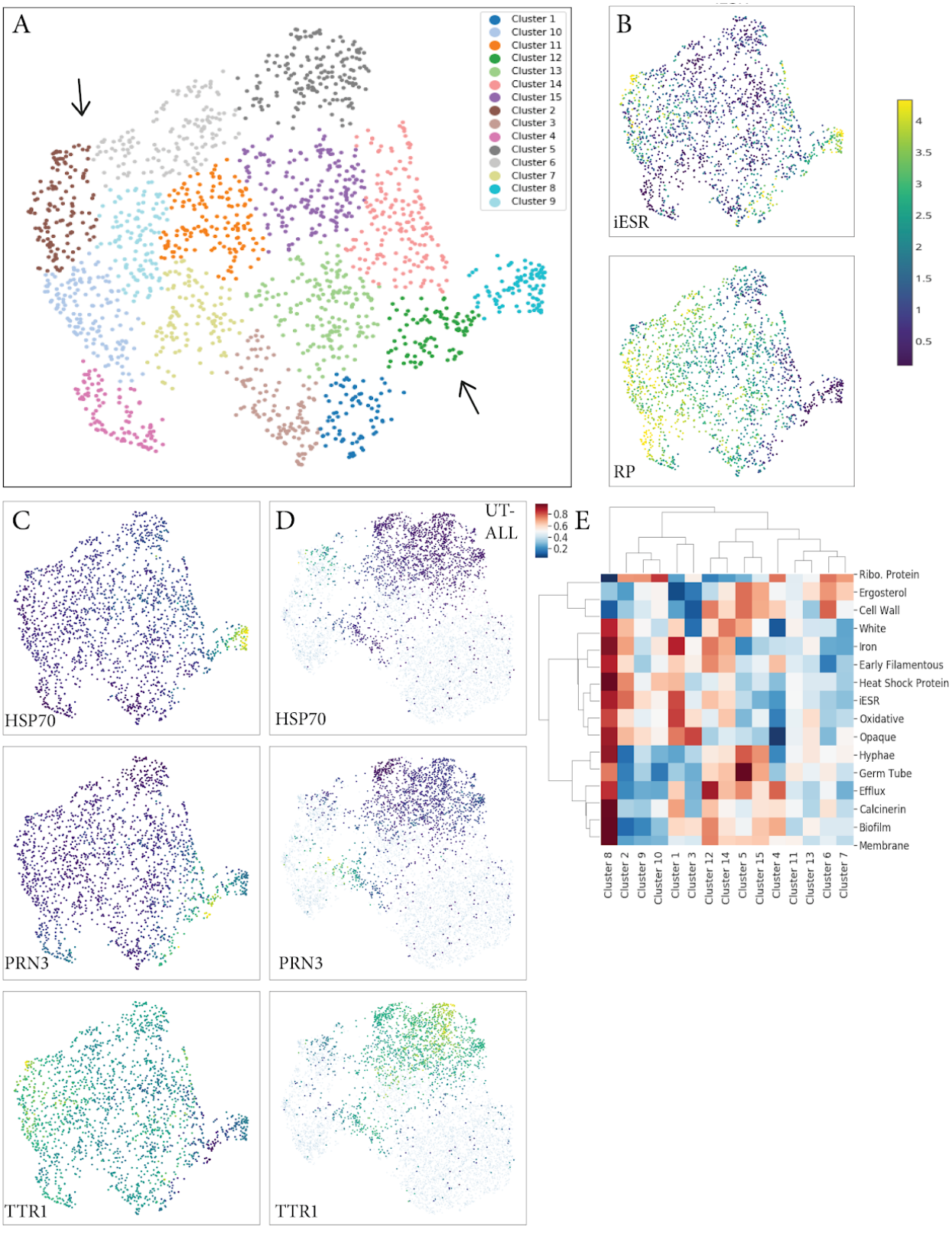
A
Cluster 1
Cluster 10
Cluster 11
Cluster 12
Cluster 13
Cluster 14
Cluster 15
Cluster 2
Cluster 3
Cluster 4
Cluster 5
Cluster 6
Cluster 7
Cluster 8
Cluster 9
B
iESR
RP
4
3.5
3
2.5
2
1.5
1
0.5
C
HSP70
D
UT-ALL
HSP70
0.8
0.6
0.4
0.2
E
Ribo. Protein
Ergosterol
Cell Wall
White
Iron
Early Filamentous
Heat Shock Protein
iESR
Oxidative
Opaque
Hyphae
Germ Tube
Efflux
Calcinerin
Biofilm
Membrane
Cluster 8
Cluster 2
Cluster 9
Cluster 10
Cluster 1
Cluster 3
Cluster 12
Cluster 14
Cluster 5
Cluster 15
Cluster 4
Cluster 11
Cluster 13
Cluster 6
Cluster 7
PRN3
PRN3
TTR1
TTR1

Figure 3 A. Visual representation (UMAP) of the relationships of only untreated (UT) cells. In total, 15 subpopulations are highlighted via Louvain clustering. **B.** Pattern of expression of the iESR and Ribosomal Protein (RP) signatures mapped onto the UMAP embedding of A. **C.** Gene expression of the endoplasmic reticulum chaperone *HSP70* (top), the ABC transporter *PRN3* (middle) and dithiol glutaredoxin *TTR1* (bottom) across UT cells. **D.** Gene expression of the endoplasmic reticulum chaperone *HSP70* (top), the ABC transporter *PRN3* (middle) and dithiol glutaredoxin *TTR1* (bottom) across all cells (drugs/timepoints) but with UT cells highlighted in the UMAP embedding of all cells. **E.** Summary of expression of all signatures across the Louvain clusters identified across only UT cells.

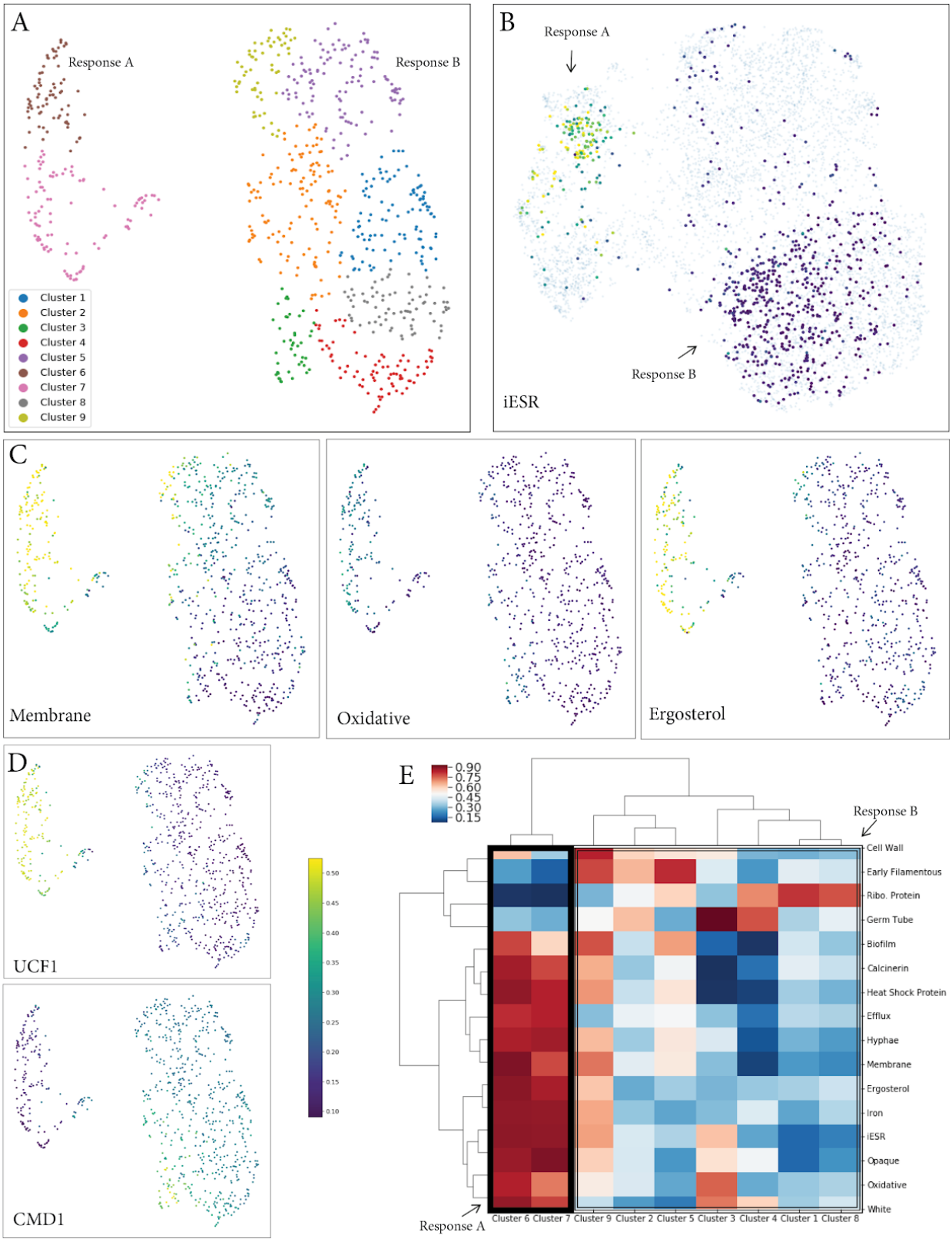
A
Response A
Response B
Cluster 1
Cluster 2
Cluster 3
Cluster 4
Cluster 5
Cluster 6
Cluster 7
Cluster 8
Cluster 9
B
Response A
Response B
iESR
C
Membrane
Oxidative
Ergosterol
D
UCF1
CMD1
0.50
0.45
0.40
0.35
0.30
0.25
0.20
0.15
0.10
E
0.90
0.75
0.60
0.45
0.30
0.15
Response B
Cell Wall
Early Filamentous
Ribo. Protein
Germ Tube
Biofilm
Calcinerin
Heat Shock Protein
Efflux
Hyphae
Membrane
Ergosterol
Iron
iESR
Opaque
Oxidative
White
Response A
Cluster 6 Cluster 7 Cluster 9 Cluster 2 Cluster 5 Cluster 3 Cluster 4 Cluster 1 Cluster 8

Figure 4 A. Visual representation (UMAP) of the relationships of only FCZ-48 cells. In total, 9 subpopulations are highlighted via Louvain clustering. **B.** Expression of the iESR across all cells (drugs/timepoints) but with FCZ-48 cells highlighted. **C.** Expression of the Membrane, Oxidative and Ergosterol signatures mapped onto the UMAP embedding of A. **D.** Gene expression of the *UCF1* (top) and *CMD1* (bottom) across FCZ-48 cells **E.** Summary of all signatures across the Louvain clusters identified across all FCZ-48 cells.

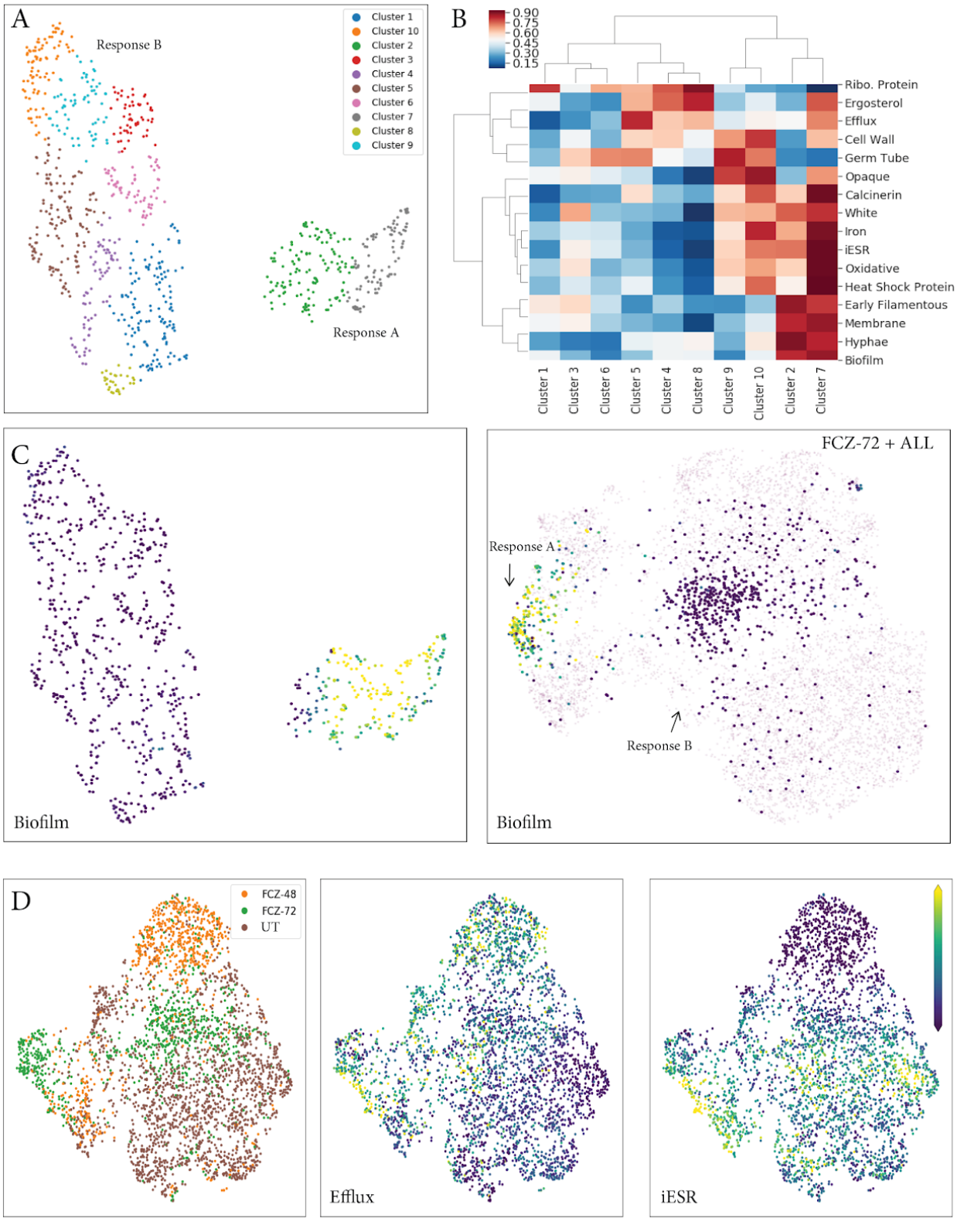
A
Response B
Response A
Cluster 1
Cluster 10
Cluster 2
Cluster 3
Cluster 4
Cluster 5
Cluster 6
Cluster 7
Cluster 8
Cluster 9
B
0.90
0.75
0.60
0.45
0.30
0.15
Ribo. Protein
Ergosterol
Efflux
Cell Wall
Germ Tube
Opaque
Calcinerin
White
Iron
iESR
Oxidative
Heat Shock Protein
Early Filamentous
Membrane
Hyphae
Biofilm
Cluster 1
Cluster 3
Cluster 6
Cluster 5
Cluster 4
Cluster 8
Cluster 9
Cluster 10
Cluster 2
Cluster 7
C
Biofilm
FCZ-72 + ALL
Response A
Response B
Biofilm
D
FCZ-48
FCZ-72
UT
Efflux
iESR

Figure 5 A. Visual representation (UMAP) of the relationships of just FCZ-72 cells. In total, 10 subpopulations are highlighted via Louvain clustering. **B.** Summary of all signatures across the Louvain clusters identified across all FCZ-72 cells. **C.** Expression of the Biofilm signature onto the UMAP embedding of A (left) and onto the UMAP embedding of all cells (drugs/timepoints) but with FCZ-72 cells highlighted (right). **D.** UMAP based visualization of the relationship between UT, FCZ-48 and FCZ-72 cells labelled by cell of origin (left), expression of the Efflux (middle) and iESR (right) signatures.

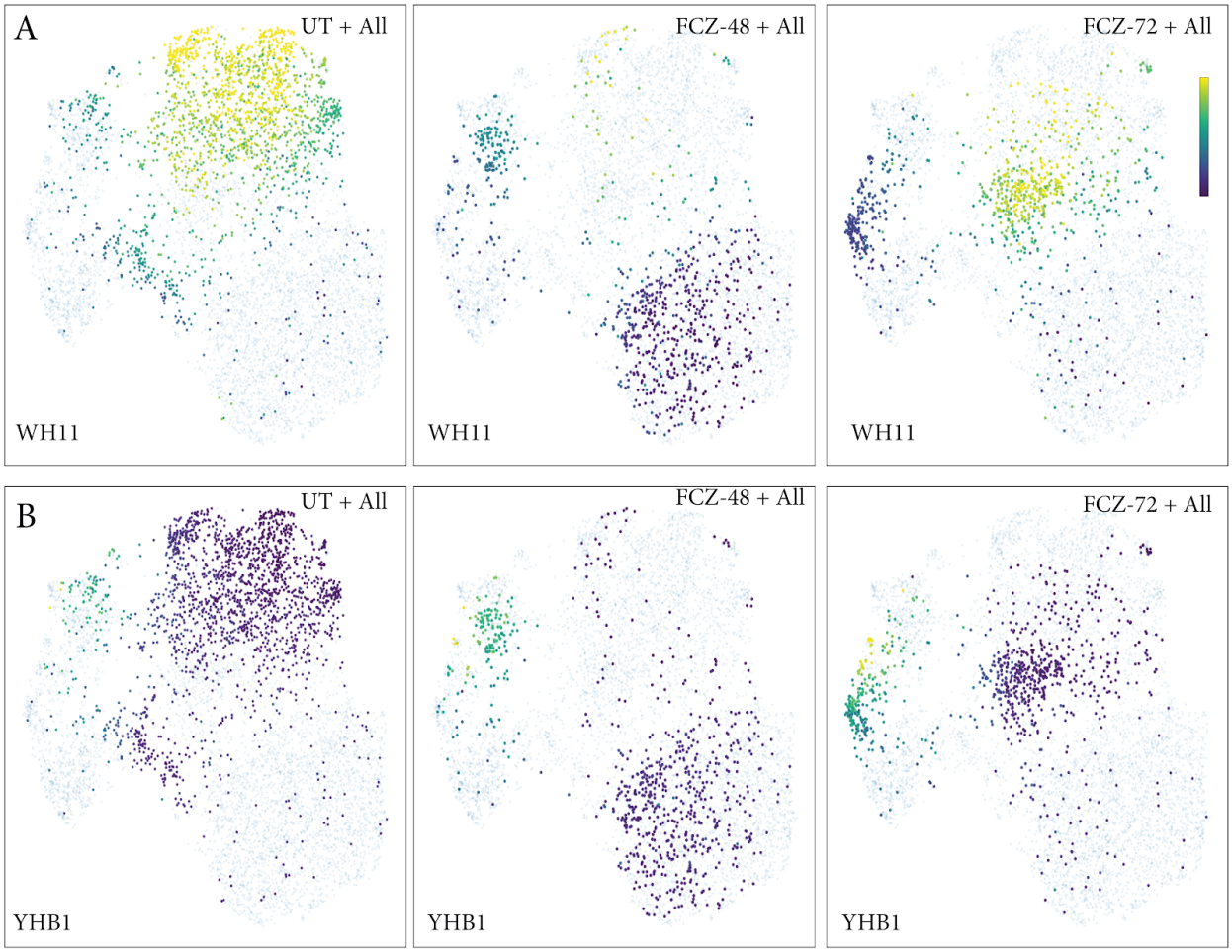

Figure 6 A. Gene expression of *WH11* across all cells (drugs/timepoints) but with UT cells highlighted (left), FCZ-48 cells (middle), and FCZ-72-cells (left) highlighted. **B.** Gene expression of *YHB1* across all cells (drugs/timepoints) but with UT cells highlighted (left), FCZ-48 cells (middle), and FCZ-72-cells (left) highlighted.

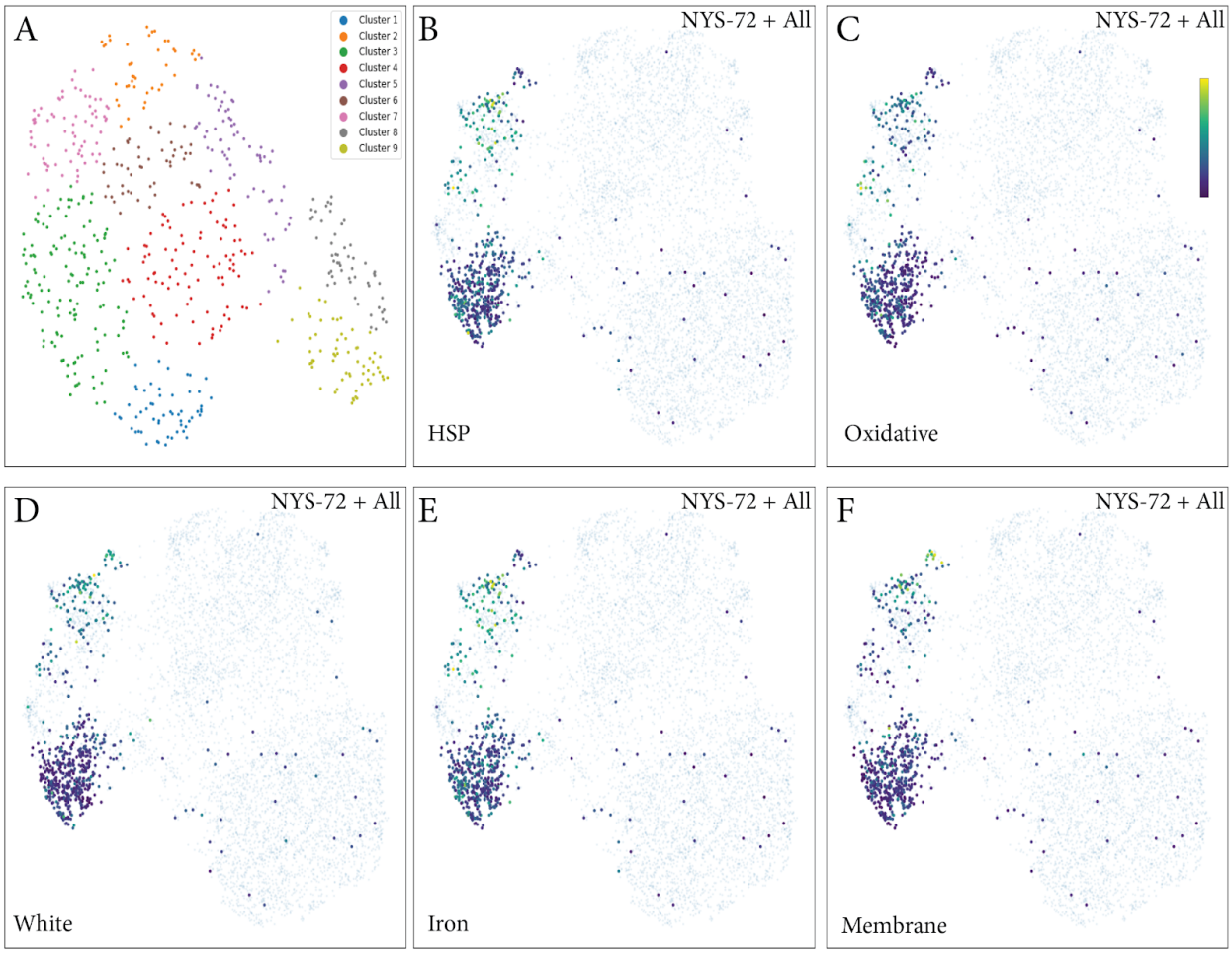

Figure 7 A. Visual representation (UMAP) of the relationships of just NYS-72 cells. In total, 9 subpopulations are highlighted via Louvain clustering. **B-F.** Expression of the Heat Shock Protein, Oxidative, White, Iron and Membrane signatures mapped onto the UMAP embedding of all cells (drugs/timepoints) but with NYS-72 cells highlighted.

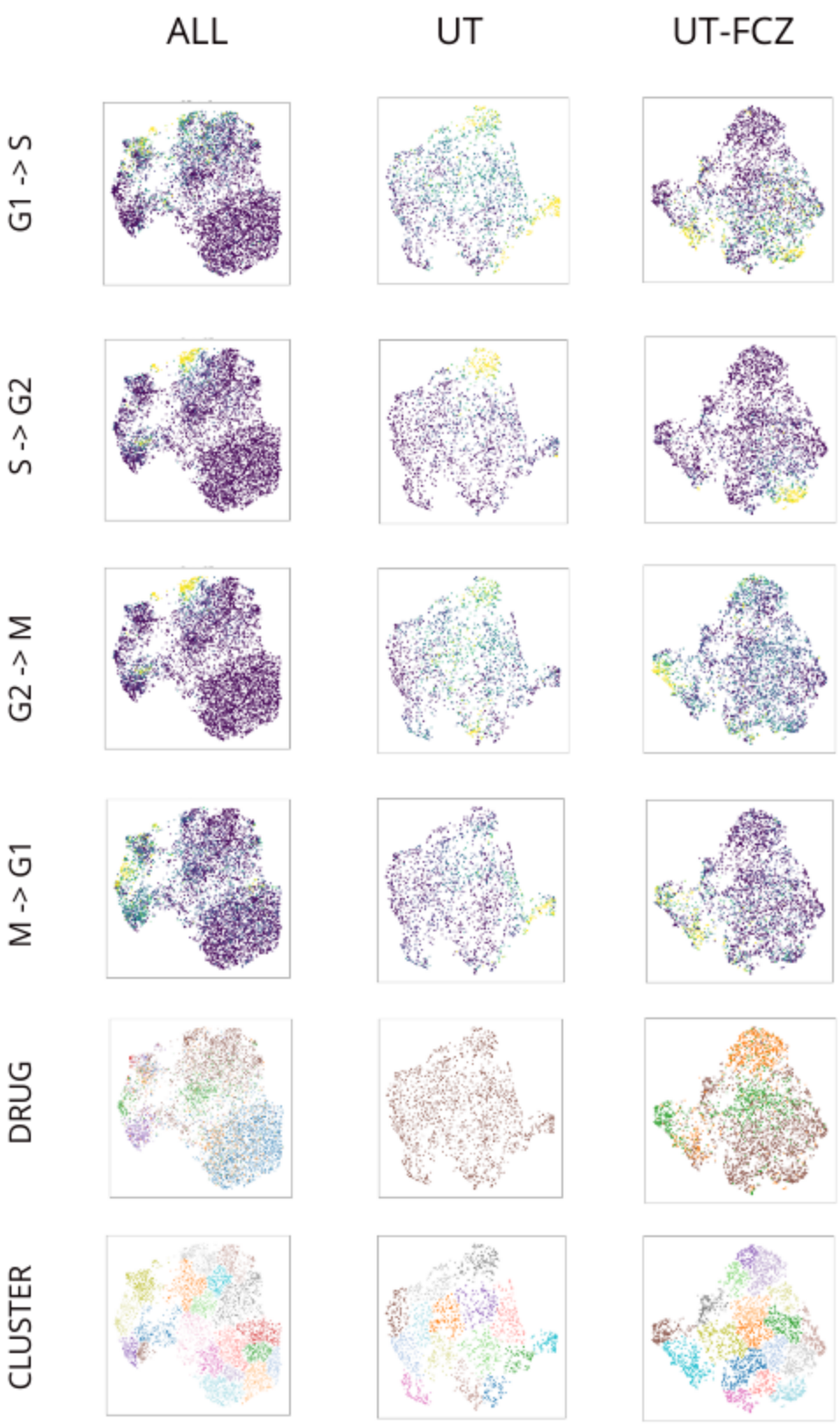
ALL
UT
UT-FCZ
G1 -> S
S -> G2
G2 -> M
M -> G1
DRUG
CLUSTER

Supplemental Figure 1 Patterns of expression of cell cycle signatures mapped onto the UMAP embedding of all cells (left), mapped onto the UMAP of UT cells (middle), and mapped onto the UMAP of UT, FCZ-48 and FCZ-72 cells (left).

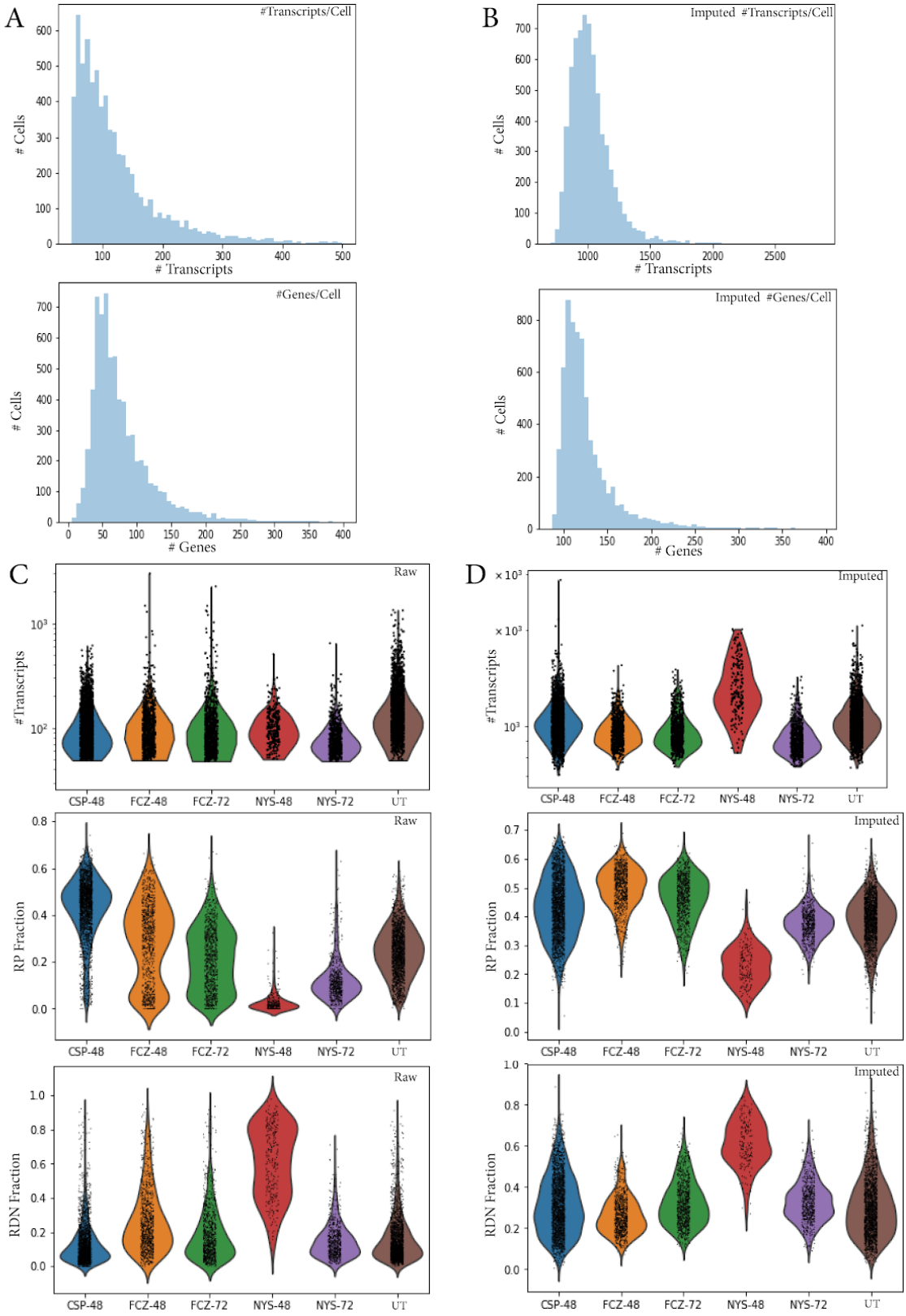
A
#Transcripts/Cell
Cells
Transcripts
#Genes/Cell
Cells
Genes
B
Imputed #Transcripts/Cell
Cells
Transcripts
Imputed #Genes/Cell
Cells
Genes
C
Raw
#Transcripts
RP Fraction
RDN Fraction
CSP-48
FCZ-48
FCZ-72
NYS-48
NYS-72
UT
D
Imputed
#Transcripts
RP Fraction
RDN Fraction
CSP-48
FCZ-48
FCZ-72
NYS-48
NYS-72
UT

Supplemental Figure 2 **A.** Histograms describing the number of cells with observed levels of transcripts (top) and genes (bottom) before normalization and imputation. **B.** Histograms describing the number of cells with observed levels of transcripts (top) and genes (bottom) after normalization and imputation. **C.** Violin plots describing the distribution of transcript number (top), fraction of transcripts of genes with an RP prefix (middle), and fraction of transcripts of genes with an RDN prefix (bottom) before normalization and imputation. **D.** Violin plots describing the distribution of transcript number (top), fraction of transcripts of genes with an RP prefix (middle), and fraction of transcripts of genes with an RDN prefix (bottom) after normalization and imputation.

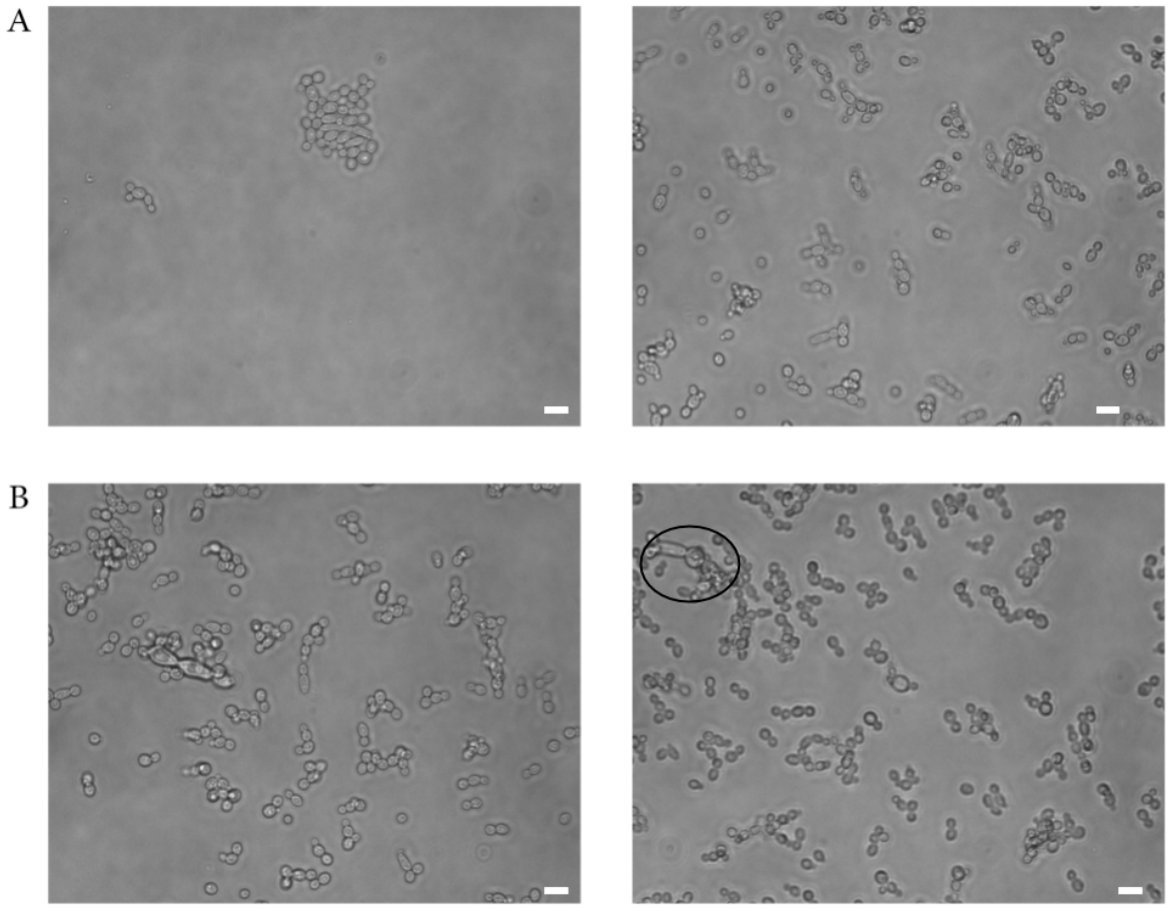

Supplemental Figure 3 **A.** Images taken under the microscope of CSP-48 cells without (left) and with a cell strainer (right). **B.** Images taken under the microscope of FCZ-48 cells without

(left) and with a cell strainer (right). The circle highlights the germ tube and small hyphae cells after applying the strainer. Scale bars represent 20 micron.

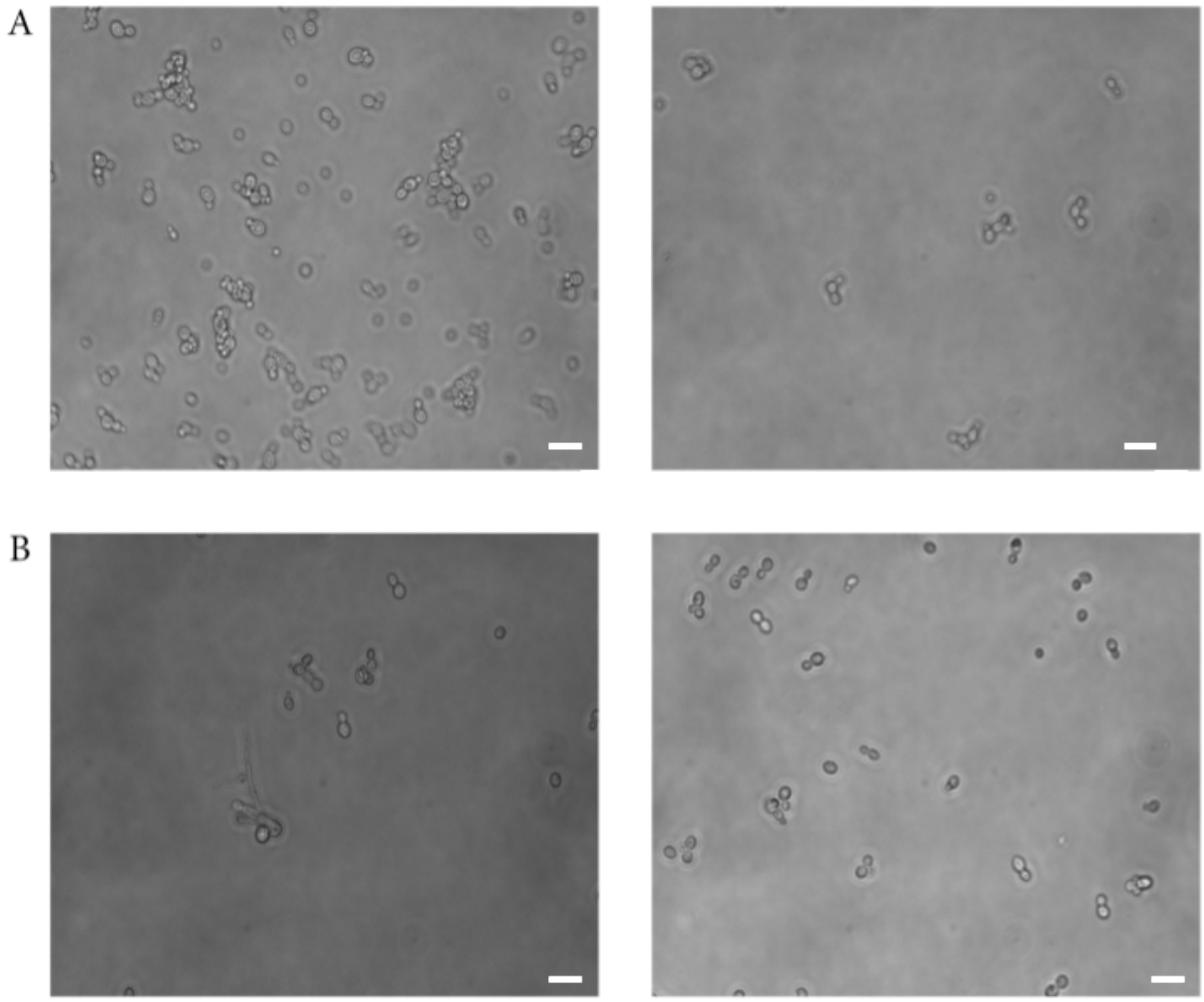

Supplemental Figure 4 **A.** Images taken under the microscope of NYS-48 cells without (left) and with a cell strainer (right). **B.** Images taken under the microscope of FCZ-72 cells without (left) and with a cell strainer (right). Scale bars represent 30 micron.

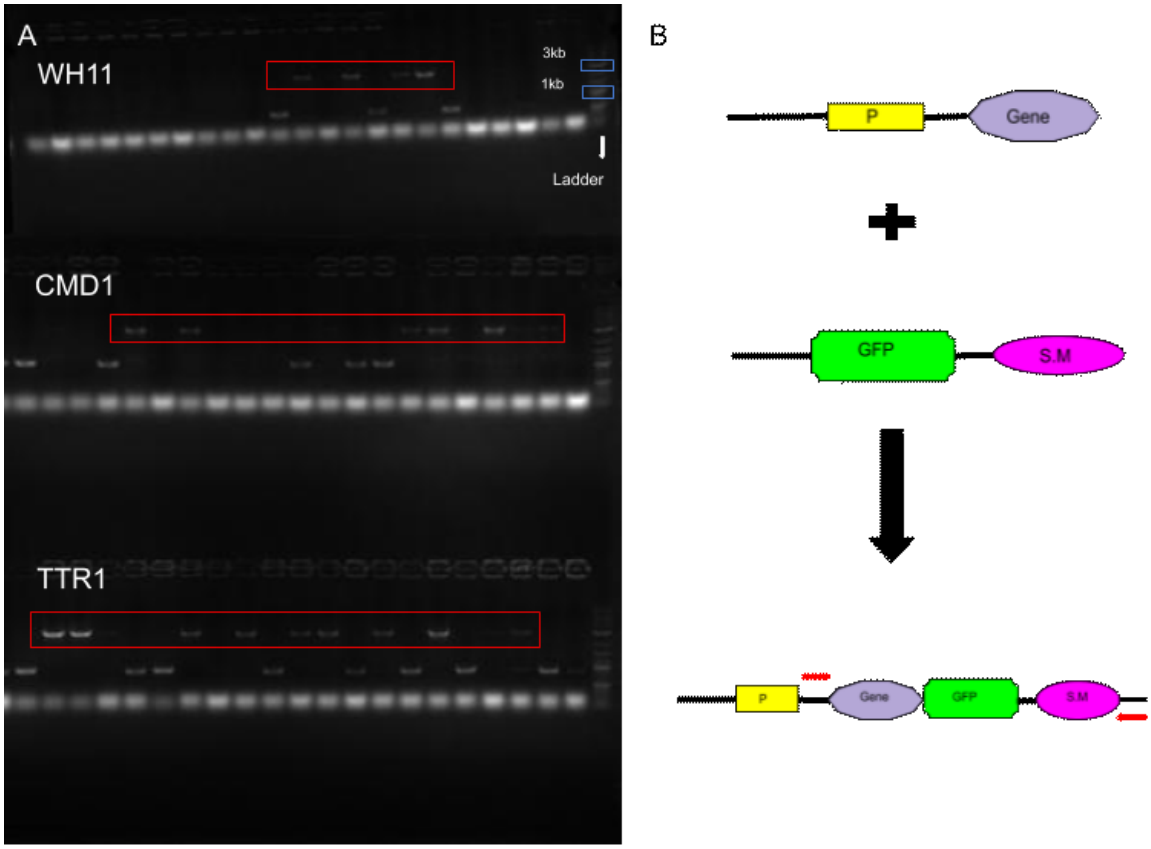

Supplemental Figure 5. **A.** Gel electrophoresis results for genes successfully tagged with *RFP*. The ~3Kb bands (bands in the red boxes) confirm that these genes are successfully tagged with *RFP* in those colonies. The size of *RFP* is almost 2400bp. The lowest row corresponds to primers. Bands in the middle row are genes not tagged with *RFP*. Therefore the bands indicate the actual size of these genes. **B.** Schematic figure showing the green fluorescent protein (GFP) tagging at the 3' position of the target gene to form the fusion protein. GFP is used for genes YHB1, UCF1, and HSP70. The same procedure was used for RFP tagging for WH11, CMD1 and TTR1. P indicates the promoter of the target gene. S.M stands for selective marker (*HIS1* in *GFP* case). Red arrows show the position of designed primers. When successful gene insertion of the PCR products occurs, the designed primers will result in big bands with combined sizes of target gene and fluorescent gene.

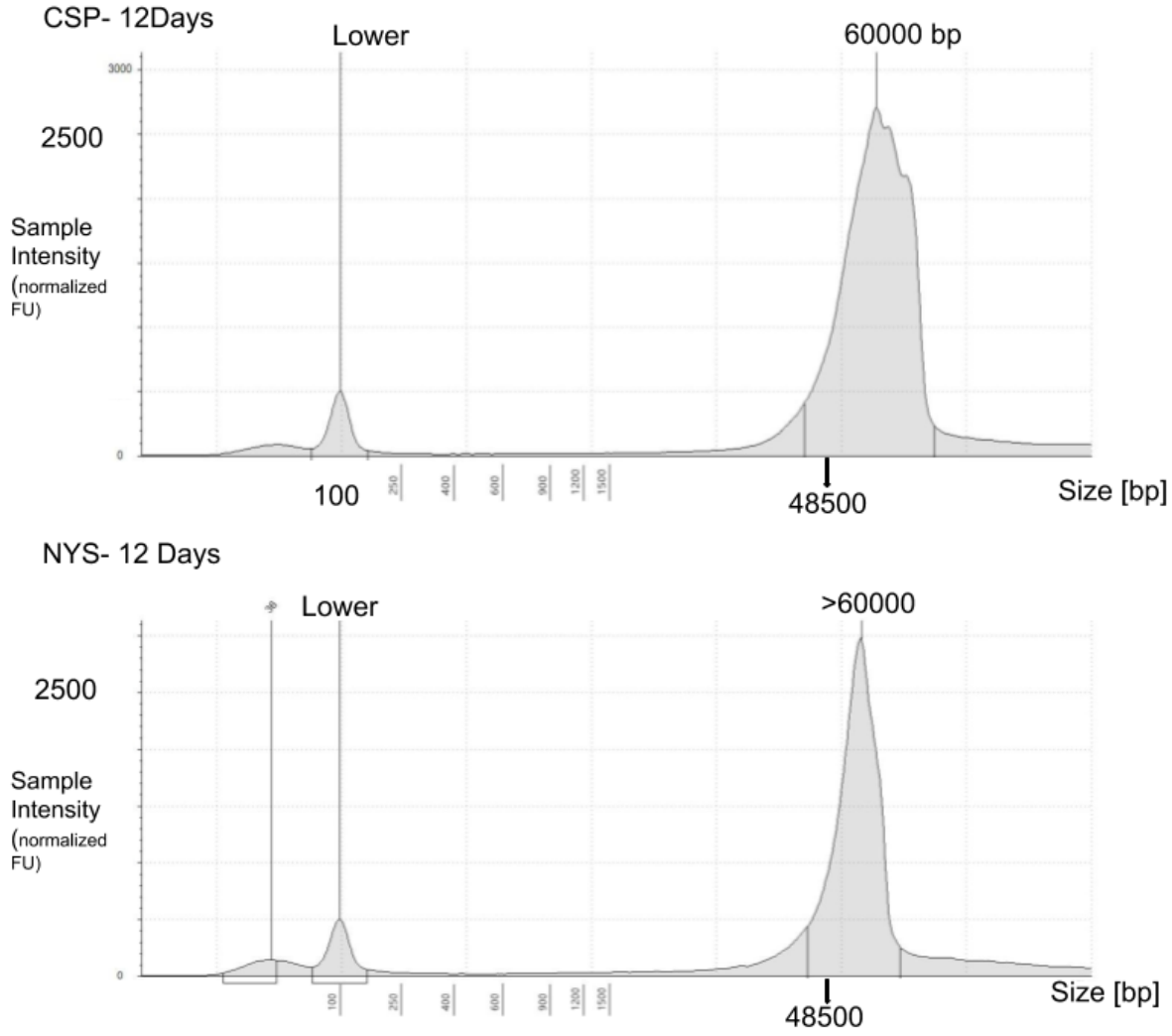

Supplemental figure 6. Concentration versus fragment length for the extracted genomic DNA via the Tapestation (Agilent Inc.). The top and bottom panels correspond to CSP and NYS at 12 days. The average size of purified DNA molecules is 40-50 kb, which is in the ideal range according to the manufacturer's protocol (MasterPure Yeast DNA purification kit, **Methods 12**). Overall concentration is more than sufficient for bulk whole genome DNA-seq via the Illumina NEXT-seq platform.

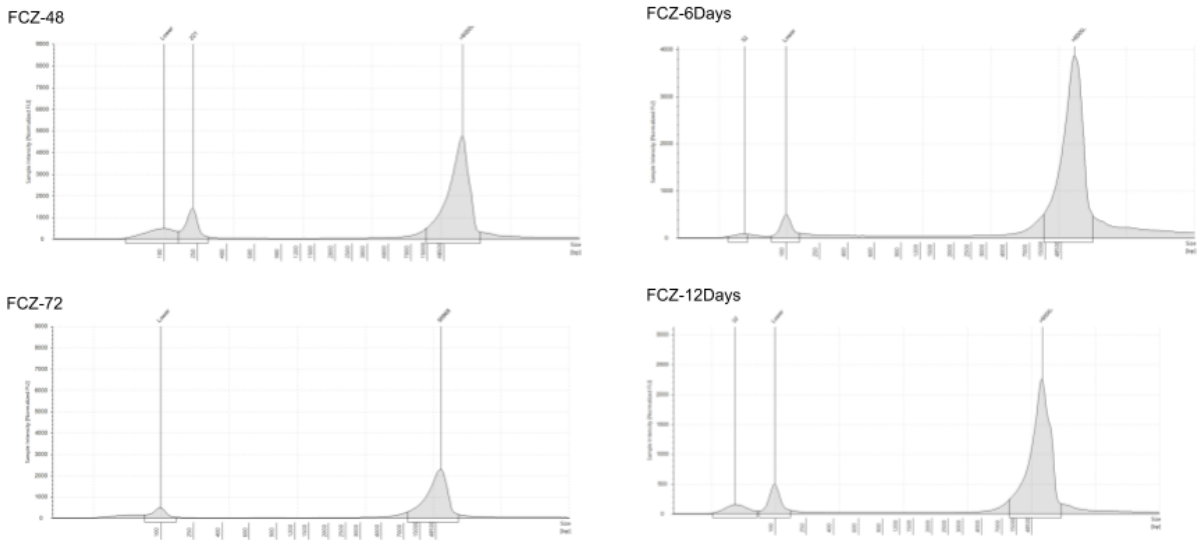

Supplemental Figure 7. Tapestation results for gDNA of FCZ-treated cells. Analogous to **Supplemental Figure 6** but for the remaining bulk whole genome DNA-sequencing.

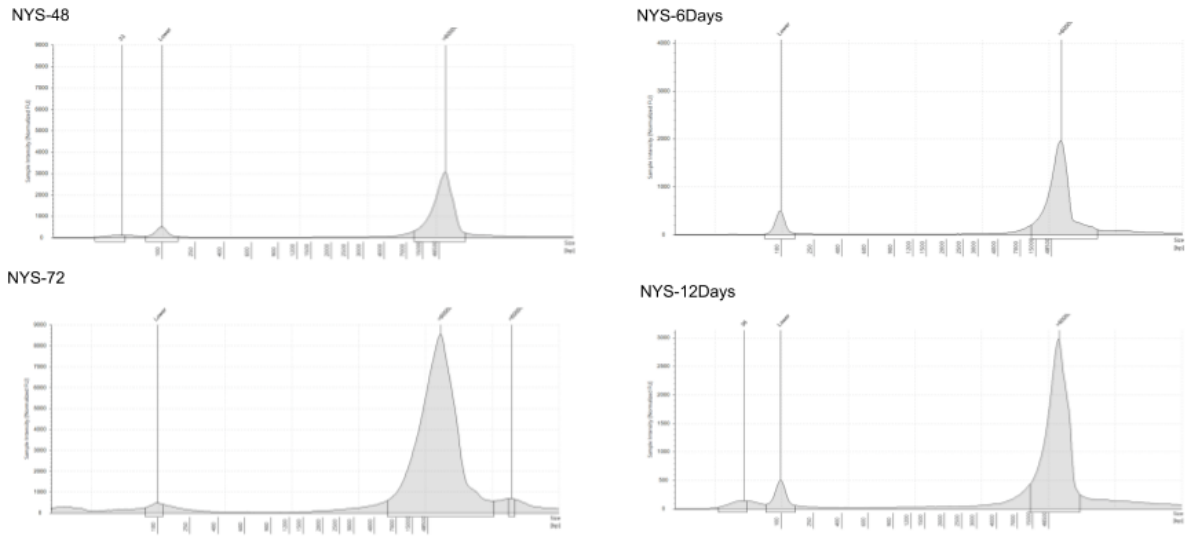

Supplemental Figure 8. Tapestation results for gDNA of NYS-treated cells. Analogous to **Supplemental Figure 6** but for the remaining bulk whole genome DNA-sequencing.

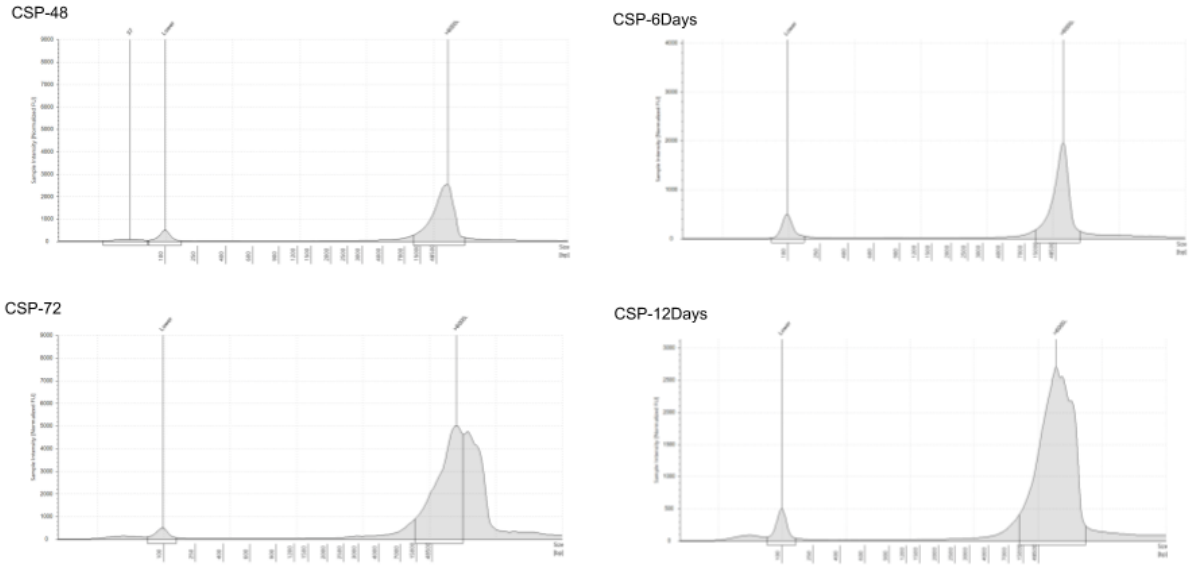

Supplemental figure 9. Tapestation results for gDNA of CSP-treated cells. Analogous to **Supplemental Figure 6** but for the remaining bulk whole genome DNA-sequencing.

Supplemental Figure 10. Our fungal DROP-seq system. The small screen is driven by a Raspberry Pi CPU and controls the pumps: two on the left for oil and cells and one on the right (vertical) for beads. The microfluidic PDMS sits on the small black platform behind the screen.

Supplemental Tables.

	Name	Sequence
1	TTR1-P3 oligo	ATTTAAACAATGTCGAACGTgttttagagctagaaatagcaagttaaa
2	TTR1-P2 oligo	ACGTTCGACATTGTTTAAATcaaattaaaaatagtttacgcaagtc
3	TTR1-RFP-For	GTCAACATATTGGTGGCAATTCCGATGTGCAAGCTTTGAAGTCTAGTGACAA ATTAGATGACAAAATCAAAGCTGCTTTAatggttatggctagaaaagtt
4	TTR1-NAT-Rev	AATTCCATTTCTTGGGGAATGTCCACTTGTTGTGCCAAAACACTGTCTTCTG TGGAATTAGAAACATGCTGAATATACCCcagcagtatagcgaccagcat
5	TTR1-Check-For	TGTTCCGTACATTATTAAC
6	TTR1-Check-Rev	ATATCTCTTTTGGTATTGTTT
7	HSP70-P3 oligo	AAGAAATAGGTAATTTACTGgttttagagctagaaatagcaagttaaa
8	HSP70-P2 oligo	CAGTAAATTACCTATTTCTTcaaattaaaaatagtttacgcaagtc
9	HSP70-GFP-For	CAGGTGGTGCCCCAGGTGCCGGTGGTCCAGGTGGTGCTACTGGTGGTGAATC AAGTGGACCAACTGTTGAAGAAGTTGATggtgctggcgcaggtgcttc
10	HSP70-HIS1-Rev	CCCATAAATAAAAAATTGTTCTAAATATTGTGCTTCTTTCTTTTTTGTTGAT CTTTACTTACTTACTTACAAAAGCAAAGccgcataggccactagtgga
11	HSP70-Check-For	TATGTCTAAAGCTGTTGGTATTGAT
12	HSP70-Check-Rev	TGTTTATCATTGTTTGCAACTTTAT
13	CMD1-P3 oligo	GTTGACATTCGTCTCTTCTGgttttagagctagaaatagcaagttaaa
14	CMD1-P2 oligo	CAGAAGAGACGAATGTCAACaaattaaaaatagtttacgcaagtc
15	CMD1-RFP-For	ATCAAATGATTAAAGAAGCTGATACCAACAATGATGGTGAGATTGATATCCA AGAATTTACTCTGTTATTAGCAGCTAAAatggttatggctagaaaagtt
16	CMD1-NAT-Rev	CCAGTATTGCCAGCTTTACAATGTAGAAAAGGAAAAAGTAGAGTAATGCTAC TAATGACAAATAATCAAATAATTAGTACcagcagtatagcgaccagcat
17	CMD1-Check-For	GTGACAGTTGTTCAAGATGA
18	CMD1-Check-Rev	TGACAGTGAATTGGAGAAAT
19	UCF1-P3 oligo	TATGTTGTTACTGTTGCTGTgttttagagctagaaatagcaagttaaa
20	UCF1-P2 oligo	ACAGCAACAGTAACAACATAcaaattaaaaatagtttacgcaagtc
21	UCF1-GFP-For	GACATTGGAGATTGGAATTGGATGTTTCTTGTACAAATGAATCAGCTATGGT TGATGTTGAATATAAATCCATTCCAATGggtgctggcgcaggtgcttc
22	UCF1-HIS1-Rev	TCATTAATTCGTAAAACGCATCATACATAAATATCATATTAAAATAAAAAAA ATAGAAGGAACAAACATAGCATCATAACcgcataggccactagtgga
23	UCF1-Check-For	TGGCGGGAAAGAAAAAGTCTAAGTC
24	UCF1-Check-Rev	CATCGTCGATAAACCTTAATTTCTCTA
25	WH11-P3 oligo	GTCAAATTTGTAGATTTGTGgttttagagctagaaatagcaagttaaa
26	WH11-P2 oligo	CACAAATCTACAAATTTGACcaaattaaaaatagtttacgcaagtc

27	WH11-RFP-For	GTGCTGCTGGTAAAGCTACTTCTGAAAACGACAAATCATTTGTCCAAAAAGC TTCTGATGCTATTTTTGGTGACTCCAAAatggttatggctagaaaagttgat
28	WH11-NAT-Rev	ATTTTTGTTTTCCTTTGTTTTTTTAATTGATTTACGCGCATCAGTTATTAAG AACGGGAACGAAAGAAGTGAGACGCGACcagcagtatagcgaccagcat
29	WH11-Check-For	TGTCCGACTTAGGTAGAAAAG
30	WH11-Check-Rev	CCAGTTCTATCAGGACGATG
31	YHB1-P3 oligo	CTGACCAACTAAGCAGAAAGgttttagagctagaaatagcaagttaaa
32	YHB1-P2 oligo	CTTTCTGCTTAGTTGGTCAGcaaattaaaaatagtttacgcaagtc
33	YHB1 -GFP-For	AGTTTATGAAAGATATCAAAGAACATTTGGGTAAAAAGAATGTTCCTGTCAA GCTTGAATATTTTGGTCCTTACGATCCTggtgctggcgcaggtgcttc
34	YHB1 -HIS1-Rev	GAGAGTATTGTTTTAATAGTAATTACACAAAACTTTAACATTTTAGATTTAG GATTTACGAAGTCGCGTTTAATATTCCGccgcataggccactagtgga
35	YHB1-Check-For	GTCGAATACGAAACCAAACA
36	YHB1-Check-rev	TATGTAGGGAGGTTTGTGTT

Supplemental Table 1. The nucleic acid sequences of forward (For) and reverse (Rev) primers used for the target genes in the live cell imaging experiments. sgRNAs (capital letters) are fused to P2 and P3 oligos.

Pathways/Stresses/Signatures	Relevant genes
Ras pathway[36]	RAS1, CYR1, TPK2, PDE2
Ergosterol biosynthesis pathway[12,90]	ERG2, ERG13, ERG27, ERG6, ERG1, ERG8, ERG25, ERG10, ERG12, ERG9, ERG11, IDI1, UPC2
Hyphae signatures[91]	RIM101, IHD1, SEC4, SEP7, RSR1, DEF1, CCH1, CDC12, TUP1, TEC1, NRG1, MID1, NRG1.1, DCK1, SEC2, CDC11, CDC42, BRG1, RAC1, MOB2
Calcineurin pathway[92,93]	HSP70, HSP90, CCH1, MID1, UTR2, CNB1
Oxidative stress[94]	TRX1, CAT1, TRR1, SOD2, CAP1, MID1, CCH1
Cell wall biosynthesis[49,95]	CHS2, CHS3, CHS8, RLM1, HOG1, MKC1, PBS2, MKK2
Efflux pumps and transporter proteins[10,11]	CDR1, TAC1, MDR1, MRR1, FLU1, MLT1, YOR1
Pseudohyphal signatures[96]	TUP1, NRG1, FKH2, TCC1, RFG1, SSN6, ACE2,

	RAP1, CLB4, GRR1
Heat shock proteins[97]	HSP12, HSP70, HSP21, HSP60, HSP90, HSP104, HSP78
Biofilm formation[38]	TYE7, ROB1, NDT80, SOH1, GCN4, TEC1, BRG1
Opaque cells signatures[98]	PGA31, SOD1, CCP1, CYC1, SDH2, QCR9, FESUR1, PCK1, OSM2, PEX4, ACO1, MET10, RBT4, CYB5, DAP1, XOG1
Iron starvation stress[56,82]	HSP12, STF2, CCP1, HMX1, PHR2, CAT1, HAP2, HAP5, HAP43, MNN2
Parasexual and meiosis genes[28,92]	SPO11, SKI8, CPH1, CAG1, DLH1, NDT80, HST6
Germ Tubes[98]	HTA2, HHF1, HTA1, HHT21, ARX1, ADE4, HAS1
White[98]	PFY1, RDI1, SOD5, YHB1, PST1, IHD1, DPM1, SPC2, ERV25, ERV46, RAS1, PDI1, CDC12, KEX2, CDC10, USO6, PRE10, CBP1, PHR1
Membrane[99]	RBT5, IHD1, PHR1, PGA7, SAP10
Early Filamentous[100]	SEC61, IHD1, HGT2, ZDS1, DCK1

Supplemental Table 2 Gene sets representing pathways, processes and morphological states in *C.albicans.*

	Genes
Log FC > 2	HSP21, CTR1, GAC1, PGA48, FGR41, YHB1, UCF1, HSP70, TYE7, SOD3, SMC6, NAD, BLP1, HGT6, XYL2, ADH2, FAB1, PGK1, YVC1, IFE2, YCF1, OXR1, GAC1, ITS1, CAS5, APE3, REG1, NDH51, ARP9, HHT21
Log FC < -2	RPL29, RPL24A, RPL43A, RPL37B, RPL30, RPS21B, NHP2, UBI3

Supplemental Table 3 Genes which are showing strong differential expression between cluster 8 versus all the remaining clusters within the population of UT cells.

	Genes
Log FC > 2.5	PGA57, PXA1, PRN3, MRV3, MRV8, RLP24, UBI4, TYE7, INN1, FMP45, TOM70, ELA1, AOX2, LOG3, ERG25, PGA31, SSY1, JIP5
Log FC < -2	GIM5, MET14, RUB1, DUT1, ALT1, X6, RIM1, GIR2, SHE9, DBF4

Supplemental Table 4 Genes which are showing strong differential expression in cluster 1 and cluster 11 of the UMAP embedding of all cells (drugs/timepoints).

	C albicans Name	CGD ID	S. cerevisiae Name	Sacc. GID	SGD ID	UID	Signature Group
C4_04480C_A	EFB1	CAL0000176377	EFB1	YAL003W	S000000003	YAL003W	RiBi
C2_06360C_A	MAK16	CAL0000176460	MAK16	YAL025C	S000000023	YAL025C	RiBi
C1_08090C_A	FUN12	CAL0000190309	FUN12	YAL035W	S000000033	YAL035W	RiBi
C1_08100W_A	DRG1	CAL0000193469	RBG1	YAL036C	S000000034	YAL036C	RiBi
C2_05460W_A	CDC19	CAL0000192883	CDC19	YAL038W	S000000036	YAL038W	RiBi
C4_04100C_A	ECM1	CAL0000196644	ECM1	YAL059W	S000000055	YAL059W	RiBi
C1_04750W_A	IFE1	CAL0000197952	BDH2	YAL061W	S000000057	YAL061W	iESR
CR_04300W_A		CAL0000192993	NCL1	YBL024W	S000000120	YBL024W	RiBi
C3_04510W_A		CAL0000196880	YBL028C	YBL028C	S000000124	YBL028C	RiBi
C1_07490C_A		CAL0000183205	POL12	YBL035C	S000000131	YBL035C	RiBi
C5_04570C_A	URA7	CAL0000193754	URA7	YBL039C	S000000135	YBL039C	RiBi
C4_03430W_A	MOH1	CAL0000187831	MOH1	YBL049W	S000000145	YBL049W	iESR
C7_02810W_A	PRX1	CAL0000196398	PRX1	YBL064C	S000000160	YBL064C	iESR
C4_01820C_A		CAL0000186972	PRS4	YBL068W	S000000164	YBL068W	RiBi
C1_05700W_A	AUT7	CAL0000182486	ATG8	YBL078C	S000000174	YBL078C	iESR
C6_01700W_A	RPL32	CAL0000179592	RPL32	YBL092W	S000000188	YBL092W	RP
C3_03470W_A		CAL0000178220	UGA2	YBR006W	S000000210	YBR006W	iESR
C1_04890W_A	YBN5	CAL0000180814	OLA1	YBR025C	S000000229	YBR025C	RiBi
C3_00200C_A	ETR1	CAL0000200874	ETR1	YBR026C	S000000230	YBR026C	iESR
C1_14160W_A		CAL0000185918	RKM3	YBR030W	S000000234	YBR030W	RiBi
C1_01030W_A	HMT1	CAL0000187520	HMT1	YBR034C	S000000238	YBR034C	RiBi

C4_02760C_A	CGR1	CAL0000196952	YBR053C	YBR053C	S000000257	YBR053C	iESR
C1_14060W_A		CAL0000194637	YBR056W	YBR056W	S000000260	YBR056W	iESR
C3_07400W_A		CAL0000176862	TRM7	YBR061C	S000000265	YBR061C	RiBi
C1_12770W_A	RPG1A	CAL0000181001	RPG1	YBR079C	S000000283	YBR079C	RiBi
C3_04500C_A	RPL19A	CAL0000180894	RPL19A	YBR084C-A	S000002156	YBR084C-A	RP
CR_07010W_A	MIS11	CAL0000181460	MIS1	YBR084W	S000000288	YBR084W	RiBi
CR_09320C_A	PHO88	CAL0000189279	PHO88	YBR106W	S000000310	YBR106W	RiBi
C1_08380W_A	TEF2	CAL0000196876	TEF2	YBR118W	S000000322	YBR118W	RiBi
C1_05290W_A	GRS1	CAL0000176302	GRS1	YBR121C	S000000325	YBR121C	RiBi
CR_05720W_A	TPS1	CAL0000182821	TPS1	YBR126C	S000000330	YBR126C	iESR
C1_05770C_A	PRC3	CAL0000190176	YBR139W	YBR139W	S000000343	YBR139W	iESR
C2_05090W_A	MAK5	CAL0000200900	MAK5	YBR142W	S000000346	YBR142W	RiBi
C2_05100C_A	ERF1	CAL0000184893	SUP45	YBR143C	S000000347	YBR143C	RiBi
C2_08130W_A	ARA1	CAL0000195767	ARA1	YBR149W	S000000353	YBR149W	iESR
C1_12820C_A		CAL0000198535	RPB5	YBR154C	S000000358	YBR154C	RiBi
C1_00560W_A	CNS1	CAL0000195791	CNS1	YBR155W	S000000359	YBR155W	RiBi
C2_03820C_A	RPS9B	CAL0000197665	RPS9B	YBR189W	S000000393	YBR189W	RP
C2_03810C_A	RPL21A	CAL0000194631	RPL21A	YBR191W	S000000395	YBR191W	RP
C1_04640W_A		CAL0000179190	LDH1	YBR204C	S000000408	YBR204C	iESR
C3_06700C_A		CAL0000189293	YBR238C	YBR238C	S000000442	YBR238C	RiBi
C2_07920W_A		CAL0000182585	RRT2	YBR246W	S000000450	YBR246W	RiBi
C7_03700C_A	ENP1	CAL0000201090	ENP1	YBR247C	S000000451	YBR247C	RiBi
C1_05110C_A	ARO4	CAL0000182853	ARO4	YBR249C	S000000453	YBR249C	RiBi
C1_01330C_A	DUT1	CAL0000195525	DUT1	YBR252W	S000000456	YBR252W	RiBi
C1_05060W_A	REI1	CAL0000177865	REI1	YBR267W	S000000471	YBR267W	RiBi
C2_02620W_A		CAL0000192813	SDH8	YBR269C	S000000473	YBR269C	iESR
C1_05530C_A	SSH1	CAL0000193960	SSH1	YBR283C	S000000487	YBR283C	RiBi
CR_07480W_A		CAL0000180922	YBR287W	YBR287W	S000000491	YBR287W	iESR
C2_02710C_A		CAL0000178916	RRP7	YCL031C	S000000536	YCL031C	RiBi
CR_07150W_A	GLK1	CAL0000189805	GLK1	YCL040W	S000000545	YCL040W	iESR
C5_01410C_A		CAL0000201797	EMC1	YCL045C	S000000550	YCL045C	RiBi
C6_04160C_A	SPB1	CAL0000201177	SPB1	YCL054W	S000000559	YCL054W	RiBi
C1_11420W_A	KRR1	CAL0000200947	KRR1	YCL059C	S000000564	YCL059C	RiBi
CR_05380C_A	YCP4	CAL0000193139	YCP4	YCR004C	S000000597	YCR004C	iESR
C3_07600W_A		CAL0000193391	YCR016W	YCR016W	S000000609	YCR016W	RiBi
C1_12790C_A	FEN1	CAL0000190970	ELO2	YCR034W	S000000630	YCR034W	RiBi
C1_06540C_A		CAL0000184319	RRP43	YCR035C	S000000631	YCR035C	RiBi
C5_02270W_A	THR4	CAL0000193606	THR4	YCR053W	S000000649	YCR053W	RiBi
CR_00800C_A	PWP2	CAL0000174443	PWP2	YCR057C	S000000653	YCR057C	RiBi
C1_10360C_A		CAL0000189087	YCR061W	YCR061W	S000000657	YCR061W	iESR
C4_05010W_A		CAL0000180486	RSA4	YCR072C	S000000668	YCR072C	RiBi

C2_10240W_A	GPD1	CAL0000200026	GPD1	YDL022W	S000002180	YDL022W	iESR
C3_05160C_A		CAL0000186628	DBP10	YDL031W	S000002189	YDL031W	RiBi
C1_07500C_A	LHP1	CAL0000195360	LHP1	YDL051W	S000002209	YDL051W	RiBi
CR_08490W_A	TSR1	CAL0000183541	TSR1	YDL060W	S000002218	YDL060W	RiBi
CR_08500W_A		CAL0000176600	SYO1	YDL063C	S000002221	YDL063C	RiBi
C1_03010W_A	RPP1A	CAL0000178222	RPP1A	YDL081C	S000002239	YDL081C	RP
C1_03020C_A	RPL13	CAL0000201310	RPL13A	YDL082W	S000002240	YDL082W	RP
C4_00220C_A	SUB2	CAL0000200240	SUB2	YDL084W	S000002242	YDL084W	RiBi
C4_03770W_A		CAL0000188816	TMA17	YDL110C	S000002268	YDL110C	iESR
C4_03840C_A	RRP42	CAL0000183621	RRP42	YDL111C	S000002269	YDL111C	RiBi
C7_03350C_A		CAL0000193623	YDL124W	YDL124W	S000002282	YDL124W	iESR
C7_03920C_A	RPP1B	CAL0000195487	RPP1B	YDL130W	S000002288	YDL130W	SGD-annotated RP
C4_02780W_A		CAL0000192278	CCT4	YDL143W	S000002302	YDL143W	RiBi
C4_02800W_A	RPC53	CAL0000175841	RPC53	YDL150W	S000002309	YDL150W	RiBi
C4_02790C_A	SAS10	CAL0000185070	SAS10	YDL153C	S000002312	YDL153C	RiBi
C1_08000W_A	NRP1	CAL0000187528	NRP1	YDL167C	S000002326	YDL167C	RiBi
C3_04960W_A	RPL35	CAL0000191177	RPL35A	YDL191W	S000002350	YDL191W	RP
CR_03850W_A	HGT3	CAL0000177617	YDL199C	YDL199C	S000002358	YDL199C	iESR
C4_04810C_A		CAL0000183898	TRM8	YDL201W	S000002360	YDL201W	RiBi
C7_02240W_A	FMP45	CAL0000192127	FMP45	YDL222C	S000002381	YDL222C	iESR
CR_00560W_A	NTH1	CAL0000200632	NTH1	YDR001C	S000002408	YDR001C	iESR
C1_14110C_A	RPL4B	CAL0000176632	RPL4B	YDR012W	S000002419	YDR012W	RP
C3_02780W_A	SES1	CAL0000183348	SES1	YDR023W	S000002430	YDR023W	RiBi
C5_01540W_A		CAL0000187802	RPS11A	YDR025W	S000002432	YDR025W	RP
CR_05390W_A	PST3	CAL0000180388	PST2	YDR032C	S000002439	YDR032C	iESR
C3_07410C_A	KRS1	CAL0000185145	KRS1	YDR037W	S000002444	YDR037W	RiBi
C6_00650C_A	RPS13	CAL0000187390	RPS13	YDR064W	S000002471	YDR064W	RP
C1_03380W_A	TPS2	CAL0000193855	TPS2	YDR074W	S000002481	YDR074W	iESR
C2_08480W_A	RRP8	CAL0000191512	RRP8	YDR083W	S000002490	YDR083W	RiBi
C3_06760W_A		CAL0000174798	RRP1	YDR087C	S000002494	YDR087C	RiBi
C1_03350C_A	RLI1	CAL0000178640	RLI1	YDR091C	S000002498	YDR091C	RiBi
C1_13170C_A	MSH6	CAL0000192796	MSH6	YDR097C	S000002504	YDR097C	RiBi
C1_03230C_A	ARX1	CAL0000194302	ARX1	YDR101C	S000002508	YDR101C	RiBi
CR_00900W_A	TRM1	CAL0000179806	TRM1	YDR120C	S000002527	YDR120C	RiBi
C7_01420W_A	GIR2	CAL0000185013	GIR2	YDR152W	S000002559	YDR152W	RiBi
C1_13370W_A		CAL0000179941	YDR161W	YDR161W	S000002568	YDR161W	RiBi
C7_02340C_A		CAL0000187643	TRM82	YDR165W	S000002572	YDR165W	RiBi
C2_09010W_A	STB3	CAL0000192161	STB3	YDR169C	S000002576	YDR169C	iESR
C2_09720W_A	SUP35	CAL0000176993	SUP35	YDR172W	S000002579	YDR172W	RiBi
C4_07150W_A		CAL0000196526	ATC1	YDR184C	S000002592	YDR184C	RiBi

C4_06800W_A		CAL0000181596	RVB1	YDR190C	S000002598	YDR190C	RiBi
C1_03160C_A	COQ4	CAL0000193093	COQ4	YDR204W	S000002612	YDR204W	iESR
C1_08600C_A	GCD6	CAL0000183518	GCD6	YDR211W	S000002619	YDR211W	RiBi
C4_04800W_A		CAL0000195123	RTN1	YDR233C	S000002641	YDR233C	RiBi
C1_04570C_A	CHL4	CAL0000188322	CHL4	YDR254W	S000002662	YDR254W	iESR
C1_04560W_A		CAL0000175041	RMD5	YDR255C	S000002663	YDR255C	iESR
C2_03390C_A	HSP78	CAL0000189244	HSP78	YDR258C	S000002666	YDR258C	iESR
C2_09260C_A	GLO2	CAL0000189186	GLO2	YDR272W	S000002680	YDR272W	iESR
C2_09160W_A		CAL0000176918	RRP45	YDR280W	S000002688	YDR280W	RiBi
C3_03200C_A		CAL0000193978	YDR286C	YDR286C	S000002694	YDR286C	iESR
CR_10580W_A	PRO1	CAL0000178490	PRO1	YDR300C	S000002708	YDR300C	RiBi
CR_10170C_A		CAL0000197030	ASP1	YDR321W	S000002729	YDR321W	RiBi
C3_02130W_A	UTP4	CAL0000184134	UTP4	YDR324C	S000002732	YDR324C	RiBi
C5_03920C_A		CAL0000182246	FCF1	YDR339C	S000002747	YDR339C	RiBi
C1_01530C_A		CAL0000176283	YDR341C	YDR341C	S000002749	YDR341C	RiBi
C1_00400W_A	SVF1	CAL0000182395	SVF1	YDR346C	S000002754	YDR346C	RiBi
C1_12760W_A		CAL0000174555	BCP1	YDR361C	S000002769	YDR361C	RiBi
C1_10970W_A		CAL0000194444	ESF1	YDR365C	S000002773	YDR365C	RiBi
CR_06860C_A	ARO10	CAL0000184409	ARO10	YDR380W	S000002788	YDR380W	iESR
C3_04680W_A	RPP2B	CAL0000199315	RPP2B	YDR382W	S000002790	YDR382W	RP
CR_10240W_A	UTP5	CAL0000191285	UTP5	YDR398W	S000002806	YDR398W	RiBi
C1_07950C_A		CAL0000175073	RRP17	YDR412W	S000002820	YDR412W	RiBi
C1_14260C_A	TIF35	CAL0000193017	TIF35	YDR429C	S000002837	YDR429C	RiBi
C3_06300W_A	DOT1	CAL0000184097	DOT1	YDR440W	S000002848	YDR440W	RiBi
C1_10870W_A	RPS17B	CAL0000195565	RPS17B	YDR447C	S000002855	YDR447C	RP
C1_10880W_A		CAL0000174108	UTP6	YDR449C	S000002857	YDR449C	RiBi
C5_03790W_A	GUK1	CAL0000178615	GUK1	YDR454C	S000002862	YDR454C	RP
C5_00680W_A	RMT2	CAL0000180017	RMT2	YDR465C	S000002873	YDR465C	RiBi
C2_05160C_A		CAL0000178700	PUF6	YDR496C	S000002904	YDR496C	RiBi
C1_11360W_A	RPL37B	CAL0000198698	RPL37B	YDR500C	S000002908	YDR500C	RP
C2_05020W_A		CAL0000192157	EMI1	YDR512C	S000002920	YDR512C	iESR
C1_00490C_A	TTR1	CAL0000190988	GRX2	YDR513W	S000002921	YDR513W	iESR
C3_02610C_A	GLX3	CAL0000194072	HSP31	YDR533C	S000002941	YDR533C	iESR
C6_03340C_A	GLC3	CAL0000188820	GLC3	YEL011W	S000000737	YEL011W	iESR
C1_01830C_A	UBC8	CAL0000197909	UBC8	YEL012W	S000000738	YEL012W	iESR
C3_04380C_A		CAL0000183109	SNU13	YEL026W	S000000752	YEL026W	RP
C3_01730C_A	UTR2	CAL0000175165	UTR2	YEL040W	S000000766	YEL040W	RiBi
C3_06120C_A	GDA1	CAL0000196532	GDA1	YEL042W	S000000768	YEL042W	RiBi
C3_02110W_A	RPL12	CAL0000181929	RPL12A	YEL054C	S000000780	YEL054C	RP
C7_03860W_A		CAL0000175297	PRB1	YEL060C	S000000786	YEL060C	iESR
C4_06210C_A		CAL0000184634	NUG1	YER006W	S000000808	YER006W	RiBi

C1_10100C_A	NTF2	CAL0000201779	NTF2	YER009W	S000000811	YER009W	RiBi
C5_02170C_A	GCD11	CAL0000197613	GCD11	YER025W	S000000827	YER025W	RP
C2_08000C_A	KRE30	CAL0000185948	ARB1	YER036C	S000000838	YER036C	RiBi
C5_04270C_A	SAH1	CAL0000201641	SAH1	YER043C	S000000845	YER043C	RiBi
C4_05460C_A	OFD1	CAL0000194379	TPA1	YER049W	S000000851	YER049W	RiBi
C2_09590C_A		CAL0000177748	PIC2	YER053C	S000000855	YER053C	iESR
C2_03160C_A	RNR1	CAL0000199428	RNR1	YER070W	S000000872	YER070W	RiBi
C1_09710C_A		CAL0000181309	UTP7	YER082C	S000000884	YER082C	RiBi
C2_05610C_A	RPS8A	CAL0000186765	RPS8B	YER102W	S000000904	YER102W	RP
C1_13480W_A	HSP70	CAL0000184706	SSA4	YER103W	S000000905	YER103W	iESR
C1_05630C_A		CAL0000182139	KAP123	YER110C	S000000912	YER110C	RiBi
C6_02070C_A	RPL23A	CAL0000187999	RPL23B	YER117W	S000000919	YER117W	RP
C1_09140C_A	SSU81	CAL0000185371	SHO1	YER118C	S000000920	YER118C	RiBi
C6_04110W_A		CAL0000175251	AVT6	YER119C	S000000921	YER119C	iESR
C3_06380W_A	NSA2	CAL0000197650	NSA2	YER126C	S000000928	YER126C	RiBi
C3_06370C_A		CAL0000175453	LCP5	YER127W	S000000929	YER127W	RiBi
C6_00720C_A	COX15	CAL0000185068	COX15	YER141W	S000000943	YER141W	iESR
C2_08420W_A		CAL0000200044	MAG1	YER142C	S000000944	YER142C	iESR
C1_03370W_A		CAL0000195952	PAB1	YER165W	S000000967	YER165W	RiBi
C5_01600C_A	SPB4	CAL0000185825	SPB4	YFL002C	S000001894	YFL002C	RiBi
C5_02110W_A		CAL0000180850	HSP12	YFL014W	S000001880	YFL014W	iESR
C1_02710W_A	FRS2	CAL0000201701	FRS2	YFL022C	S000001872	YFL022C	RiBi
C5_02010C_A		CAL0000185005	BUD27	YFL023W	S000001871	YFL023W	RiBi
C4_04390W_A		CAL0000196794	RPL22B	YFL034C-A	S000006436	YFL034C-A	SGD-annotated RP
C1_02440C_A		CAL0000186385	OTU1	YFL044C	S000001850	YFL044C	iESR
C1_02480W_A	PMM1	CAL0000183926	SEC53	YFL045C	S000001849	YFL045C	RiBi
C3_02040C_A		CAL0000180322	LOC1	YFR001W	S000001897	YFR001W	RiBi
C1_11060C_A	RPL2	CAL0000174265	RPL2A	YFR031C-A	S000002104	YFR031C-A	RP
C1_11040W_A	RPL29	CAL0000175799	RPL29	YFR032C-A	S000006437	YFR032C-A	SGD-annotated RP
C6_04580W_A	HXK1	CAL0000186127	HXK1	YFR053C	S000001949	YFR053C	iESR
C3_01250W_A	PMC1	CAL0000196416	PMC1	YGL006W	S000002974	YGL006W	iESR
C3_00720W_A	PMA1	CAL0000187161	PMA1	YGL008C	S000002976	YGL008C	RiBi
C2_01660C_A		CAL0000177781	MPO1	YGL010W	S000002978	YGL010W	iESR
C1_11000C_A		CAL0000173953	CGR1	YGL029W	S000002997	YGL029W	RiBi
C4_04900W_A	RPL30	CAL0000189848	RPL30	YGL030W	S000002998	YGL030W	RP
C4_04890C_A	RPL24A	CAL0000190222	RPL24A	YGL031C	S000002999	YGL031C	RP
C7_03520W_A	PNC1	CAL0000183035	PNC1	YGL037C	S000003005	YGL037C	iESR
C2_07200W_A		CAL0000191376	RPB9	YGL070C	S000003038	YGL070C	RiBi
C1_05720W_A		CAL0000182421	RPL7A	YGL076C	S000003044	YGL076C	RP

C1_10030W_A	DBP3	CAL0000185988	DBP3	YGL078C	S000003046	YGL078C	RiBi
C1_12650C_A		CAL0000191589	MMS2	YGL087C	S000003055	YGL087C	iESR
C7_02040C_A	CUP9	CAL0000195705	TOS8	YGL096W	S000003064	YGL096W	iESR
C7_02780W_A		CAL0000200421	SRM1	YGL097W	S000003065	YGL097W	RiBi
C6_02230W_A		CAL0000183488	LSG1	YGL099W	S000003067	YGL099W	RiBi
CR_03030C_A	RPL28	CAL0000198266	RPL28	YGL103W	S000003071	YGL103W	RP
C2_07960C_A	NSA1	CAL0000184567	NSA1	YGL111W	S000003079	YGL111W	RiBi
C3_01560W_A		CAL0000191988	PRP43	YGL120C	S000003088	YGL120C	RiBi
C1_01480C_A	RPS21	CAL0000191073	RPS2	YGL123W	S000003091	YGL123W	RP
CR_07710W_A	ARO2	CAL0000185781	ARO2	YGL148W	S000003116	YGL148W	RiBi
C4_02360W_A	AMS1	CAL0000179816	AMS1	YGL156W	S000003124	YGL156W	iESR
C7_00330C_A		CAL0000197105	SUA5	YGL169W	S000003137	YGL169W	RiBi
C1_12600C_A	CHR1	CAL0000178978	ROK1	YGL171W	S000003139	YGL171W	RiBi
C4_04450C_A	ATG1	CAL0000188572	ATG1	YGL180W	S000003148	YGL180W	iESR
C2_01610C_A	RPS26A	CAL0000180001	RPS26A	YGL189C	S000003157	YGL189C	RP
C6_03890C_A	SKI8	CAL0000201104	SKI8	YGL213C	S000003181	YGL213C	RiBi
C1_07700C_A	VRG4	CAL0000182900	VRG4	YGL225W	S000003193	YGL225W	RiBi
C5_02290W_A	PDE1	CAL0000177603	PDE1	YGL248W	S000003217	YGL248W	iESR
C2_04190C_A	UGA1	CAL0000181031	UGA1	YGR019W	S000003251	YGR019W	iESR
C1_02330C_A		CAL0000201086	RPL26B	YGR034W	S000003266	YGR034W	RP
C1_02430C_A		CAL0000199029	YGR054W	YGR054W	S000003286	YGR054W	RiBi
C3_05120C_A		CAL0000183866	PAC10	YGR078C	S000003310	YGR078C	RiBi
C2_06850W_A		CAL0000183209	SLX9	YGR081C	S000003313	YGR081C	RiBi
C3_07250W_A	GCD2	CAL0000182407	GCD2	YGR083C	S000003315	YGR083C	RiBi
C2_06810C_A	RPL11	CAL0000192242	RPL11B	YGR085C	S000003317	YGR085C	RP
C2_06640C_A	VAS1	CAL0000181624	VAS1	YGR094W	S000003326	YGR094W	RiBi
C2_09320C_A	PES1	CAL0000200824	NOP7	YGR103W	S000003335	YGR103W	RiBi
C3_01710C_A	PPT1	CAL0000195801	PPT1	YGR123C	S000003355	YGR123C	RiBi
C2_09060C_A	ASN1	CAL0000188342	ASN2	YGR124W	S000003356	YGR124W	RiBi
CR_03260W_A		CAL0000196868	YGR127W	YGR127W	S000003359	YGR127W	iESR
C3_00330W_A	UTP8	CAL0000200844	UTP8	YGR128C	S000003360	YGR128C	RiBi
C7_03540C_A	ENP2	CAL0000177364	ENP2	YGR145W	S000003377	YGR145W	RiBi
C1_10460W_A		CAL0000184780	YGR149W	YGR149W	S000003381	YGR149W	iESR
CR_02140W_A	RSR1	CAL0000199219	RSR1	YGR152C	S000003384	YGR152C	RiBi
CR_02550C_A		CAL0000191642	MTR3	YGR158C	S000003390	YGR158C	RiBi
CR_00290W_A		CAL0000200149	RTS3	YGR161C	S000003393	YGR161C	iESR
C2_08760C_A	TIF4631	CAL0000188458	TIF4631	YGR162W	S000003394	YGR162W	RiBi
C5_04900C_A		CAL0000184764	RBG2	YGR173W	S000003405	YGR173W	RiBi
C4_02980W_A	TYS1	CAL0000188062	TYS1	YGR185C	S000003417	YGR185C	RiBi
C4_02050W_A	HGH1	CAL0000178023	HGH1	YGR187C	S000003419	YGR187C	RiBi
C4_05300W_A	XKS1	CAL0000191735	XKS1	YGR194C	S000003426	YGR194C	iESR

C4_02090C_A		CAL0000180234	SKI6	YGR195W	S000003427	YGR195W	RiBi
C4_02850W_A		CAL0000181143	ELP2	YGR200C	S000003432	YGR200C	RiBi
C3_05370C_A	YST1	CAL0000191976	RPS0A	YGR214W	S000003446	YGR214W	RP
C1_07870C_A	SMI1	CAL0000199204	SMI1	YGR229C	S000003461	YGR229C	RiBi
C5_04960W_A		CAL0000181504	YGR237C	YGR237C	S000003469	YGR237C	iESR
CR_05660W_A	SDA1	CAL0000201072	SDA1	YGR245C	S000003477	YGR245C	RiBi
C5_04840C_A		CAL0000189299	NOP19	YGR251W	S000003483	YGR251W	RiBi
C5_04700C_A	MES1	CAL0000178172	MES1	YGR264C	S000003496	YGR264C	RiBi
C4_04520W_A		CAL0000197682	PXR1	YGR280C	S000003512	YGR280C	RiBi
C4_02870C_A	ZUO1	CAL0000192667	ZUO1	YGR285C	S000003517	YGR285C	RiBi
C1_13050W_A	RPL14	CAL0000179395	RPL14B	YHL001W	S000000993	YHL001W	RP
C2_02510W_A	PRS1	CAL0000176742	PRS3	YHL011C	S000001003	YHL011C	RiBi
C5_01110W_A		CAL0000189600	OTU2	YHL013C	S000001005	YHL013C	RiBi
CR_08150W_A	RPS20	CAL0000185871	RPS20	YHL015W	S000001007	YHL015W	SGD-annotated RP
C7_04310C_A		CAL0000176874	AIM17	YHL021C	S000001013	YHL021C	iESR
C1_12390C_A	RPL27A	CAL0000176884	RPL27A	YHR010W	S000001052	YHR010W	RP
CR_10400W_A		CAL0000201001	ARD1	YHR013C	S000001055	YHR013C	RiBi
C7_03670W_A	DED81	CAL0000197236	DED81	YHR019C	S000001061	YHR019C	RiBi
C7_03660C_A		CAL0000176548	YHR020W	YHR020W	S000001062	YHR020W	RiBi
CR_07630C_A	RPS27	CAL0000200692	RPS27B	YHR021C	S000001063	YHR021C	RP
C5_00650C_A	THR1	CAL0000196189	THR1	YHR025W	S000001067	YHR025W	RiBi
C1_13280C_A		CAL0000187987	VMA16	YHR026W	S000001068	YHR026W	RiBi
C4_03180W_A	NCP1	CAL0000197218	NCP1	YHR042W	S000001084	YHR042W	RiBi
C6_01170W_A	CIC1	CAL0000187983	CIC1	YHR052W	S000001094	YHR052W	RiBi
C4_04700W_A	SSZ1	CAL0000182719	SSZ1	YHR064C	S000001106	YHR064C	RiBi
CR_09740W_A		CAL0000176052	RRP3	YHR065C	S000001107	YHR065C	RiBi
CR_09730C_A	SSF1	CAL0000187750	SSF1	YHR066W	S000001108	YHR066W	RiBi
C3_02180C_A		CAL0000180114	DYS1	YHR068W	S000001110	YHR068W	RiBi
C2_07630C_A		CAL0000176228	RTC3	YHR087W	S000001129	YHR087W	iESR
C4_03270W_A	RPF1	CAL0000187860	RPF1	YHR088W	S000001130	YHR088W	RiBi
C1_11550W_A	GAR1	CAL0000187800	GAR1	YHR089C	S000001131	YHR089C	RiBi
C5_02930C_A	GRE3	CAL0000192827	GRE3	YHR104W	S000001146	YHR104W	iESR
CR_09010C_A		CAL0000185607	YHR112C	YHR112C	S000001154	YHR112C	iESR
C5_03390C_A	FUR1	CAL0000201707	FUR1	YHR128W	S000001170	YHR128W	RP
C4_05560C_A	ARO9	CAL0000197694	ARO9	YHR137W	S000001179	YHR137W	iESR
C4_02340W_A		CAL0000188954	YHR138C	YHR138C	S000001180	YHR138C	iESR
C1_14390W_A	RPC10	CAL0000192095	RPC10	YHR143W-A	S000001185	YHR143W-A	RiBi
C1_14310W_A		CAL0000182387	DCD1	YHR144C	S000001187	YHR144C	RiBi
CR_00460C_A		CAL0000189738	IMP3	YHR148W	S000001191	YHR148W	RiBi
CR_05630W_A	DBP8	CAL0000181153	DBP8	YHR169W	S000001212	YHR169W	RiBi

CR_06720W_A	NMD3	CAL0000185434	NMD3	YHR170W	S000001213	YHR170W	RiBi
CR_06730W_A	APG7	CAL0000178896	ATG7	YHR171W	S000001214	YHR171W	iESR
C3_04140C_A	EGD2	CAL0000185584	EGD2	YHR193C	S000001236	YHR193C	RiBi
C3_07750W_A	UTP9	CAL0000175459	UTP9	YHR196W	S000001239	YHR196W	RiBi
C4_05230C_A		CAL0000185245	RIX1	YHR197W	S000001240	YHR197W	RiBi
C4_05650W_A		CAL0000182332	FAF1	YIL019W	S000001281	YIL019W	RiBi
C4_05640C_A		CAL0000175514	HIS6	YIL020C	S000001282	YIL020C	RiBi
C4_05630W_A		CAL0000186561	RPB3	YIL021W	S000001283	YIL021W	RiBi
C1_06890C_A		CAL0000185373	RPL34B	YIL052C	S000001314	YIL052C	RP
C3_00090W_A	RPS24	CAL0000180342	RPS24B	YIL069C	S000001331	YIL069C	SGD-annotated RP
C5_00110C_A	THS1	CAL0000177380	THS1	YIL078W	S000001340	YIL078W	RiBi
C3_05860C_A		CAL0000182639	BMT5	YIL096C	S000001358	YIL096C	RiBi
C3_05850W_A		CAL0000193350	FYV10	YIL097W	S000001359	YIL097W	iESR
C3_01320C_A	SGA1	CAL0000178932	SGA1	YIL099W	S000001361	YIL099W	iESR
C2_05860C_A		CAL0000190238	XBP1	YIL101C	S000001363	YIL101C	iESR
C2_05830C_A		CAL0000201076	SHQ1	YIL104C	S000001366	YIL104C	RiBi
C1_08950W_A	PFK26	CAL0000176014	PFK26	YIL107C	S000001369	YIL107C	iESR
C1_09040C_A		CAL0000175693	HPM1	YIL110W	S000001372	YIL110W	RiBi
CR_04210C_A	QDR1	CAL0000179875	QDR1	YIL120W	S000001382	YIL120W	iESR
C3_00900C_A	AYR1	CAL0000181438	AYR1	YIL124W	S000001386	YIL124W	iESR
C3_01430W_A		CAL0000186307	RRT14	YIL127C	S000001389	YIL127C	RiBi
C1_00180W_A	RPL16A	CAL0000175593	RPL16A	YIL133C	S000001395	YIL133C	RP
CR_01470W_A	CSP37	CAL0000182669	OM45	YIL136W	S000001398	YIL136W	iESR
C5_05340W_A		CAL0000180910	SQT1	YIR012W	S000001451	YIR012W	RiBi
CR_03570C_A	YVH1	CAL0000184045	YVH1	YIR026C	S000001465	YIR026C	RiBi
C6_00850W_A		CAL0000196844	HYR1	YIR037W	S000001476	YIR037W	iESR
C3_03600C_A	GTT12	CAL0000179604	GTT1	YIR038C	S000001477	YIR038C	iESR
C3_05530W_A	OST1	CAL0000177262	OST1	YJL002C	S000003539	YJL002C	RiBi
C5_05120W_A	CCT3	CAL0000198447	CCT3	YJL014W	S000003551	YJL014W	RiBi
C4_02830C_A	HCA4	CAL0000199884	HCA4	YJL033W	S000003570	YJL033W	RiBi
C7_03400C_A		CAL0000198236	MTR4	YJL050W	S000003586	YJL050W	RiBi
C1_05370C_A		CAL0000176582	IKS1	YJL057C	S000003593	YJL057C	iESR
CR_03120W_A		CAL0000191885	MPM1	YJL066C	S000003602	YJL066C	iESR
CR_09670C_A		CAL0000178864	YJL068C	YJL068C	S000003604	YJL068C	iESR
C7_04190C_A	UTP18	CAL0000175893	UTP18	YJL069C	S000003605	YJL069C	RiBi
C1_11860W_A		CAL0000181643	SCP160	YJL080C	S000003616	YJL080C	RiBi
C1_07170C_A	ZCF23	CAL0000175205	GSM1	YJL103C	S000003639	YJL103C	iESR
C1_14080W_A		CAL0000180258	UTP10	YJL109C	S000003645	YJL109C	RiBi
C7_00160C_A		CAL0000182219	ALB1	YJL122W	S000003658	YJL122W	RiBi
CR_08940W_A		CAL0000194641	GCD14	YJL125C	S000003661	YJL125C	RiBi

C1_01370C_A	RPS21B	CAL0000190545	RPS21B	YJL136C	S000003672	YJL136C	RP
C1_01350C_A	TIF	CAL0000186279	TIF2	YJL138C	S000003674	YJL138C	RP
C2_04660C_A	YAK1	CAL0000193813	YAK1	YJL141C	S000003677	YJL141C	iESR
C1_10260C_A	RPA34	CAL0000179921	RPA34	YJL148W	S000003684	YJL148W	RiBi
CR_08550W_A		CAL0000186425	FBP26	YJL155C	S000003691	YJL155C	iESR
C3_05380W_A		CAL0000179271	YJL163C	YJL163C	S000003699	YJL163C	iESR
C2_04600C_A	RPL17B	CAL0000193181	RPL17B	YJL177W	S000003713	YJL177W	RP
C1_02400C_A	MNN11	CAL0000193393	MNN11	YJL183W	S000003719	YJL183W	RiBi
C1_06470W_A		CAL0000189989	RPL39	YJL189W	S000003725	YJL189W	RP
C1_06460C_A	RPS22A	CAL0000188584	RPS22A	YJL190C	S000003726	YJL190C	RP
C1_06450C_A	RPS14B	CAL0000196584	RPS14B	YJL191W	S000003727	YJL191W	RP
C5_00280C_A		CAL0000174323	NUC1	YJL208C	S000003744	YJL208C	RiBi
C2_00070C_A	MPP10	CAL0000175136	MPP10	YJR002W	S000003762	YJR002W	RiBi
C4_05310W_A		CAL0000183261	YJR003C	YJR003C	S000003763	YJR003C	RiBi
C1_06960W_A	SUI2	CAL0000201409	SUI2	YJR007W	S000003767	YJR007W	RiBi
C1_14030W_A		CAL0000191113	MHO1	YJR008W	S000003768	YJR008W	iESR
C4_00770C_A		CAL0000192770	TMA22	YJR014W	S000003775	YJR014W	RiBi
CR_05440W_A		CAL0000184857	BNA1	YJR025C	S000003786	YJR025C	iESR
C3_04370C_A		CAL0000187255	URB2	YJR041C	S000003802	YJR041C	RiBi
C1_05850W_A	POL32	CAL0000193896	POL32	YJR043C	S000003804	YJR043C	RiBi
C6_01710C_A	PTK2	CAL0000186778	PTK2	YJR059W	S000003820	YJR059W	iESR
C2_07300C_A	RPA12	CAL0000195650	RPA12	YJR063W	S000003824	YJR063W	RiBi
C2_07310W_A	CCT5	CAL0000189768	CCT5	YJR064W	S000003825	YJR064W	RiBi
C2_07290W_A		CAL0000183521	LIA1	YJR070C	S000003831	YJR070C	RiBi
C3_06860C_A		CAL0000185942	YJR096W	YJR096W	S000003857	YJR096W	iESR
C4_02320C_A	SOD1	CAL0000185037	SOD1	YJR104C	S000003865	YJR104C	iESR
C5_03070W_A	RPS5	CAL0000175293	RPS5	YJR123W	S000003884	YJR123W	RP
C5_03940C_A		CAL0000181747	YJR124C	YJR124C	S000003885	YJR124C	RiBi
C2_06100W_A	PMT4	CAL0000192933	PMT4	YJR143C	S000003904	YJR143C	RiBi
C1_01640W_A	RPS42	CAL0000191446	RPS4A	YJR145C	S000003906	YJR145C	RP
C6_02770W_A	MRT4	CAL0000181896	MRT4	YKL009W	S000001492	YKL009W	RiBi
C4_05330C_A		CAL0000187814	MAK11	YKL021C	S000001504	YKL021C	RiBi
CR_04660C_A	UGP1	CAL0000175518	UGP1	YKL035W	S000001518	YKL035W	iESR
CR_00860C_A	TMA19	CAL0000181023	TMA19	YKL056C	S000001539	YKL056C	RP
C5_02890W_A	YNK1	CAL0000191707	YNK1	YKL067W	S000001550	YKL067W	iESR
C6_01040C_A		CAL0000190791	DHR2	YKL078W	S000001561	YKL078W	RiBi
C2_08190W_A	VMA5	CAL0000198252	VMA5	YKL080W	S000001563	YKL080W	RiBi
C2_08180C_A		CAL0000200640	RRP14	YKL082C	S000001565	YKL082C	RiBi
CR_03360W_A		CAL0000180806	UTP11	YKL099C	S000001582	YKL099C	RiBi
C3_02170C_A	LAP41	CAL0000183019	APE1	YKL103C	S000001586	YKL103C	iESR
CR_03370C_A	KTI12	CAL0000192073	KTI12	YKL110C	S000001593	YKL110C	RiBi

C1_01940C_A		CAL0000197941	SRP21	YKL122C	S000001605	YKL122C	RiBi
C7_03890C_A		CAL0000180066	SSH4	YKL124W	S000001607	YKL124W	iESR
C4_04430W_A	MRP8	CAL0000198349	MRP8	YKL142W	S000001625	YKL142W	iESR
CR_10650W_A	LTV1	CAL0000196926	LTV1	YKL143W	S000001626	YKL143W	RiBi
C1_05230W_A		CAL0000199486	RPC25	YKL144C	S000001627	YKL144C	RiBi
C6_02040W_A	MCR1	CAL0000182452	MCR1	YKL150W	S000001633	YKL150W	iESR
C6_02030C_A		CAL0000185966	YKL151C	YKL151C	S000001634	YKL151C	iESR
CR_07660C_A		CAL0000180632	SRP102	YKL154W	S000001637	YKL154W	RiBi
C1_05510C_A	RPS27A	CAL0000198357	RPS27A	YKL156W	S000001639	YKL156W	RP
C2_04570W_A		CAL0000183510	EBP2	YKL172W	S000001655	YKL172W	RiBi
C5_00260W_A		CAL0000189135	PRS1	YKL181W	S000001664	YKL181W	RiBi
C1_12100C_A	PXA2	CAL0000196592	PXA2	YKL188C	S000001671	YKL188C	iESR
C2_04020C_A	SDS22	CAL0000176734	SDS22	YKL193C	S000001676	YKL193C	iESR
C7_04200C_A		CAL0000200169	LOS1	YKL205W	S000001688	YKL205W	RiBi
C3_00810C_A	FOX2	CAL0000176075	FOX2	YKR009C	S000001717	YKR009C	iESR
C7_01200C_A	DBP7	CAL0000199731	DBP7	YKR024C	S000001732	YKR024C	RiBi
C7_01210C_A		CAL0000182770	RPC37	YKR025W	S000001733	YKR025W	RiBi
C7_01220W_A	GCN3	CAL0000186383	GCN3	YKR026C	S000001734	YKR026C	RiBi
C2_07420W_A		CAL0000182609	SHB17	YKR043C	S000001751	YKR043C	RiBi
C1_01380C_A	TRM2	CAL0000192336	TRM2	YKR056W	S000001764	YKR056W	RiBi
C2_04700C_A		CAL0000194786	UTP30	YKR060W	S000001768	YKR060W	RiBi
C3_02480C_A	CCP1	CAL0000199533	CCP1	YKR066C	S000001774	YKR066C	iESR
C2_02890W_A	SCT2	CAL0000191565	GPT2	YKR067W	S000001775	YKR067W	iESR
CR_02130W_A	ECM4	CAL0000196854	ECM4	YKR076W	S000001784	YKR076W	iESR
C3_00420W_A		CAL0000186672	TRZ1	YKR079C	S000001787	YKR079C	RiBi
C2_05230C_A	RPF2	CAL0000180822	RPF2	YKR081C	S000001789	YKR081C	RiBi
CR_02980C_A	SRP40	CAL0000197163	SRP40	YKR092C	S000001800	YKR092C	RiBi
CR_10550W_A	DRS1	CAL0000182242	DRS1	YLL008W	S000003931	YLL008W	RiBi
C3_00560C_A	SOF1	CAL0000196031	SOF1	YLL011W	S000003934	YLL011W	RiBi
C1_13470W_A	KNS1	CAL0000194707	KNS1	YLL019C	S000003942	YLL019C	iESR
CR_08250C_A	HSP104	CAL0000200274	HSP104	YLL026W	S000003949	YLL026W	iESR
C5_02120C_A	RIX7	CAL0000179059	RIX7	YLL034C	S000003957	YLL034C	RiBi
CR_06450W_A		CAL0000182248	GRC3	YLL035W	S000003958	YLL035W	RiBi
C3_07480W_A		CAL0000186688	PRP19	YLL036C	S000003959	YLL036C	RiBi
C3_07270C_A	UBI4	CAL0000186339	UBI4	YLL039C	S000003962	YLL039C	iESR
C3_05240C_A	RPL8B	CAL0000183492	RPL8B	YLL045C	S000003968	YLL045C	RP
C7_00260C_A		CAL0000199507	YLR001C	YLR001C	S000003991	YLR001C	iESR
C7_03850W_A		CAL0000177493	NOC3	YLR002C	S000003992	YLR002C	RiBi
C1_07790C_A		CAL0000195062	CMS1	YLR003C	S000003993	YLR003C	RiBi
C4_00510C_A	RLP24	CAL0000179590	RLP24	YLR009W	S000003999	YLR009W	RP
C3_03790W_A	MEU1	CAL0000179927	MEU1	YLR017W	S000004007	YLR017W	RiBi

C4_06570C_A	PDC11	CAL0000201027	PDC1	YLR044C	S000004034	YLR044C	RiBi
C3_07800C_A		CAL0000179596	FCF2	YLR051C	S000004041	YLR051C	RiBi
CR_01760C_A	FRS1	CAL0000190210	FRS1	YLR060W	S000004050	YLR060W	RiBi
CR_01780W_A		CAL0000181125	BMT6	YLR063W	S000004053	YLR063W	RiBi
C1_01950C_A		CAL0000175736	ENV10	YLR065C	S000004055	YLR065C	RiBi
C1_02450C_A		CAL0000190982	BUD20	YLR074C	S000004064	YLR074C	RiBi
C1_02460W_A	RPL10	CAL0000194016	RPL10	YLR075W	S000004065	YLR075W	RP
CR_07180W_A	EMP46	CAL0000179572	EMP46	YLR080W	S000004070	YLR080W	iESR
C4_02550C_A	EMP70	CAL0000181076	EMP70	YLR083C	S000004073	YLR083C	RiBi
C1_08290C_A	DIP2	CAL0000188650	DIP2	YLR129W	S000004119	YLR129W	RiBi
C5_02600W_A	PUT1	CAL0000197353	PUT1	YLR142W	S000004132	YLR142W	iESR
C1_13330C_A		CAL0000192204	SPE4	YLR146C	S000004136	YLR146C	RiBi
C7_03280C_A		CAL0000191424	YLR149C	YLR149C	S000004139	YLR149C	iESR
C3_04810C_A		CAL0000197338	STM1	YLR150W	S000004140	YLR150W	RiBi
C4_07180W_A	UBI3	CAL0000178202	RPS31	YLR167W	S000004157	YLR167W	RP
C5_03700C_A		CAL0000183474	DPH5	YLR172C	S000004162	YLR172C	RiBi
C1_10620W_A		CAL0000194674	CBF5	YLR175W	S000004165	YLR175W	RiBi
C5_00930C_A	TFS1	CAL0000201755	TFS1	YLR178C	S000004168	YLR178C	iESR
C1_11350C_A	TOS4	CAL0000194861	TOS4	YLR183C	S000004173	YLR183C	RiBi
C1_11380W_A	NEP1	CAL0000197320	EMG1	YLR186W	S000004176	YLR186W	RiBi
C4_01450W_A	PWP1	CAL0000198308	PWP1	YLR196W	S000004186	YLR196W	RiBi
CR_09950C_A	SIK1	CAL0000178436	NOP56	YLR197W	S000004187	YLR197W	RiBi
C1_04710C_A		CAL0000175312	RSA3	YLR221C	S000004211	YLR221C	RiBi
C5_02550C_A	UTP13	CAL0000184822	UTP13	YLR222C	S000004212	YLR222C	RiBi
C4_06790W_A		CAL0000198582	GPN3	YLR243W	S000004233	YLR243W	RiBi
C5_01580C_A	CEF3	CAL0000190871	YEF3	YLR249W	S000004239	YLR249W	RiBi
C5_01980C_A		CAL0000197371	SSP120	YLR250W	S000004240	YLR250W	iESR
C2_06430C_A		CAL0000199251	SYM1	YLR251W	S000004241	YLR251W	iESR
C7_00710W_A	RPS28B	CAL0000196464	RPS28B	YLR264W	S000004254	YLR264W	RP
C7_01190W_A		CAL0000181791	DCS1	YLR270W	S000004260	YLR270W	iESR
C6_01890C_A		CAL0000180288	DBP9	YLR276C	S000004266	YLR276C	RiBi
C7_00300W_A		CAL0000175025	YLR290C	YLR290C	S000004281	YLR290C	iESR
C2_03990W_A	GCD7	CAL0000187213	GCD7	YLR291C	S000004282	YLR291C	RiBi
C2_06310C_A	GSP1	CAL0000182095	GSP1	YLR293C	S000004284	YLR293C	RiBi
C1_00550W_A	CIS2	CAL0000184736	ECM38	YLR299W	S000004290	YLR299W	iESR
C2_00210W_A	RPL38	CAL0000195876	RPL38	YLR325C	S000004317	YLR325C	RP
C2_00250W_A	STF2	CAL0000185307	TMA10	YLR327C	S000004319	YLR327C	iESR
C5_03540C_A	RPS25B	CAL0000173943	RPS25B	YLR333C	S000004325	YLR333C	RP
CR_03650W_A	SGD1	CAL0000199737	SGD1	YLR336C	S000004328	YLR336C	RiBi
C7_00990W_A	RPP0	CAL0000189629	RPP0	YLR340W	S000004332	YLR340W	RP
C1_02320C_A		CAL0000179837	YLR345W	YLR345W	S000004337	YLR345W	iESR

C6_01140C_A	ARC18	CAL0000196412	ARC18	YLR370C	S000004362	YLR370C	iESR
C2_03230C_A	FEN12	CAL0000193175	ELO3	YLR372W	S000004364	YLR372W	RiBi
CR_08480C_A		CAL0000180472	RPS29A	YLR388W	S000004380	YLR388W	RP
CR_08590W_A		CAL0000185208	AFG2	YLR397C	S000004389	YLR397C	RiBi
C2_02420C_A		CAL0000188545	DUS3	YLR401C	S000004393	YLR401C	RiBi
C5_00290W_A	DUS4	CAL0000191650	DUS4	YLR405W	S000004397	YLR405W	RiBi
C2_05410W_A		CAL0000188731	RPL31B	YLR406C	S000004398	YLR406C	SGD-annotated RP
C2_02430W_A	UTP21	CAL0000192006	UTP21	YLR409C	S000004401	YLR409C	RiBi
C5_00250C_A		CAL0000178313	BER1	YLR412W	S000004404	YLR412W	RiBi
C1_03060C_A	TSR2	CAL0000185349	TSR2	YLR435W	S000004427	YLR435W	RiBi
C4_00020W_A		CAL0000178095	VMA6	YLR447C	S000004439	YLR447C	RiBi
C1_03110W_A	RPL6	CAL0000181737	RPL6B	YLR448W	S000004440	YLR448W	RP
C1_00500C_A	GLO1	CAL0000175730	GLO1	YML004C	S000004463	YML004C	iESR
C3_06420C_A		CAL0000179869	YML018C	YML018C	S000004480	YML018C	RiBi
C2_01430W_A	APT1	CAL0000192887	APT1	YML022W	S000004484	YML022W	RP
C7_00960W_A	RPS18	CAL0000197056	RPS18B	YML026C	S000004488	YML026C	RP
C4_02020W_A	CAT2	CAL0000184947	CAT2	YML042W	S000004506	YML042W	iESR
CR_06480C_A	RRN11	CAL0000185586	RRN11	YML043C	S000004507	YML043C	RiBi
C2_06390C_A	IMH3	CAL0000175344	IMD4	YML056C	S000004520	YML056C	RiBi
C7_03910W_A	OGG1	CAL0000183658	OGG1	YML060W	S000004525	YML060W	RiBi
C1_03090W_A	RPS1	CAL0000192592	RPS1B	YML063W	S000004528	YML063W	RP
C2_09500W_A		CAL0000188810	DUS1	YML080W	S000004545	YML080W	RiBi
CR_09800C_A		CAL0000180872	UTP14	YML093W	S000004558	YML093W	RiBi
CR_01650W_A	URA5	CAL0000176894	URA5	YML106W	S000004574	YML106W	RiBi
C2_05470W_A	COQ5	CAL0000175801	COQ5	YML110C	S000004578	YML110C	iESR
CR_09140C_A		CAL0000184548	MSC1	YML128C	S000004597	YML128C	iESR
C2_05130W_A		CAL0000187542	YML131W	YML131W	S000004600	YML131W	iESR
CR_00680W_A	BUD22	CAL0000194312	BUD22	YMR014W	S000004616	YMR014W	RiBi
C4_00380W_A		CAL0000175239	ARA2	YMR041C	S000004644	YMR041C	iESR
C1_04130W_A	ERB1	CAL0000194713	ERB1	YMR049C	S000004652	YMR049C	RiBi
C5_00480C_A	SEC14	CAL0000199482	SEC14	YMR079W	S000004684	YMR079W	RiBi
CR_00090C_A		CAL0000190190	YMR090W	YMR090W	S000004696	YMR090W	iESR
C2_08670C_A	UTP15	CAL0000175436	UTP15	YMR093W	S000004699	YMR093W	RiBi
CR_02820W_A	PGM2	CAL0000201506	PGM2	YMR105C	S000004711	YMR105C	iESR
C1_00410C_A		CAL0000181570	HFD1	YMR110C	S000004716	YMR110C	iESR
C7_01250W_A	ASC1	CAL0000180554	ASC1	YMR116C	S000004722	YMR116C	RP
CR_04100C_A	RPL15A	CAL0000190553	RPL15B	YMR121C	S000004728	YMR121C	RP
C2_00410C_A		CAL0000195316	ECM16	YMR128W	S000004735	YMR128W	RiBi
C1_12680W_A		CAL0000198380	RRB1	YMR131C	S000004738	YMR131C	RiBi
C2_02530W_A		CAL0000198820	GAT2	YMR136W	S000004744	YMR136W	iESR

C2_04290W_A	RIM11	CAL0000186692	RIM11	YMR139W	S000004747	YMR139W	iESR
C1_03030W_A	RPS16A	CAL0000175363	RPS16A	YMR143W	S000004751	YMR143W	RP
C1_02790W_A	TIF34	CAL0000192484	TIF34	YMR146C	S000004754	YMR146C	RP
C4_04250W_A		CAL0000193728	YMR155W	YMR155W	S000004764	YMR155W	iESR
C2_09220W_A	DDR48	CAL0000176590	DDR48	YMR173W	S000004784	YMR173W	iESR
C2_03960W_A	RPL39	CAL0000177209	RPL36A	YMR194W	S000004807	YMR194W	RP
C3_03410C_A		CAL0000188430	YMR196W	YMR196W	S000004809	YMR196W	iESR
C3_03400C_A	VTI1	CAL0000188283	VTI1	YMR197C	S000004810	YMR197C	iESR
C1_09360C_A		CAL0000200870	EFR3	YMR212C	S000004825	YMR212C	RiBi
C1_09490C_A	GUA1	CAL0000179678	GUA1	YMR217W	S000004830	YMR217W	RiBi
C2_02540W_A		CAL0000188474	RRP5	YMR229C	S000004842	YMR229C	RiBi
C6_03260W_A		CAL0000187941	RNH1	YMR234W	S000004847	YMR234W	RiBi
C3_01990W_A	RNA1	CAL0000191775	RNA1	YMR235C	S000004848	YMR235C	RiBi
C4_04830W_A	DCR1	CAL0000189883	RNT1	YMR239C	S000004852	YMR239C	RiBi
C2_02200W_A		CAL0000192596	ZRC1	YMR243C	S000004856	YMR243C	RiBi
C1_11660W_A	GAD1	CAL0000195622	GAD1	YMR250W	S000004862	YMR250W	iESR
CR_01710W_A		CAL0000189317	TMA23	YMR269W	S000004882	YMR269W	RiBi
C3_07460W_A		CAL0000184913	FCP1	YMR277W	S000004890	YMR277W	RiBi
C5_04750C_A	HAS1	CAL0000175982	HAS1	YMR290C	S000004903	YMR290C	RiBi
C3_04550C_A	CMK1	CAL0000190479	TDA1	YMR291W	S000004905	YMR291W	iESR
C7_03360W_A	CPY1	CAL0000177922	PRC1	YMR297W	S000004912	YMR297W	iESR
CR_03620C_A		CAL0000182841	YME2	YMR302C	S000004917	YMR302C	iESR
C2_10050W_A		CAL0000182786	UBP15	YMR304W	S000004920	YMR304W	iESR
C1_00220W_A	PHR2	CAL0000181783	GAS1	YMR307W	S000004924	YMR307W	RiBi
C1_08110W_A		CAL0000200179	PSE1	YMR308C	S000004925	YMR308C	RiBi
C4_01490W_A	NIP1	CAL0000176830	NIP1	YMR309C	S000004926	YMR309C	RiBi
C4_02260C_A		CAL0000191193	YMR310C	YMR310C	S000004927	YMR310C	RiBi
C6_02560W_A		CAL0000178081	YMR315W	YMR315W	S000004932	YMR315W	iESR
CR_03070W_A	DOM34	CAL0000193423	DOM34	YNL001W	S000004946	YNL001W	RiBi
CR_06120W_A	RPL7	CAL0000194902	RLP7	YNL002C	S000004947	YNL002C	RP
C2_07140W_A		CAL0000187183	YNL010W	YNL010W	S000004955	YNL010W	RiBi
CR_02030C_A		CAL0000178878	RCM1	YNL022C	S000004967	YNL022C	RiBi
C1_04100C_A	POR1	CAL0000182381	POR1	YNL055C	S000005000	YNL055C	iESR
CR_04170W_A		CAL0000190202	NOP2	YNL061W	S000005005	YNL061W	RiBi
CR_04160C_A		CAL0000185106	GCD10	YNL062C	S000005006	YNL062C	RiBi
C6_00820W_A	SUN41	CAL0000175157	SUN4	YNL066W	S000005010	YNL066W	RiBi
C3_02470C_A	RPL9B	CAL0000184881	RPL9B	YNL067W	S000005011	YNL067W	RP
CR_07950W_A	IMP4	CAL0000181923	IMP4	YNL075W	S000005019	YNL075W	RiBi
C3_04300C_A	POL1	CAL0000174261	POL1	YNL102W	S000005046	YNL102W	RiBi
C7_00690W_A	NOP15	CAL0000196813	NOP15	YNL110C	S000005054	YNL110C	RiBi
CR_02520W_A	RPC19	CAL0000179133	RPC19	YNL113W	S000005057	YNL113W	RiBi

C6_00250W_A		CAL0000196053	YNL115C	YNL115C	S000005059	YNL115C	iESR
CR_03550W_A	NCS2	CAL0000189560	NCS2	YNL119W	S000005063	YNL119W	RP
CR_04110W_A		CAL0000196049	NAF1	YNL124W	S000005068	YNL124W	RiBi
CR_04240C_A		CAL0000178904	KRE33	YNL132W	S000005076	YNL132W	RiBi
CR_03300C_A		CAL0000183745	YNL134C	YNL134C	S000005078	YNL134C	iESR
C2_06970W_A	AAH1	CAL0000194200	AAH1	YNL141W	S000005085	YNL141W	RiBi
CR_02720C_A	RPC31	CAL0000174952	RPC31	YNL151C	S000005095	YNL151C	RiBi
C4_05860W_A		CAL0000198712	GIM3	YNL153C	S000005097	YNL153C	RiBi
C1_10390C_A	RPL42	CAL0000190451	RPL42A	YNL162W	S000005106	YNL162W	RP
C1_07140C_A	RIA1	CAL0000176174	RIA1	YNL163C	S000005107	YNL163C	RiBi
C3_07300W_A	NOP13	CAL0000196304	NOP13	YNL175C	S000005119	YNL175C	RiBi
CR_04810W_A	RPS3	CAL0000200765	RPS3	YNL178W	S000005122	YNL178W	RP
C1_06760C_A		CAL0000201524	IPI3	YNL182C	S000005126	YNL182C	RiBi
C1_06780W_A	NPR1	CAL0000199299	NPR1	YNL183C	S000005127	YNL183C	iESR
C4_03440C_A	DOT4	CAL0000187993	UBP10	YNL186W	S000005130	YNL186W	RiBi
C1_02220C_A		CAL0000191549	YNL200C	YNL200C	S000005144	YNL200C	iESR
C3_05710W_A	RCT1	CAL0000178441	YNL208W	YNL208W	S000005152	YNL208W	iESR
CR_08090W_A	SSB1	CAL0000194973	SSB2	YNL209W	S000005153	YNL209W	RP
CR_03240C_A		CAL0000195354	JJJ1	YNL227C	S000005171	YNL227C	RiBi
C1_08980C_A	ZWF1	CAL0000192089	ZWF1	YNL241C	S000005185	YNL241C	iESR
C1_13030C_A		CAL0000188986	YNL247W	YNL247W	S000005191	YNL247W	RiBi
C2_01070W_A		CAL0000186371	RPA49	YNL248C	S000005192	YNL248C	RiBi
C5_01910W_A	GIS2	CAL0000183688	GIS2	YNL255C	S000005199	YNL255C	RiBi
C5_00770C_A	FOL1	CAL0000194395	FOL1	YNL256W	S000005200	YNL256W	RiBi
C1_02980W_A	GOR1	CAL0000192040	GOR1	YNL274C	S000005218	YNL274C	iESR
C5_01180W_A	PUS4	CAL0000191725	PUS4	YNL292W	S000005236	YNL292W	RiBi
CR_06560C_A		CAL0000175245	BXI1	YNL305C	S000005249	YNL305C	iESR
C3_02350W_A		CAL0000194501	KRI1	YNL308C	S000005252	YNL308C	RiBi
C2_10740C_A		CAL0000193421	EMW1	YNL313C	S000005257	YNL313C	RiBi
CR_03500W_A	CIT1	CAL0000197786	CIT1	YNR001C	S000005284	YNR001C	iESR
C2_06680W_A	FRP3	CAL0000177981	ATO2	YNR002C	S000005285	YNR002C	iESR
C6_03210C_A		CAL0000189174	RPC34	YNR003C	S000005286	YNR003C	RiBi
C1_00070W_A	MVD	CAL0000181620	MVD1	YNR043W	S000005326	YNR043W	RiBi
C6_03640W_A	NOG2	CAL0000182741	NOG2	YNR053C	S000005336	YNR053C	RiBi
C5_02070C_A		CAL0000181506	ESF2	YNR054C	S000005337	YNR054C	RiBi
C7_02930C_A		CAL0000182014	TSR4	YOL022C	S000005382	YOL022C	RiBi
CR_08360C_A	RPP2A	CAL0000175968	RPP2A	YOL039W	S000005399	YOL039W	RP
C3_04670C_A	RPS15	CAL0000179139	RPS15	YOL040C	S000005400	YOL040C	RP
C2_04120C_A		CAL0000199505	NOP12	YOL041C	S000005401	YOL041C	RiBi
CR_08380C_A		CAL0000201421	RRT8	YOL048C	S000005408	YOL048C	iESR
C1_12310C_A	CSI2	CAL0000186593	BRX1	YOL077C	S000005437	YOL077C	RiBi

C2_08140C_A	PHM7	CAL0000191215	PHM7	YOL084W	S000005444	YOL084W	iESR
C1_12380C_A	WRS1	CAL0000182691	WRS1	YOL097C	S000005457	YOL097C	RiBi
C3_05100C_A	RPL18	CAL0000188970	RPL18A	YOL120C	S000005480	YOL120C	RP
C3_05200W_A	RPS19A	CAL0000200926	RPS19A	YOL121C	S000005481	YOL121C	RP
C3_05140C_A		CAL0000185296	TRM11	YOL124C	S000005484	YOL124C	RiBi
C6_01970C_A	RPL25	CAL0000200350	RPL25	YOL127W	S000005487	YOL127W	RP
C6_03240W_A		CAL0000179051	GRE2	YOL151W	S000005511	YOL151W	iESR
C1_05050C_A	RRP6	CAL0000183418	RRP6	YOR001W	S000005527	YOR001W	RiBi
CR_02420W_A		CAL0000197728	UTP23	YOR004W	S000005530	YOR004W	RiBi
C2_03130W_A		CAL0000176044	SFM1	YOR021C	S000005547	YOR021C	RiBi
C2_02920W_A		CAL0000185278	TMC1	YOR052C	S000005578	YOR052C	iESR
C2_09430W_A	RPL3	CAL0000201023	RPL3	YOR063W	S000005589	YOR063W	RP
C3_01480C_A	RKI1	CAL0000188418	RKI1	YOR095C	S000005621	YOR095C	RiBi
C3_01490W_A	RPS7A	CAL0000199878	RPS7A	YOR096W	S000005622	YOR096W	RP
CR_10410C_A		CAL0000173996	PNO1	YOR145C	S000005671	YOR145C	RiBi
C1_00310W_A		CAL0000201857	PNS1	YOR161C	S000005687	YOR161C	iESR
C7_00550C_A	GLN4	CAL0000198388	GLN4	YOR168W	S000005694	YOR168W	RiBi
CR_03770C_A	RPS30	CAL0000193815	RPS30B	YOR182C	S000005708	YOR182C	RP
C1_03710C_A	MSB1	CAL0000199709	MSB1	YOR188W	S000005714	YOR188W	RiBi
CR_05520W_A	NOC2	CAL0000192871	NOC2	YOR206W	S000005732	YOR206W	RiBi
C7_04040C_A	NPT1	CAL0000174810	NPT1	YOR209C	S000005735	YOR209C	RiBi
C4_03040W_A		CAL0000183011	RPB10	YOR210W	S000005736	YOR210W	RiBi
C2_05790C_A	RFC1	CAL0000180025	RFC1	YOR217W	S000005743	YOR217W	RiBi
C7_01700W_A		CAL0000179241	RCN2	YOR220W	S000005746	YOR220W	iESR
CR_04780W_A	RPB8	CAL0000181508	RPB8	YOR224C	S000005750	YOR224C	RiBi
C2_10270W_A	PUS7	CAL0000177714	PUS7	YOR243C	S000005769	YOR243C	RiBi
C1_09330W_A		CAL0000197859	TMA16	YOR252W	S000005778	YOR252W	RiBi
CR_04070W_A	NAT5	CAL0000188442	NAT5	YOR253W	S000005779	YOR253W	RiBi
CR_03990C_A	GCD1	CAL0000190232	GCD1	YOR260W	S000005786	YOR260W	RiBi
C1_09470C_A		CAL0000177270	FSF1	YOR271C	S000005797	YOR271C	RiBi
C1_09510W_A	YTM1	CAL0000176486	YTM1	YOR272W	S000005798	YOR272W	RiBi
C1_09350W_A		CAL0000199949	CAF20	YOR276W	S000005802	YOR276W	RiBi
CR_07030C_A		CAL0000179560	RRP36	YOR287C	S000005813	YOR287C	RiBi
C2_00770W_A		CAL0000200626	YOR289W	YOR289W	S000005815	YOR289W	iESR
C2_08040C_A	RPS10	CAL0000177647	RPS10A	YOR293W	S000005819	YOR293W	RP
C1_00900W_A	RRS1	CAL0000188560	RRS1	YOR294W	S000005820	YOR294W	RiBi
C6_00370C_A	NOP5	CAL0000190357	NOP58	YOR310C	S000005837	YOR310C	RiBi
C4_01520C_A	RPL20B	CAL0000200399	RPL20B	YOR312C	S000005839	YOR312C	RP
C7_01450C_A	PRT1	CAL0000183631	PRT1	YOR361C	S000005888	YOR361C	RiBi
C3_07150C_A	RPS12	CAL0000200890	RPS12	YOR369C	S000005896	YOR369C	RP
C1_04680W_A	PIL1	CAL0000179346	LSP1	YPL004C	S000005925	YPL004C	iESR

C1_11650W_A	EGD1	CAL0000174763	EGD1	YPL037C	S000005958	YPL037C	RiBi
C1_04390C_A	NOP4	CAL0000184653	NOP4	YPL043W	S000005964	YPL043W	RiBi
C3_06040W_A		CAL0000176267	LEE1	YPL054W	S000005975	YPL054W	iESR
C3_06060W_A	ELP3	CAL0000193262	ELP3	YPL086C	S000006007	YPL086C	RiBi
C4_07050W_A	YDC1	CAL0000177800	YDC1	YPL087W	S000006008	YPL087W	iESR
C4_01270W_A	RPS6A	CAL0000181351	RPS6A	YPL090C	S000006011	YPL090C	RP
C7_01790C_A	RPL5	CAL0000178607	RPL5	YPL131W	S000006052	YPL131W	SGD-annotated RP
C2_05710C_A		CAL0000183633	RPL33A	YPL143W	S000006064	YPL143W	RP
C2_05750W_A		CAL0000191069	NOP53	YPL146C	S000006067	YPL146C	RiBi
C3_03830W_A		CAL0000193039	RRD2	YPL152W	S000006073	YPL152W	iESR
C2_07400C_A	01-Apr	CAL0000197684	PEP4	YPL154C	S000006075	YPL154C	iESR
CR_01690C_A	CDC60	CAL0000201312	CDC60	YPL160W	S000006081	YPL160W	RiBi
C1_02080W_A	SET6	CAL0000174725	SET6	YPL165C	S000006086	YPL165C	iESR
C6_04530C_A		CAL0000188018	RTT10	YPL183C	S000006104	YPL183C	RiBi
C3_02540C_A	OXR1	CAL0000197295	OXR1	YPL196W	S000006117	YPL196W	iESR
C2_07210C_A	TPK2	CAL0000181882	TPK2	YPL203W	S000006124	YPL203W	iESR
C6_02290C_A		CAL0000201526	TYW1	YPL207W	S000006128	YPL207W	RiBi
C6_02360W_A	NIP7	CAL0000185986	NIP7	YPL211W	S000006132	YPL211W	RiBi
C6_02350C_A		CAL0000183350	PUS1	YPL212C	S000006133	YPL212C	RiBi
C3_01000W_A	BMS1	CAL0000199005	BMS1	YPL217C	S000006138	YPL217C	RiBi
C6_02240C_A	RPL10A	CAL0000174170	RPL1A	YPL220W	S000006141	YPL220W	RP
CR_09370W_A	ELF1	CAL0000177541	NEW1	YPL226W	S000006147	YPL226W	RiBi
CR_06440C_A	BCR1	CAL0000177853	USV1	YPL230W	S000006151	YPL230W	iESR
C7_01810W_A	RVB2	CAL0000176498	RVB2	YPL235W	S000006156	YPL235W	RiBi
C7_04130C_A	SUI3	CAL0000188940	SUI3	YPL237W	S000006158	YPL237W	RiBi
C1_13720W_A		CAL0000187064	KEL3	YPL263C	S000006184	YPL263C	RiBi
C1_13730C_A	DIM1	CAL0000196194	DIM1	YPL266W	S000006187	YPL266W	RiBi
C1_08410C_A	SAM4	CAL0000183325	SAM4	YPL273W	S000006194	YPL273W	RiBi
C7_00570W_A	RPA135	CAL0000201405	RPA135	YPR010C	S000006214	YPR010C	RiBi
CR_07080W_A		CAL0000186684	TIF6	YPR016C	S000006220	YPR016C	RiBi
C1_06940C_A	ATC1	CAL0000186706	ATH1	YPR026W	S000006230	YPR026W	iESR
C5_05490C_A	HTS1	CAL0000190585	HTS1	YPR033C	S000006237	YPR033C	RiBi
C1_03310W_A		CAL0000201344	ARP7	YPR034W	S000006238	YPR034W	RiBi
C5_02490C_A	TIF5	CAL0000179125	TIF5	YPR041W	S000006245	YPR041W	RiBi
C5_04590C_A	RPL43A	CAL0000185522	RPL43A	YPR043W	S000006247	YPR043W	RP
C1_11500C_A	ARO7	CAL0000179531	ARO7	YPR060C	S000006264	YPR060C	RiBi
C3_06900W_A	ISA2	CAL0000191195	ISA2	YPR067W	S000006271	YPR067W	iESR
C1_08320W_A	TKL1	CAL0000174068	TKL1	YPR074C	S000006278	YPR074C	RiBi
C2_08370C_A	TEF1	CAL0000196936	TEF1	YPR080W	S000006284	YPR080W	RiBi
C1_13190W_A		CAL0000182808	YPR098C	YPR098C	S000006302	YPR098C	iESR

C2_05340C_A	RPC40	CAL0000195273	RPC40	YPR110C	S000006314	YPR110C	RiBi
C3_02020W_A		CAL0000192627	MRD1	YPR112C	S000006316	YPR112C	RiBi
C2_01160W_A		CAL0000191452	MRI1	YPR118W	S000006322	YPR118W	RiBi
C1_06580W_A	RPS23A	CAL0000197722	RPS23B	YPR132W	S000006336	YPR132W	RP
CR_02710W_A	RRP9	CAL0000183718	RRP9	YPR137W	S000006341	YPR137W	RiBi
C2_09380W_A	RRP15	CAL0000177236	RRP15	YPR143W	S000006347	YPR143W	RiBi
C2_07340W_A	NOC4	CAL0000199787	NOC4	YPR144C	S000006348	YPR144C	RiBi
C3_04910C_A	NCE102	CAL0000190917	NCE102	YPR149W	S000006353	YPR149W	iESR
C6_01630W_A	TIF3	CAL0000196640	TIF3	YPR163C	S000006367	YPR163C	RiBi
C1_08870C_A	JIP5	CAL0000174164	JIP5	YPR169W	S000006373	YPR169W	RiBi
C4_05140C_A	GDB1	CAL0000189511	GDB1	YPR184W	S000006388	YPR184W	iESR
C5_03360W_A	RPO26	CAL0000199338	RPO26	YPR187W	S000006391	YPR187W	RiBi
CR_02890C_A		CAL0000174854	RPC82	YPR190C	S000006394	YPR190C	RiBi

Supplemental Table 5. *S. cerevisiae* ESR ortholog genes in *C.albicans.* RP(Ribosomal Protein), RiBi(Ribosome Biogenesis), iESR(involved in Environmental Stress Response)